

https://dspace.org/

Applications of low-temperature crystallography

Billing, David Gordon

1991

http://hdl.handle.net/10539/20826

Billing, David Gordon (1991) Applications of low-temperature crystallography, University of Witwatersrand, Johannesburg, <http://wiredspace.wits.ac.za/handle/10539/20826>

Downloaded from a DSpace repository. https://dspace.org/

Applications of Small Molecule Crystallography

by

David Gordon Billing

A thesis submitted in the Faculty of Science,
University of the Witwatersrand, Johannesburg,
for the Degree of Doctor of Philosophy.

February, 1995

Abstract

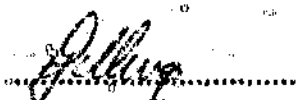
A detailed knowledge and understanding of the three-dimensional structure of molecules is important in many branches of chemistry. The majority of this is obtained via the results of small molecule crystallographic analyses. The application of the techniques and methods of small molecule X-ray crystallography is however not straight forward. Many systematic as well as random factors could affect the collection of the necessary diffraction data. The subsequent derivation of the crystal structure from the diffraction data is also not always obvious and without problems.

In this thesis, the results obtained from the successful refinement of 19 crystal structures are presented. These structure determinations, in addition to them contributing to the general body of known crystal structures, were undertaken for a number of chemically important reasons. These included an investigation into the nature of some chemical bonds, the conformational preferences of some molecules, hydrogen bonding in crystals of triglycine sulphate, as well as the identification and characterisation of some reaction products.

Also, because of the advantages obtained from performing the crystallographic at low temperatures, a previously unreliable cryostat was significantly modified and tested. The modified cryostat proved to be far more reliable, as well as stable and easier to use.

Declaration

I declare that this thesis is my own, unaided work. It is being submitted for the degree of Doctor of Philosophy in the Faculty of Science in the University of the Witwatersrand, Johannesburg. It has not been submitted for any degree or examination in any other University or Institution.



David Gordon Billing

February, 1995

Acknowledgements

I am grateful to my supervisor, Prof. J.C.A. Boeyens, for his support and guidance during the course of this project, and for the endless patience and advice that was needed during the preparation of this manuscript.

I would also like to express my gratitude towards the following people:

Prof. D.H. Reid for providing me with the heterapentalene crystals and his interest in my work.

Johan du Toit for his support, useful insights and discussions shared over numerous cups of coffee, as well as for proof-reading parts of this manuscript

My wife Caren, for her help and support throughout all this.

I would like to dedicate this work to my late father,

Gordon Donald Billing.

Publications

The following publications have resulted from some of the work presented in this thesis as well as from related work.

1. The structure and conformation of 1,1'-Bipyrrolidene-2,2'dithione.
   J.P.Michael, D.G.Billing, J.C.A.Boeyens, L.Carlton, L.Denner, I.Hindmarch.
   J.Mol.Struc.,**238**,(1990),391-401.

2. Conformational analysis of rotational barriers n N-Arylpyrrolidin-2-ones.
   D.G.Billing, J.C.A.Boeyens, L.Denner, K.du Plooy, G.C.Long, J.P Michael.
   Acta Cryst., (1991), **B47**, 284-288.

3. Structure of 6,7-Dihydro-2-phenyl-5h-2aλ^4-thia-3-selena-1,2-diaza cyclopent-[*cd*]indene.
   D.G.Billing, D.C. Levendis, D.H.Reid.
   Acta Cryst.,(1991), **C47**, 759-761.

4. The structure of uns-*cis*-mer(Pyridene-2-carboxylato-N,O)(ethylenediamine diacetato- N,N',O,O')cobalt(III).
   D.G.Billing, S.M.Dobson, G.Pattrick, L.Carlton.
   Acta Cryst.,(1991), **C47**,1964-1966.

5. Comparison of the NMR coupling paths in leucodrin and conocarpin by low temperature X-ray analysis.
   D.G.Billing, J.C.A.Boeyens, L.Carlton, D.C.Levendis, G.W.Perold.
   J. Chem. Soc. Perkin Trans. 2, (1991) 695-700.

6. Control of metal ion size-based selectivity through the structure of the oxygen donor pendant groups on Lariat ethers. A crystallographic and thermodynamic study.
K.V.Damu, R.D.Hancock, P.W.Wade, J.C.A.Boeyens, D.G.Billing and S.M.Dobson.
J. Chem. Soc. Dalton Trans. (1991), 293.

7. Structure of 2,3-Dicyclohexyl-6,7-dihydro-5H-2aλ^4-thia-2,3,4a,7a-tetra-azacyclopent[*cd*]indene-1(2H),4(2H)-diselone.
D.G.Billing, J.C.A.Boeyens, L.Denner, M.D.Hellyar, L.Le, A.J.Matthee and D.H.Reid.
Acta Cryst.(C) (1991), **C47**, 2564-2567.

8. Structure and stability of some complexes of Lariat ethers with sterically hindered pyridyl groups as pendent donors.
K.V.Damu, R.D.Hancock, J.C.A.Boeyens, D.G.Billing and S.M.Dobson.
S.A.J. of Chem.,(1991), **44**, 65-70.

9. Crystallographic study of N-arylpyrrolidin-2-ones.
D.G.Billing, J.C.A.Boeyens, D.C.Levendis and J.P.Michael.
S.A.J. of Chem..(1991), **44**, 75-79.

10. Metal Dimer Chemistry: Me_3NO induced substitution reactions of $(\eta^5\text{-}C_5H_5)MoMn(CO)_6$. X-ray structure determinations of $(\eta^5\text{-}C_5H_5)MoMn(CO)_4[P(OMe)_3]$.
W. E. Ingham, David G. Billing, Demetrius C. Levendis and Neil J. Coville.
Inorg. Chem. Acta. (1991), **187**, 17-21.

11. Novel production of 3-Benzoyl-2,1-benzisoxazoles from 2-Phenyl-4(1H)-quinolinones.
B. Staskun, T. van Es, D.G. Billing and J.C.A. Boeyens.
J. Chem. Soc. Chem. Comm., (1991), 927.

12. Is the metal-metal bond length in $MnRe(CO)_{10}$ anomalous? The X-ray structure determination of $MnRe(CO)_9L$ (L = ^tBuNC, $P(CH_2C_6H_5)_3$) and $MnRe(CO)_8(CN(Bu^t)(PPh_3)$.
A.E. Leins, D.G. Billing, D.C. Levendis, J. du Toit and N.J. Coville.
Inorg. Chem., (1992), **31**, 4756 - 4761.

13. Structures of 2,3-Diethyl-6,7-dihydro-5*H*-2aλ^4-selena-2,3,4a,7a-tetraaza-cyclopent[*cd*]indene-1(2*H*),4(2*H*)-diselone and 1,4-Bisethylimino-5,6-dihydro- 2,2aλ^4,3-triselena-4a,6a-diazacyclopenta[*cd*]pentalene.
D.G Billing, E.E Ferg, L. Lai, D.C. Levendis and D.H Reid.
Acta Cryst. C, (1993), **C49**,

14. Structure of 5,10-Dihydro-3-phenylimino-1,2,4-Thiaselenazolo[4,5-*b*][2,4] benzo diazepine.
D.G. Billing, J.C.A. Boeyens, W. Haag, L.L. Lai and D.H. Reid.
Acta Cryst. C, (1993), **C49**, 1781-1782

15. Crystal and molecular structure of 6-*exo*-methyl-6-*endo*-nitro-2-*exo*-phenylbi-cyclo[2.2.1]heptan-2-*endo*-ol
J.P. Michael, D.G. Billing and T.L. Maqutu
J. Chem. Crystall., (1994), **24**, 309-312

16. Crystal structure of 2,3-Diethyl-5,6,7,8-tetrahydro-2aλ^4-thia-2,3,4a,8a-tetraazacyclopent[*cd*]azulene-1(2*H*),4(3*H*)-diselone.
D.G. Billing, J.C.A. Boeyens, L.L. Lai and D.H. Reid.
Acta Cryst. C, (1994), (in press)

17. Crystal structure of 5,6,7,8 - Tetrahydro - 2,3-diphenyl - 2aλ⁴- thia - 2,3,4a, 8a-tetraazacyclopent[*cd*]azulene -1[*2H*],4[*3H*] - diselone.
D.G. Billing, J.C.A. Boeyens, L.L. Lai and D.H. Reid.
Acta Cryst. C, (1994), (in press)

18. 3,5-Diphenyl-2,2'-pyridylamino-1-thia-6,6aλ⁴-diselenapentalene.
D.G. Billing, D.C. Levendis, D.H. Reid and B.G. Rose
Acta Cryst. C, (1994), (accepted for publication)

19. 5-thylamino-3-p-toiyl-1λ⁴,2,4-thia-selenazol-1-ylium Bromide.
D.G. Billing, J.C.A. Boeyens, L.L. Lai and D.H. Reid.
Acta Cryst. C, (1994), (submitted for publication)

Contents

		page
Abstract		ii
Declaration		iii
Acknowledgements		iv
Dedication		v
Publications		vi
Contents		x
List of Computer programs used		xiii
Chapter		
1	Introduction	1
2	Crystal structure determination	
	2.1 Introduction	11
	2.2 Crystal growth	15
	2.3 Specimen selection and preparation	17
	2.4 Crystal mounting	18
	2.5 Data collection	20
	2.6 Data reduction	24
	2.7 Structure solution	25
	2.8 Structure refinement	28
	2.9 Geometrical parameters	31
	2.10 Graphical representation of structures	33
3	Cryostat design, construction and testing	
	3.1 Introduction	35
	3.2 Modification concepts and criteria	37
	3.3 Prototype construction	38
	3.4 Discussion and conclusion	40

4 The metal-metal bond length in MnRe dimers

4.1 Introduction 41

4.2 Crystallographic analysis. 43

4.3 Results and Discussion. 51

5 Bonding in Heterapentalene type compounds

5.1 Introduction 53

5.2 Crystal structure of 5,6-Dihydro-1,4-bis-*p*-tolylimino-2aλ⁴-thia-2,3,diselena-4a,6a-diazacyclopent[*cd*]pentalene. 55

5.3 Crystal structure of 3,5-Diphenyl-2,2'-pyridylamino-1-thia-6,6aλ⁴-diselenapentalene. 60

5.4 Crystal structure of *N*-Phenyl-2-(5-phenyl-*3H*-1,2-diselenol-3-ylidine)acetamide. 65

5.5 Crystal structure of 1,4-Bis(ethylimino)-5,6-dihydro-2,2aλ⁴,3-triselena-4a,6a-diazacyclopenta[*cd*]pentalene. 69

5.6 Crystal structure of 2,3-Diethyl-6,7-dihydro-5*H*-2aλ⁴-selena-2,3,4a,7a-tetraazacyclopent[*cd*]indene-1(2*H*),4(3*H*)-diselone. 73

5.7 Crystal structure of 5-*p*-Methoxyphenyl-2-*p*-methoxyphenylimino-3,2-phenyl-1,6,6aλ⁴-triselenapentalene. 77

5.8 Crystal structure of 1,4-Bis-*p*-ethoxyphenylimino-5,6-dihydro-2,3-dithia-2aλ⁴-selena-4a,6a-diazacyclopenta[*cd*]pentalene. 81

5.9 Crystal structure of 2,3-Diethyl-5,6,7,8-tetrahydro-2aλ⁴-thia-2,3,4a,8a-tetraazacyclopent[*cd*]azulene-1(2*H*),4(3*H*)-diselone. 86

5.10 Crystal structure of 5,6,7,8-Tetrahydro-2,3-diphenyl-2aλ⁴-thia-2,3,4a,8a-tetraazacyclopent[*cd*]azulene-1(2*H*),4(3*H*)-diselone. 90

5.11 Crystal structure of 6,7-Dihydro-2-phenyl-5*H*-2aλ⁴-thia-3-selena-1,2-diazacyclopent[*cd*]indene. 95

5.12 Discussion. 99

6	Conformation preferences in single *ortho*, N-substituted acetanilide derivatives.	108
7	X-ray Diffraction study of TGS.	115
8	The crystal structure of 5-Ethylamino-3-p-tolyl-1λ⁴,2,4-thia-selenazol- 1-ylium Bromide.	125
9	The crystal structure of 3-Benzoyl-5-methyl-2,1-benzisoxazole.	129
10	Concluding discussion.	133
Bibliography		135
References		136
Appendix		139

List of computer programs used.

The following computer programs were used during the course of the work:

CAD4 - Diffractometer control program by Enraf Nonius

PROFIT - Data reduction program, including profile fitting (Strel'tsov *et al*, 1989)

SHELXS86 - Structure solution program (Sheldrick; 1985)

SHELXL93 - Structure refinement program (Sheldrick; 1993)

XTAL 3.2 - Suite of programs (Hall *et al*; 1992)

in particular the following routines were used:

ABSCAL - Scale diffractometer data for psi-scan absorption.

ABSORB - Apply Gaussian, analytical and spherical absorption corrections.

ADDATM - Load atom parameters to binary file.

ADDREF - Place and reduce reflection data onto binary file.

ATABLE - Prepare table of atomic parameters for publication.

BONDLA - Calculate bond lengths and angles.

CONTRS - Contour Fourier maps.

CRYLSQ - Refine atomic parameters by least-squares.

DIFDAT - Process CAD4, Nicolet and other diffractometer tapes.

FC - Calculate structure factors.

FOURR - Map Patterson and Fast Fourier transform.

LATCON - Refine lattice constants from two theta values.

ORTEP - Calculate thermal ellipsoid data for plotting.

PIG - Display and manipulate molecular coordinates.

PLOTX - Apply plot commands for specific graphics devices.

SLANT - Interpolate slanted map from FOURR map.

SORTRF - Sort and merge reflection data on F, F^2 and I.

STARTX - Create and update binary data file with cell and symmetry data.

NRCVAX - Suite of programs (Gabe *et al*, 1989)

SCHAKAL - Produces graphical representations of molecules. (Keller; 1988)

The Cambridge Crystallographic Database.

CHAPTER 1

Introduction

From the time when it was first postulated that atoms could interact with each other to form molecules, chemists have been interested in the nature and properties of these atomic aggregates. It was soon realised that some knowledge of the structures of these molecules would be central in the understanding of their properties. As chemists knowledge and understanding grew, their concept of a molecular structure also evolved. From where it was little more than an enumeration of the ratios of the various elements in the structure, to a point where it also includes information about the connectivity between these atoms, and their relative positions in three dimensional space. Today the fundamental laws governing molecular structures are still far from well understood and is the source of much speculation and research in many branches of chemistry. This, however, has not prevented chemists from using structural information, with great success when, for example, designing synthetic routes to new products, investigating the properties of materials or when studying the reactions of molecules.

There are many techniques available that can be used to obtain structural information about a molecule of interest. Most of these are based on the interaction of electromagnetic radiation with a sample containing the molecule. So, for example, techniques such as infrared spectroscopy, ultraviolet and visible spectroscopy as well as nuclear magnetic resonance spectroscopy are based on the absorption of electromagnetic radiation by the molecule under investigation. Such techniques can generally be used to obtain information concerning the atomic connectivity and functional groups present in the molecule. The appeal of these methods lie therein that they are relatively easy to use and that liquids and solutions can be used as samples.

To obtain detailed structural information, including interatomic distances and stereochemical data, it is necessary to use one of the diffraction-based techniques. Of these, single-crystal X-ray diffraction has assumed a leading position, mainly

because of the affordability and hence availability of equipment. In this technique a single crystal is exposed to a monochromatic beam of x-rays, and the angular distribution and intensities of the diffracted beams are recorded. From these the electron density distribution in the crystal may be determined and hence the positions of atoms inferred.

Because of the internal regularity of crystals, X-rays are diffracted by the crystal lattice according to the equation:

$$2d_{hkl} \sin\theta_{hkl} = n\lambda$$

which is known as Bragg's law. X-rays are diffracted by a set of crystal planes when, and only when this equation is satisfied. The diffracted beam then appears to have been reflected from the *hkl* lattice planes. Each diffracted beam is identified by the Miller indices of the set of parallel planes causing the reflection *hkl*. The wave scattered by the contents of the unit cell in the direction of the *hkl* reflection is described in amplitude and phase by the structure factor, F_{hkl}. This may be derived by noting that the radiation scattered by one atom will interfere constructively and destructively with radiation scattered by other atoms in the unit cell and therefore the scattering from the entire crystal will depend on where each atom lies in the unit cell. The structure factor is then given by:

$$F_{hkl} = F_{hkl} \exp(i\alpha_{hkl}) = \sum_j f_j \exp\left[2\pi\left(hx_j + ky_j + lz_j\right)\right]$$

where α_{hkl} and F_{hkl} are the phase and amplitude, respectively, of the diffracted beam. The sum is over all atoms in the unit cell and f_j is the scattering factor of the j-th atom at the value of $\sin\theta/\lambda$ corresponding to the Bragg reflection *hkl*. The positional coordinates of the atoms, x_j, y_j and z_j, are expressed as the fractions of the unit cell edges. Thus if the atomic positions are known, then F_{hkl} can be calculated and so can the phase angle α_{hkl}.

It is important to realize that each atom in the unit cell (and hence in the crystal) contributes to the intensity of each reflection by an amount that depends on its position in the unit cell, its scattering power and, to a lesser extent, the scattering angle. Thus each F_{hkl} contains information about the entire crystal structure.

The electron density in a crystal is normally represented by means of a three-dimensional map of the electron-density function, $\rho(xyz)$, calculated by Fourier synthesis at various points in the unit cell. Fourier summation methods are used because the electron density within a crystal is a triply periodic function and hence can be expressed by the triple summation of appropriately phased waves. Thus it is the simulation of the action of a lens and is a summation of waves of known amplitude F_{hkl} and phase α_{hkl}. The electron-density distribution is given by the following equation:

$$\rho(xyz) = \frac{1}{V} \sum_{hkl} \mathbf{F}_{hkl} \exp[-2\pi i(hx + ky + lz)]$$

where V is the volume of the unit cell. This equation can also be written in the from :

$$\rho(xyz) = \frac{1}{V} \sum_{hkl} F_{hkl} \cos[2\pi(hx + ky + lz) - \alpha_{hkl}]$$

where the amplitudes, F_{hkl}, and the phases, α_{hkl}, of the diffracted beams appear explicitly. Note that while the structure amplitudes are directly accessible by experiment, the phase angles are not; they have to be obtained in some way if we wish to calculate the electron-density map.

Since the electron-density function may be expressed as a Fourier series with the structure factors as coefficients, the structure factors may also be expressed in terms of the electron density. Thus the structure factor, $\mathbf{F}_{hkl}$, is the Fourier transform of the electron density $\rho(xyz)$:

$$\mathbf{F}_{hkl} = \int_{cell} \rho(xyz) \exp(i\phi)\, dV$$

(where ϕ is $2\pi(hx + ky + lz)$), and the electron density is the inverse Fourier transform of the structure factor:

$$\rho(xyz) = \frac{1}{V} \sum_{hkl} F_{hkl} \exp(-i\phi)$$

In this last equation a triple summation is used because F_{hkl} is only observed at discrete points. Thus the intensity of a Bragg reflection is proportional to the value at that reciprocal-lattice point, *hkl*, of the square of the Fourier transform of the electron density.

So far only the kinetic theory of X-ray diffraction has been considered. That is, only the interference effects between the elementary waves scattered within the volume of the crystal have been considered. In fact, this theory neglects two important phenomena. Firstly, when the incident wave propagates through the crystal its intensity decreases gradually because a part of its energy is transferred to the scattered beam. And secondly, the diffracted waves interfere with each other and with the incident beam. The theory which takes all these phenomena into account and analyses the wave-field set up as a whole is called the dynamic theory of diffraction. It was initiated by Ewald, and later on Laue showed that Ewald's theory is equivalent to analysing the propagation of any electromagnetic field through a medium having a periodically varying complex dielectric constant.

Dynamic effects develop gradually in a crystal, and it may be shown that for sufficiently small thicknesses the incident beam is not weakened considerably. The diffracted waves are not so strong as to give rise to remarkable interference effects with the incident beam and the effects of absorption are negligible. Under these conditions (theoretically, thicknesses $<10^{-3}$ - 10^{-4} cm) the kinematic theory is a fairly accurate approximation to dynamic theory. In practice however, the corresponding equations proved to be valid even for crystals having dimensions of several tenths of a millimeter. This is due to the structure of real crystals.

A simplified model of a real crystal was proposed by Darwin (1914 &1922) when he showed that it can be ideally schematised like a mosaic of crystalline blocks with dimensions of about 10^{-5} cm, tilted very slightly to each other at angles of the order of fractions of a minute of arc. Each block is separated by faults and cracks from other blocks. The interference between waves only occurs inside every single block, whose dimensions satisfy the theoretical conditions of applicability of the kinematic theory. Because of the loss of coherence between the waves diffracted from different blocks, the diffracted intensity from the whole crystal is equal to the sum over the intensities diffracted from every single block.

A great advantage of the X-ray method is its ability to show some totally unexpected and surprising structures with complete certainty.

The detailed structure, that is obtained from an X-ray structure analysis, is important to chemists because it provides the chemist with the following information about the molecule:

- The atomic connectivity
- Interatomic distances (such as bond lengths)
- Conformational information
- Stereochemical data
- Information about non-bonded interaction (such as hydrogen bonding)
- Information concerning the motion of atoms in the crystal

In some cases where exceptional care was taken during the collection of the diffraction data, it is also possible to obtain reliable electron density information. This information is of great use in theoretical studies concerning bonding and molecular shape.

In this project, a number of compounds were studied by X-ray crystallographic methods. These structures were then used to answer questions relating to :

i. The metal-metal bond length in Mn-Re dimers.
ii. Bonding in heterapentalenes.
iii. Conformational preferences in single -*ortho*, N-substituted acetanilide derivatives.

iv. Hydrogen bonding in Triglycine Sulfate.
v. Reaction product identification and characterisation.

In most cases, the structures could be solved by routine structure determination techniques. For the purposes of this project, this is considered to involve the solution of a structure not influenced by disorder or any other systematic problem. In a number of cases, however, these routine methods failed to give data reliable enough to answer the questions at hand. In these cases it was generally possible to improve the accuracy and precision of the experiment in order to obtain the information at the desired accuracy. This was done by reducing the effects of some of the known systematic errors. The systematic effects encountered in this project and the methods by which they were minimised are listed in Table 1.1.

Table 1.1: Systematic problems in X-ray analysis

Systematic problem	Possible actions
Absorption	1. smaller crystal 2. empirical absorption corrections 3. Apply analytical absorption correction
Crystal decay	1. Apply linear decay correction 2. Apply non-linear absorption correction 3. Perform study at low temperature
Extinction	Consider during refinement
Thermal diffuse scattering	Perform study at low temperature
Disorder	1. include disorder model in refinement 2. Perform study at low temperature

When the diffraction experiment is performed at low temperature, the X-ray diffraction pattern obtained from crystalline matter would change. The extent of the changes depends on the crystal under investigation as well as the temperature range through which cooling has taken place. A small change in temperature could lead to hardly any discernible change in the diffraction pattern, unless the crystal undergoes a phase change. In this case the diffraction pattern could change dramatically, depending on the nature of the phase change that takes place. Thus, for example a disorder-order phase transition could result in diffuse layer lines in the diffraction pattern resolving into sharp reflections. This and other types of phase transition could also be associated with changes in the unit cell, which on its own has a dramatic effect on the spatial distribution of reflections.

On the other hand, if a crystal does not undergo a phase change on cooling, the changes in the diffraction pattern are more subtle, even for large changes in temperature. Firstly, the unit cell of the crystal will undergo a slight reduction in size due to thermal contraction. This would cause a slight spreading out of the reflections in the diffraction pattern. One must also bear in mind that the structure factor expression as written previously refers to atoms at rest, with f_j corresponding to a stationary atomic model. The thermal motion of an atom can be taken into account if the scattering factor for the stationary atom is replaced by the scattering factor a vibrating atom, f', which has the form:

$$f' = f \exp\left[\frac{-B \sin^2\theta}{\lambda^2}\right]$$

The quantity B, known as the Debye-Waller factor, is related to the atomic vibration by:

$$B = 8\pi^2 u^2$$

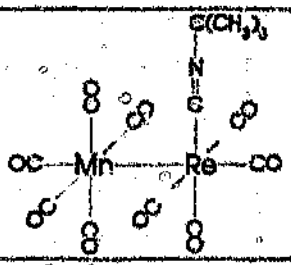
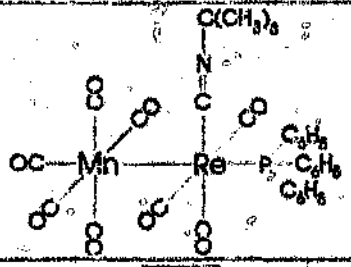
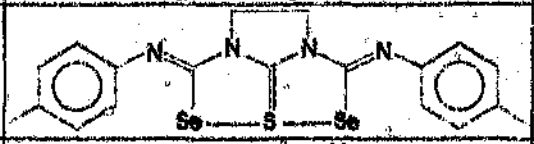
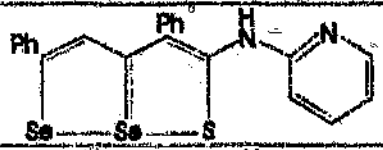
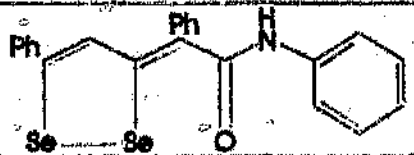
where u is the root-mean-square amplitude of atomic vibration. The effect of the additional factor in the struture factor expression, is to cause an increased fall-off of intensity with respect to $\sin\theta / \lambda$.

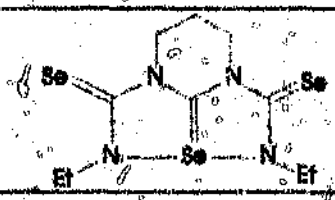
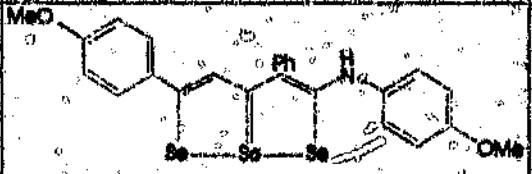
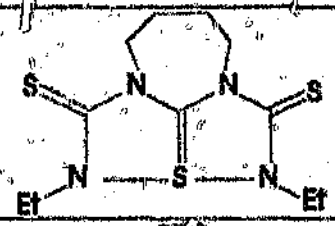
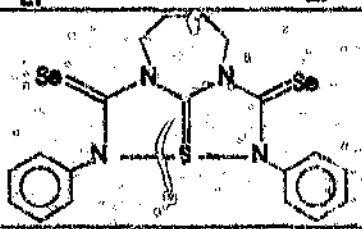
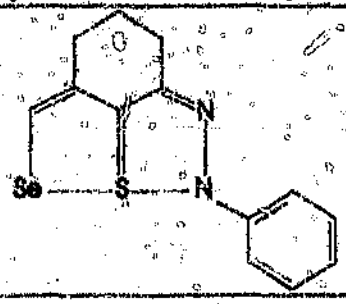
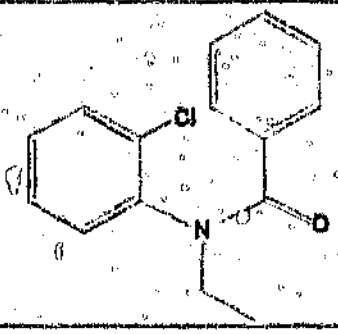
Thus on cooling, high order reflections show the most obvious changes, in the sense that they become more intense. More importantly, they become measurable. Therefore the number of measured reflections included in a data set increases significantly. This results in better, more precise structure refinements, including improved figures of merit.

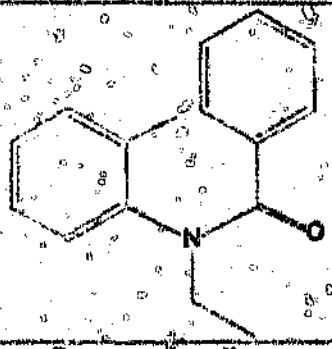
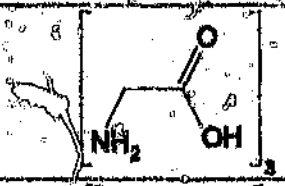
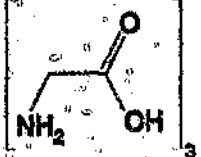
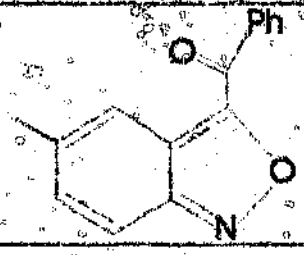
With this in mind and because of problems encountered with the cryostat used in previous projects, a computer controlled cryostat was also designed and built. It was then tested by collecting the low temperature data used in this project.

Table 1.2 lists the structures determined during the course of this project, and is fairly representative of the type of structures amenable to study by small molecule X-ray diffraction methods.

Table 1.2: Structures determined in this project

Structure Code	Molecular Formula	Chemical formula
1		$C_{14}H_9MnO_8Re$
2		$C_{30}H_{21}MnO_8PRe$
3		$C_{31}H_{24}MnNO_8PRe$
4		$C_{18}H_{18}N_4SSe_2$
5		$C_{22}H_{16}N_2SSe_2$
6		$C_{23}H_{17}NOSe_2$
7		$C_9H_{14}N_4Se_3$

8		$C_{10}H_{18}N_4Se_3$
9		$C_{28}H_{21}NO_2Se_3$
10		$C_{21}H_{22}N_4O_2S_2Se$
11		$C_{11}H_{18}N_4S_3$
12		$C_{19}H_{18}N_4SSe_2$
13		$C_{13}H_{12}N_2SSe$
14		$C_{15}H_{14}ClNO$

15		$C_{16}H_{17}NO$
16	 H_2SO_4	$C_8H_{17}N_3O_{10}S$
17	 H_2SO_4	$C_8H_{17}N_3O_{10}S$
18		$C_{11}H_{13}BrN_2SSe$
19		$C_{15}H_{11}NO_2$

CHAPTER 2

Crystal Structure Determination

2.1 Introduction

The object of a crystal structure determination is to identify and locate the positions of all the atoms within the unit cell, and thus, to completely define the structure of the crystal. For X-ray diffraction methods this can be accomplished because of the Fourier relationship which exists between the electron density distribution within the unit cell and the intensities of the X-ray beams diffracted by the crystal. The positions of atoms are then assumed to correspond to the centres of ovoids of charge. To accomplish this in practice it is necessary for a number of distinct stages to be completed successfully. And as these stages are to be completed in sequence it is important that as few errors as possible be introduced at each stage. Figure 2.1 shows the sequence of events that comprises the average modern X-ray structure determination. The principal steps being:

- Crystal growth
- Specimen selection and preparation
- Crystal mounting
- Data collection
- Structure solution
- Structure refinement
- Calculation of geometrical parameters
- Graphical representation of the structure

In the remainder of this chapter each of these steps will be discussed briefly.

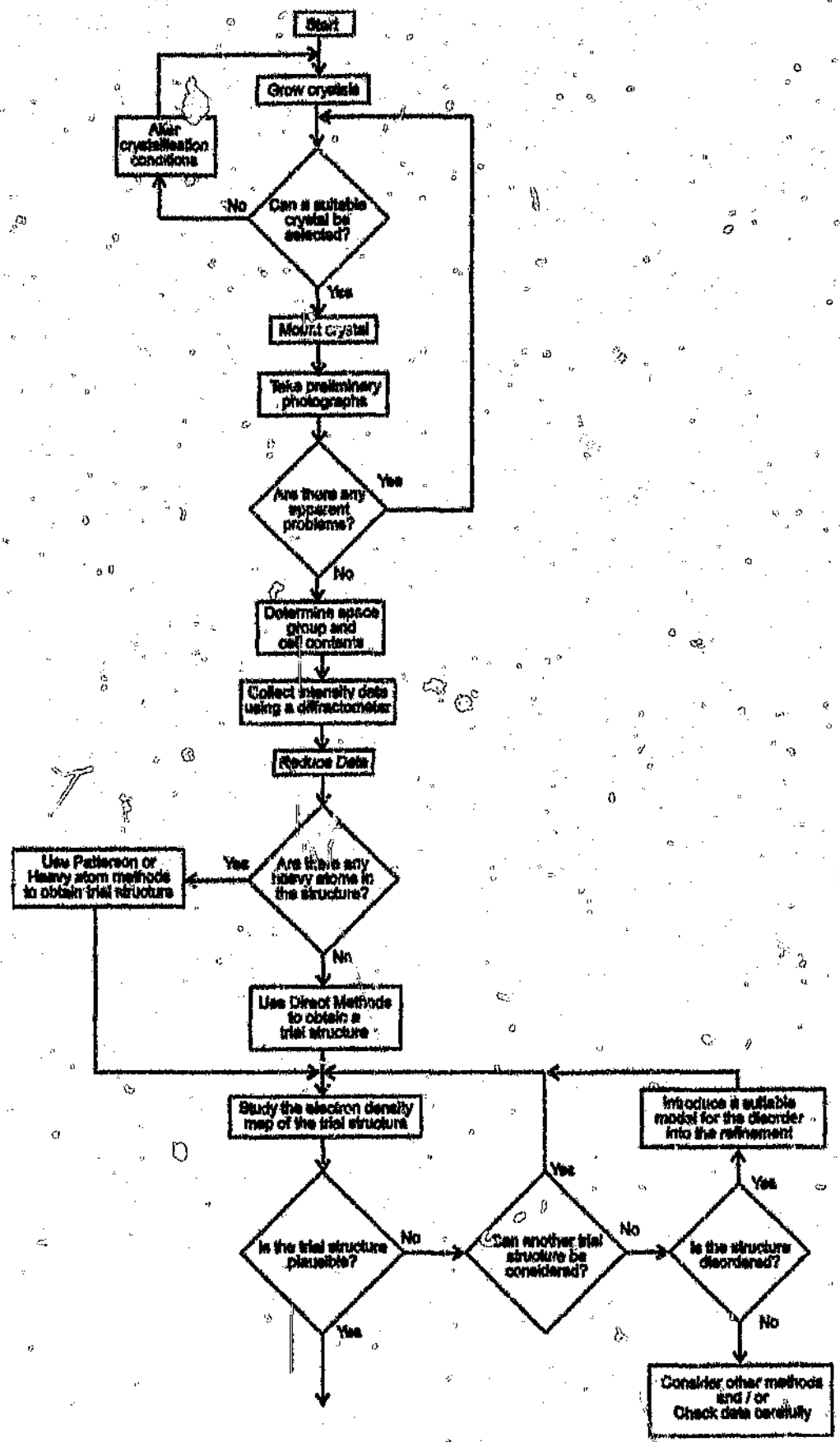


Figure 2.1 : The course of a modern structure determination

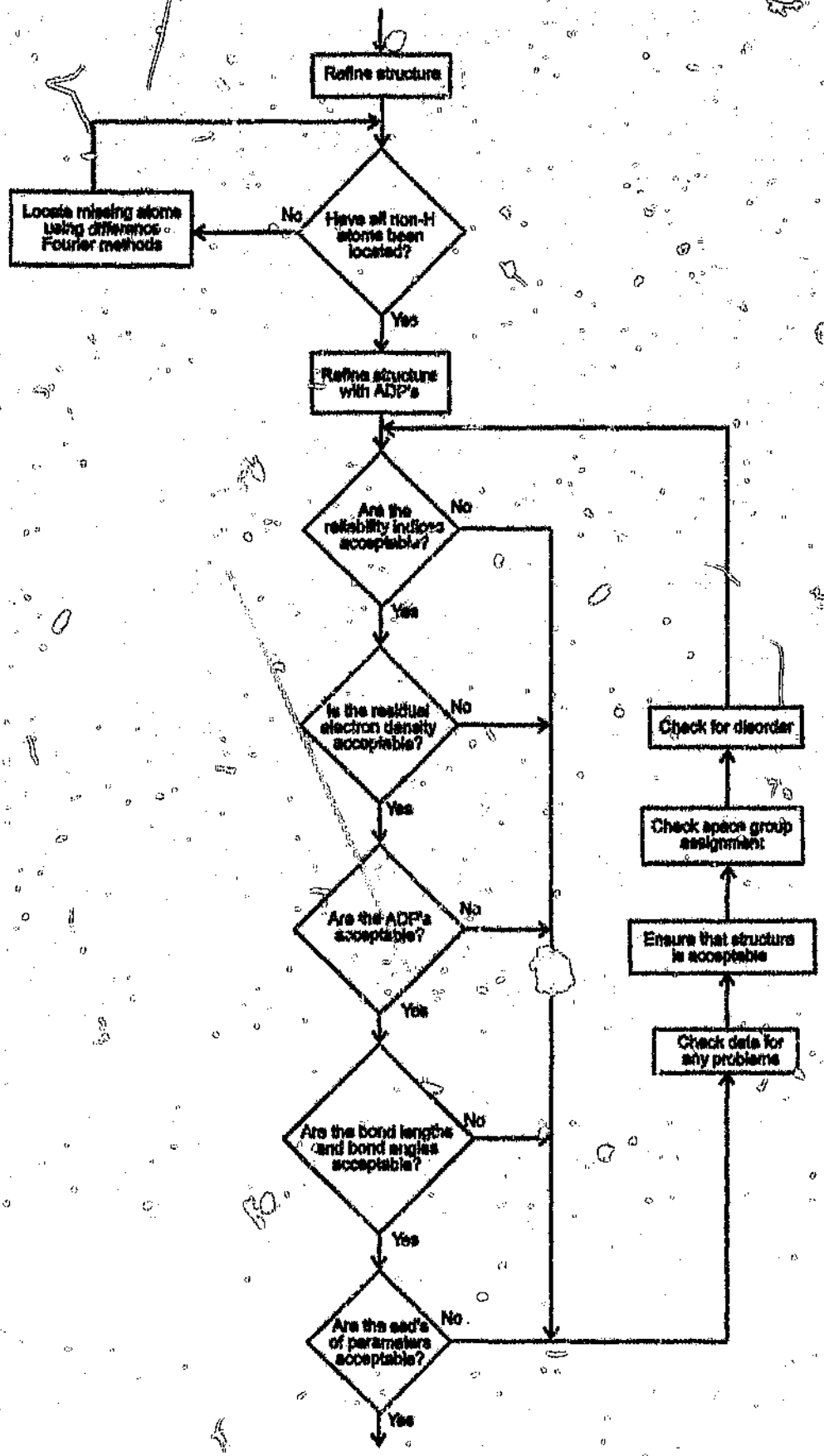


Figure 2.1 (Cont.)

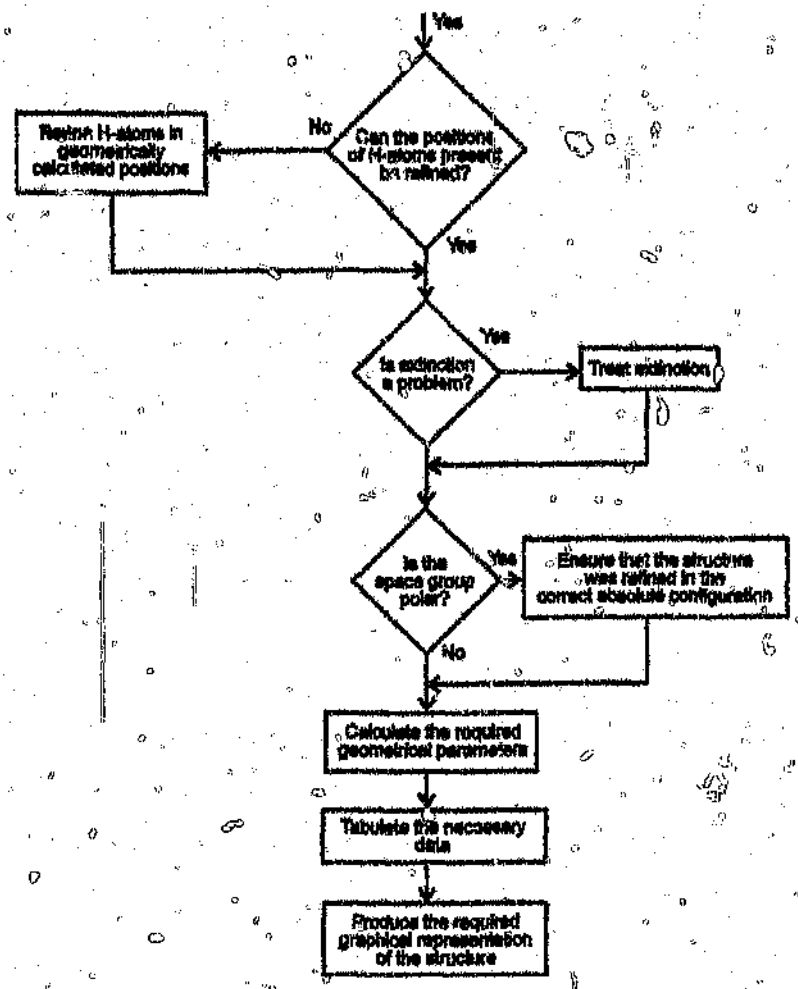


Figure 2.1 (Cont.)

2.2 Crystal growth

It is obvious that suitable crystals should be available before the crystal structure of a material can be determined. Unfortunately, because of the quality and the size of the crystals needed, it is often neccessary for crystals to be grown specially for the diffraction analysis. In general the growth should be slow so that a regular arrangement of molecules or ions, leading to a well-formed crystal, may be obtained. The aim is to reach a point at which the soluton is just saturated and then to slowly lower the saturation point while limiting the rate of nucleation, so that only a few crystals can grow to a relatively large size.

The method most frequently employed is slow evaporation, which unfortunately often deposits crystals as a microcrystalline crust on the walls of the container just at the surface of the solution. As the solvent evaporates, the solution recedes, leaving the crust in a position where it is not effective in inducing good crystal growth. Futhermore, it is so difficult to control the evaporation from small volumes of solution that appreciable amounts of solvent, a few milliliters, are required.

The second method commonly used is slow cooling. Cooling rates from elevated temperatures for solutions contained in laboratory vessels of ordinary size are often too rapid to produce anything but microscopic crystals. The rate of cooling can be slowed somewhat by placing the vessel containing the solution in a large container of hot water or by surrounding it with sufficient insulating material. The whole process can also be carried out with advantage in a Dewar vessel. Extremely slow rates of cooling can be obtained in a well-insulated and thermostatted oven by reducing the thermostat settings gradually.

If difficulty is experienced in growing satisfactory crystals from single solvents by either of the above methods, mixtures of two or more solvents should be tried. Changing the nature of the solvent often has a pronounced effect on the crystal habit and the size of the crystals grown, since properties that may influence crystal

growth, such as density, dielectric constant, viscosity, solvation and solubilty, can be varied in a controlled manner over wide ranges.

Another method that can often give good single crystals with milligram amounts of solute is by altering the solvent by vapour diffusion as illustrated in Figure 2.2

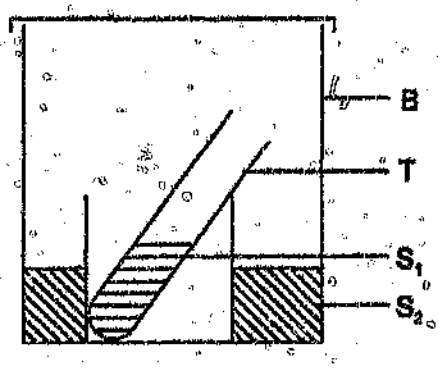


Figure 2.2: Crystallisation by vapour diffusion

A solution of the substance in solvent S_1 is contained in tube T. A second solvent S_2, placed in the closed beaker B, is chosen such that it produces with S_1 a mixture in which the solute is less soluble that in S_1 alone. Slow diffusion of S_2 into T (and S_1 out) will cause crystallisation, which under favourable conditions, can result in the growth of relatively large single crystals. If S_2 is more volatile than S_1, it is possible for the volume of the solution to increase during crystallisation and thus avoid the troublesome crusts that often form when solutions evaporate. In order to obtain good mixing of S_1 and S_2 as they diffuse together it is helpful that their densities be relatively similar, or, preferably that S_2 be denser that S_1.

Diffusion in the liquid phase can also be used to grow crystals. Figure 2.3 shows one arrangement that depends on the differences in density to maintain the initial separation between solvents S_1 and S_2. The solute must always be dissolved in the solvent in which it is more soluble. Crystals appear at the interface between S_1 and S_2 and grow as the solvents mix by diffusion.

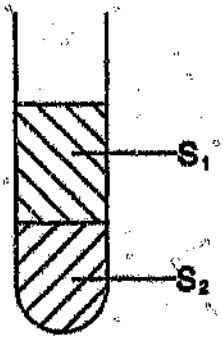


Figure 2.3 : Crystallisation by liquid diffusion

Satisfactory crystals can sometimes also be grown from the melt by slow cooling. This method is not amenable to the wide variations in conditions attainable with the methods already outlined, and has only limited application in growing crystals of organic compounds. For certain inorganic substances and metals, however, melting and crystallizing in a zone growth technique is capable of producing very large and pure crystals.

Sublimation is another method of limited applicability, but one that sometimes works well. If a solid vapourises readily without decomposition, sublimation can be considered as an alternative to other methods. If a gas condenses rapidly as a solid on a relatively cold surface, crystal growth is impaired and only a microcrystalline mass results. However, if sublimation is carried out slowly, so that large crystals grow at the expense of smaller ones, very large crystals may sometimes be obtained.

2.3 Specimen selection and preparation

A crystal whose structure is to be determined must be a single crystal, not cracked or a conglomerate. This may be checked by examining it under a polarizing microscope. If rotated about an axis normal to the polarising material, the crystal should either appear uniformly dark in all positions or be bright and extinguish, that is appear uniformly dark, once every 90°. Crystals made up of two or more fragments with different orientations will often reveal themselves by displaying both dark and light regions at the same time.

Choosing a crystal of suitable size is also important. If it is too large it would not be bathed homogeneously by the collimated beam of X-rays. If it is too small on the other hand it would result in difficulties in measuring the diffracted intensities reliably. Another important effect in determining a suitable crystal size is the absorption of x-rays by the crystal, and it can be shown that the optimum thickness is a function of the linear aborption coefficient and is given by:

$$t_{opt} = 2/\mu$$

All these phenomena could lead to serious systematic errors in the measured diffraction intensities.

If a crystal is too large it may be possible to cut it with a razor blade or with a solvent coated fibre. Ideally one should try to find a crystal that is, or can be ground into an approximately spherical shape, as this would minimize absorption effects. Alternatively a crystal with well defined faces should be selected, as these faces can be indexed, measured and used for calculating analytical absorption corrections. However, some crystals are too soft, fragile or sensitive for even delicate cutting and manipulation and must be used in the shape in which they grew.

2.4 Crystal mounting

For preliminary studies as well as the subsequent intensity data collection using a diffractometer, the selected crystal is generally attached to the end of a glass fibre using an adhesive. In cases where the crystal is unstable, the crystal may be put inside a thin-walled capillary (Lindemann tube) and the capillary sealed. An appropriate atmosphere may be maintained within the capillary to ensure stability. The fibre or capillary in turn is fixed into a brass pin using sealing wax. (See figures 2.4 and 2.5). The pin is used for handling the assembly and attaching it to the goniometer head.

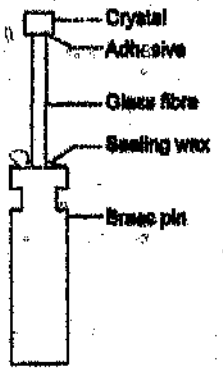


Figure 2.4 : Crystal mounted on glass fibre.

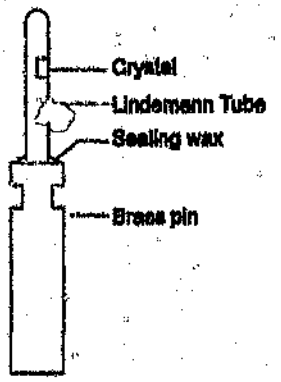


Figure 2.5 : Crystal mounted in glass capillary

These mounts are however not suitable for use in low temperature studies. The glues used to bind the crystal to the rod and the different coefficients of expansion of the materials used in these mounts may cause stresses on the crystal. It has been shown (Argoud & Muller; 1989) that these stresses could lead to strong modifications of diffraction intensities. The suggested method for mounting crystals for low temperature studies is illustrated in Figure 2.6, where the crystal is attached to a quartz rod, that had been drawn into a fibre, using a **small** amount of silicone grease.



Figure 2.6 : Low temperature mount

2.5 Data collection

The collection of crystallographic diffraction data poses two quite different problems. The first is the determination of the geometry of diffraction, from which the size, shape, and symmetry of the direct and reciprocal lattices may be calculated. The second is the assignment of an observed intensity to every point in the reciprocal lattice, which may ultimately be related to the distribution of electrons in the unit cell. Historically photographic methods served both ends, but automated diffractometers have largely replaced them for intensity data collection. Photographs, however, reveal significant portions of the reciprocal lattice simultaneously, making them ideal for confirming the quality of a crystal and for establishing the crystal system and space group of a crystal.

In photographic methods a camera containing a piece of film is placed behind or around the crystal, with allowance for entry of the direct beam from the collimator. The cameras used are constructed so that the indexing of the reflections is unambiguous and, with the precession camera, simple. The indices of the diffracted beams and the orders of diffraction may be determined by inspection or by calculation from the positions of the spots on the film. With most cameras, direct recording of the diffracted beams gives dark spots on the photographic film. In recent years Polaroid film has been used for preliminary indexing and space group determination; in this an intensifier (such zinc sulfide) faces the X-ray source and the visible light emitted is recorded on the Polaroid film. Such films give positive images rather than negative ones. The degree of blackness (or whiteness) of a spot depends on the exposure time, on the intensity of the diffracted beam and, to some extent, the conditions of development of the film.

In a diffractometer, the film is replaced by a photon detector and the intensity of a diffracted beam is determined by counting the photons associated with it. Generally such detectors can only measure a single beam at a time, and thus the diffracted beam intensities have to be measured sequentially. This could result in difficulties when collecting diffraction data for crystals which show significant radiation damage.

Diffractometer principles

Most contemporary diffractometers are of the four-circle type and are completely computer controlled. The essential geometry of a four-circle diffractometer is shown in figure 2.7. The incident X-ray beam and the diffracted beam, when orientated for measurement, lie in the horizontal plane which contains the crystal. The crystal can be rotated about three axes and the detector about a fourth axis; all four axes must intersect at the crystal. The crystal is mounted on a goniometer head which is attached to a spindle. The head is provided with centering slides and a height adjustment so that the crystal can be precisely positioned at the intersection of the three axes about which it can be rotated. The spindle, on which the head is mounted, can be rotated about its axis, which is designated the φ–axis, by the controlling computer. The spindle assembly, including the crystal, can be rotated about a perpendicular axis, designated the χ–axis, by rotation of ring **B** inside the stationary ring **A** (figure 2.7). This χ-ring together with the spindle assembly and the crystal can be rotated about a vertical axis, designated the ω–axis.

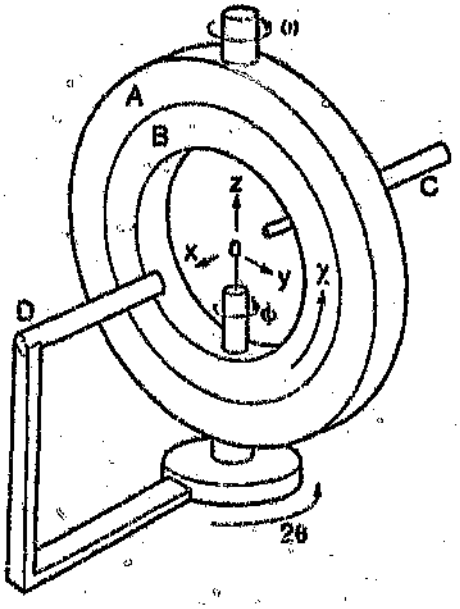


Figure 2.7 : The geometry of a four-circle diffractometer

The purpose of the three rotation axes, φ, χ and ω, is to enable the normal to a selected reflecting plane *hkl* to be brought into the horizontal plane, defined by the axes of the collimator **C** and the detector **D**, so that it is inclined to the incident beam at an angle of $90° - \theta$. The detector **D**, usually a scintillation counter, is mounted on an arm which enables it to be rotated about a vertical axis, designated the 2θ axis, coincident with the ω–axis so that it is inclined in the horizontal plane at 2θ to the forward direction of the incident beam; the detector is then correctly positioned to measure the intensity of the X-ray beam reflected from the selected *hkl* plane. The fact that the crystal can be rotated about three axes, leads to a degree of flexibility in the way in which it can be moved into the reflecting position for any given set of *hkl* planes.

Since the crystal is mounted at random, it is initially necessary to determine the orientation of its reciprocal lattice relative to the fixed reference axes of the diffractometer, X, Y, Z. These reference axes are orthogonal, right-handed, and such that X is directed along the forward direction of the incident X-ray beam while Z is vertical (figure 2.6). If the *hkl* reciprocal lattice vector, $\mathbf{d}^*_{hkl}$ where $|\mathbf{d}^*_{hkl}| = \lambda/d_{hkl}$, has coordinates X, Y, Z when the scales of φ, χ and ω are zero, then it is apparent that in order to bring $\mathbf{d}^*_{hkl}$ into the reflecting position the rotation on ϕ must be $\tan^{-1} X/Y$, on χ, $\sin^{-1}(-Z/d^*_{hkl})$, and on ω, $\sin^{-1} \frac{1}{2}d^*_{hkl}$, where $d^*_{hkl} = \sqrt{X^2+Y^2+Z^2}$. In order to be able to calculate these angles for a particular reflection it is necessary to know X, Y, Z for the corresponding reciprocal lattice vector, which implies the necessity to know the orientation of the reciprocal lattice axes relative to the diffractometer reference axes. This can be achieved by searching a predetermined θ range for reflections and then deducing the orientation of the reciprocal unit-cell from the measured ϕ, χ, and θ of the recorded reflections. If the components of the reciprocal lattice vector $\mathbf{a}^*$ along the diffractometer reference axes X, Y, Z are a^*_X, a^*_Y, a^*_Z, the components of $\mathbf{b}^*$ are b^*_X, b^*_Y, b^*_Z, and the components of $\mathbf{c}^*$ are c^*_X, c^*_Y, c^*_Z, then the coordinates X, Y, Z of the *hkl* reciprocal lattice point are given by the operation of what is known as the *UB matrix* on the indices *hkl*

$$\begin{bmatrix} X \\ Y \\ Z \end{bmatrix} = \begin{bmatrix} a^*_X & b^*_X & c^*_X \\ a^*_Y & b^*_Y & c^*_Y \\ a^*_Z & b^*_Z & c^*_Z \end{bmatrix} \begin{bmatrix} h \\ k \\ l \end{bmatrix}$$

Since crystals usually reflect over a small range of θ and since it is the total intensity reaching the detector from a given reflection that is required, the crystal is rotated through the reflecting position about the ω–axis at constant speed. For accurate intensity measurements it is important both to set the limits of such a scan correctly for each reflection and to maintain the intensity of the incident beam at a constant magnitude within acceptable limits. The background intensity is estimated from measurements at the limits of the chosen ω–scan and subtracted from the peak measurements to yield the *net integrated intensity* of the reflection.

The χ–ring permits complete rotation of the crystal about the χ–axis, but its construction involves quite sophisticated engineering, which is expensive, and moreover, its thickness may inhibit the measurement of diffracted beams as well as restricting rotation on the ω–axis by the necessity to avoid collision with the collimator. In the so-called *kappa-axis diffractometer* an axis designated κ is inclined at 50° to the ω–axis and can be rotated about the ω–axis; the κ–axis substitutes for the χ–axis of the Eulerian four-circle diffractometer. In the kappa-axis diffractometer the ϕ–axis is mounted on an arm attached to the κ–axis so that it can be rotated on a small circle about the κ–axis. The whole ϕκ assembly can be rotated about the ω–axis. The kappa-axis diffractometer is in its engineering simpler than the Eulerian four-circle diffractometer and has the advantage that the X-ray reflection from any *hkl* plane can be recorded as the plane is rotated through 360° about its normal. Such an azimuthal scan may be utilised for making empirical absorption corrections to intensity measurements. With the Eulerian four-circle diffractometer, azimuthal scans are also possible, but are limited by the necessity to avoid collision of the χ-ring with the collimator and by the obstruction of the diffracted beam by the χ-ring.

Diffractometer practice.

As has already been indicated, most modern diffractometers are computer controlled and many software routines have been implemented to facilitate the tasks of the operator. With these routines the operator, having centered the crystal on the diffractometer, could:

- Search through a region of space and use the reflections to determine an orientation matrix and unit cell.
- Transfrom the cell if necessary.
- Identify reflections to be used as position and intensity controls.
- Set up a procedure for automatically collecting the data.

Data reduction

Once the *net integrated intensity*, I_{hkl}, of a Bragg reflection has been measured, it must be corrected by some factors that take into account the relative length of time the crystal was in the diffracting position, the extent of polarization of the X-ray beam and the absorption of X-rays by the crystal. This may be done by the following equation :

$$F^2_{hkl} = I_{hkl}(KLpA)^{-1}$$

where F_{hkl} is the structure amplitude, The Lorentz factor, L, takes into consideration how long each set of lattice planes was in the diffracting position, and depends on the technique used for data collection. The polarization factor, p, originates from the fact that the variation of the reflection efficiency of X-rays with the scattering angle depends on the polarization status of the incident beam. The transmission factor, A, takes into account the reduction of the intensity due to absorption of the X-rays by the crystal. It may be computed geometrically from path lengths in a crystal of known shape and size or estimated by measuring the variation in intensity of a reflection as the crystal is rotated about the scattering vector.

2.7 Structure solution

From the equation

$$\rho(x,y,z) = \frac{1}{V}\sum_h\sum_k\sum_l F_{hkl}\, e^{-2\pi i\,(hx+ky+lz)}$$

where V is the cell volume and F_{hkl} the structure factor for a particular set of indices h, k and l, the electron density distribution throughout the unit cell may be obtained, provided that both the magnitudes and the phases of the structure factors are known. As has already been seen the magnitudes of the structure factors may readily be derived from the intensities of the diffracted X-ray beams. Unfortunately the relative phases cannot be determined experimentally, which represents one of the main obstacles that have to be overcome during the course of a structure analysis. This situation as been called the "phase problem" within crystallographic circles.

Therefore a vital aspect of any X-ray structure determination is the determination of a set of phases which corresponds to a trial structure which is chemically meaningful. Some of the main techniques that have been developed with the aim of accomplishing this initial structure solution will now briefly be considered.

Trial and error methods

A tentative atomic arrangement is found in some way and the phase angles are calculated from the coordinates in the model. A number of arrangements can be tested systematically; the correct model is usually identified by comparing the observed and calculated structure amplitudes. This method was the one used originally but is not used much any longer, unless the structure is extremely simple.

Direct methods

The electron density must be positive or zero but never negative since electrons are never less than absent. This requirement, together with the information that there are peaks at atomic positions but that elsewhere the map is fairly flat (near zero), implies that there are mathematical constraints on possible phase angles (Karle and

Hauptman; 1950). The best set of phases may be found by 'direct methods'. In these methods the phases are chosen to give the least negative electron-density map. The simplest case is that of centrosymmetric structures, where the phase problem reduces to that of determining the sign of each A_{hkl}. For example, for three intense reflections with indices *hkl*, *h'k'l'* and *h+h',k+k',l+l'*, the signs of the respective A terms in the structure factor expression are related by the following equation

$$s(hkl) \times s(h'k'l') \approx s(h+h', k+k', l+l')$$

where *s* means 'sign of' (ie. + or -) and ≈ means 'probably equal to' and stresses the importance of the probability aspects of these equations. If two of these signs (phases) are known, it is possible to derive the third. From such relationships it is often possible to derive phases for almost all intense Bragg reflections. Since it is these intense Bragg reflections that dominate the electron-density map, it is possible to obtain a good approximation to that map. Analogous methods are used for non- centrosymmetric structures.

For such analyses the structure amplitudes are normalised by removing the effects of fall-off of scattering with angle so that only the geometric component, E_{hkl}, is left. Usually only the highest *E* values are used; any intense high-θ reflections are thereby given high weight in the calculations that follow. An analysis of the statistical distribution of the *E* values will indicate whether the structure is centrosymmetric or non-centrosymmetric. The triple products among high *E* values, that is any triplets with indices *hkl*, *h'k'l'*, and *h+h',k+k',l+l'* are found and, after fixing the phases of some origin determining reflections, the signs of as many *E* values as possible are developed from triple products of the type listed above and probability formulae. Usually there are several sets that satisfy the truncated data set so used. Often it is possible to identify the correct set on the basis of the probability associated with sign relationships. Otherwise several electron-density maps (computed from *E* values) may have to be calculated and searched for reasonable geometry of peak positions.

Patterson and heavy atom methods

If one or a few atoms in a structure have high atomic numbers and therefore dominate the scattering, the structure determination may be simplified by first finding the positions of these few atoms. The method for doing this is to calculate a *Patterson function* (Patterson, 1934, 1935), which uses the squares of the amplitudes of the diffracted beams and a cosine function

$$P(u,v,w) = \frac{1}{V}\sum_h\sum_k\sum_l F_{hkl}^2 \cos[2\pi(hu + kv + lw)]$$

When compared with the equation for the electron density distribution in the unit cell, two main differences become apparent. The structure factors are squared and there are no phase terms in the equation. Thus this equation may be evaluated directly from the experimental data. Peaks in the Patterson map can be shown to represent vectors between atoms; the height of the peak being proportional to the product of the atomic numbers of the two atoms at the ends of the vector. So, a Patterson map for a unit cell containing N atoms will contain about N^2 peaks, however, if one or two atoms have high atomic numbers the vectors between them will be very high and will dominate the map. Therefore, if the space group of a crystal is known, then the positions of the heavy atoms within the unit cell can be determined.

Isomorphous replacement

Isomorphous compounds are isostructural and capable of forming solid solutions. In the method of isomorphous replacement , differences in intensities from crystals of isostructural compounds differing only in the identity of one atom is measured. The varying atom, usually a heavy atom, is located by Patterson methods, and from this phases may be derived if the structure is centrosymmetric. Otherwise more isomorphs must be studied. This method of solving the phase problem is of great value in protein crystallography (Blundell and Johnson; 1976), but is only occasionally applied to small molecules.

2.8 Structure refinement

In general, just after the structure has been solved, the calculated diffraction pattern does not agree optimally with that obtained experimentally. It is also quite feasible that the trial structure obtained during the solution is not yet complete or contains some structural anomalies. These situations may be resolved by the use of least-squares refinement and difference Fourier methods.

In essence, the least-squares process involves the adjusting of a scale factor and the positional and displacement parameters of the atoms in the unit cell so as to obtain the best agreement between the experimental $|F_o|$ and the calculated $|F_c|$ quantities derived from the structure model. In its most usual application, the technique minimizes the function.

$$R = \sum_h w(|F_o| - G|F_c|)^2$$

where the sum is taken over the entire set of crystallographically independent terms h, w is the weight for each term, and G is the reciprocal of the scale factor K for $|F_c|$. Let p_j ($j = 1,2,....n$) be the variables in $|F_c|$ whose values are to be refined. Then

$$\frac{\delta R}{\delta p_j} = 0$$

or

$$\sum_h w\Delta\frac{\delta|F_c|}{\delta p_j} = 0$$

where Δ is $|F_o| - |F_c|$. For a trial set of parameters not too different from the correct values, Δ is expanded as a Taylor series to the first order:

$$\Delta(\mathbf{p} + \xi) = \Delta(\mathbf{p}) - \sum_{j=1}^{n} \xi_j \frac{\delta|F_c|}{\delta p_j}$$

where the shift ξ_i is the correction to be applied to parameter p_i and $\mathbf{p}$ and ξ represent the complete sets of variables and corrections. Substituting back leads to the normal equations

$$\sum_{i=1}^{n}\left[\sum_{\mathbf{h}} w\frac{\delta|F_o|}{\delta p_i}\frac{\delta|F_o|}{\delta p_j}\right]\xi_i = \sum_{\mathbf{h}} w\Delta\frac{\delta|F_o|}{\delta p_j}$$

The *n* normal equations may be expressed neatly in matrix form:

$$A\xi = \mathbf{b} \text{ or } \sum_i a_{ij}\xi_i = b_j$$

where

$$a_{ij} = \sum_{\mathbf{h}} w\frac{\delta|F_o|}{\delta p_i}\frac{\delta|F_c|}{\delta p_j}$$

and

$$b_j = \sum_{\mathbf{h}} w\Delta\frac{\delta|F_o|}{\delta p_j}$$

The normal equations are solved by standard mathematical procedures. It is important to remember that the least-squares procedure provides the best fit for the parameters that have been included into the model. Hence, it is essential to examine the final difference Fourier map at the completion of a least-squares refinement, after several cycles of calculations have led to negligible differences ξ_i.

If the Fourier series with $|F_o|$ coefficients is represented as $\rho_o(x, y, z)$ and the corresponding synthesis with $|F_c|$ as $\rho_c(x, y, z)$, then the difference-Fourier synthesis $\Delta\rho(x, y, z)$ may be obtained in a single-stage calculation from the equation

$$\Delta\rho(x,y,z) = \frac{2}{V_o}\sum_h\sum_k\sum_l (|F_o| - |F_c|)\cos[2\pi(hx + ky + lz) - \alpha_c]$$

Since the phases are substantially correct at this stage of the structure determination, it is in effect, a subtraction, point by point, of the 'calculated' or trial

Fourier synthesis from that of the 'observed' or experimentally based synthesis. This map should be featureless, as any peaks or troughs could indicate errors in the structure model used for the refinement.

The agreement between the scaled observed and the calculated structure-factor amplitudes may also be evaluated by means of a reliability factor. An overall reliability factor (R-factor) may be defined as:

$$R = \left(\sum_{hkl} |K|F_o| - |F_c|| \right) / \sum_{hkl} K|F_o|$$

For a well-refined structure model, the value of R approaches a small value (about 1% at best) corresponding to the errors in both the experimental data and the model. Another useful index used in structure refinement is the so called 'goodness of fit' where:

$$S = \left[\frac{\Sigma\, w(|F_o| - |F_c|)^2}{n - m} \right]^{\frac{1}{2}}$$

for n refinable parameters and m observations, w is the weight factor associated with each structure amplitude. S is a measure of the degree to which the found distribution of differences between $|F_o|$ and $|F_c|$ fits the distribution expected from the weights used in the refinement. If these weights are correct, which implies that the errors in the data are strictly random and correctly estimated, and if the model properly represents the structure that gives rise to the data, the value of S is 1.0.

The very weak reflections in an X-ray diffraction data set have relatively large errors and those for which the background exceeds the peak will have negative net intensities. They are undefined and cannot, therefore, be used when refining against $|F_o|$. It is customary to eliminate the very weak reflections by use of a threshold, that is, reflections with intensities less than some positive threshold value such as $2\sigma(I)$ are given zero weight. The use of any threshold, however, introduces a bias in the data and is indefensible in principle; it is therefore much better to refine against $|F_o|^2$ so that all data can be included. Accordingly the function

$$R' = \sum_{hkl} w_{hkl}\left(|F_o|^2 - |kF_c|^2\right)^2$$

is minimised. This again leads to a set of normal equations as seen before, as well as related reliability factors etc.

When comparing refined structures it is important to note what parameters were used in the refinement as well as the criteria used to evaluate the refinement.

2.9 Geometrical parameters

Following a crystallographic analysis, the atomic positions within the unit cell are normally expressed in terms of fractional coordinates. To interpret and compare molecular structures chemically, it is useful to describe the structure in terms of bond lengths, bond angles, torsion angles etc. Relations used to calculate the geometrical parameters include:

Bond Lengths:

In the triclinic case, the distance between two points in fractional coordinates (x_1, y_1, z_1) and (x_2, y_2, z_2) is given by the law of cosines in three dimension,

$$l = \left\{ \begin{array}{c} (\Delta x a)^2 + (\Delta y b)^2 + (\Delta z c)^2 - 2ab\Delta x\Delta y\cos\gamma \\ -2ac\Delta x\Delta z\cos\beta - 2bc\Delta y\Delta z\cos\alpha \end{array} \right\}^{\frac{1}{2}}$$

where a, b, c, α, β, γ are the unit-cell parameters.

Bond angles:

The angle θ subtended by bonds *AB* and *AC* (Figure 2.8) can be calculated in various ways. If the lengths *AB*, *AC* and *BC* are known, then the law of cosines provides a direct means of computing the angle

$$\theta = \cos^{-1}\left[\frac{(AB)^2 + (AC)^2 - (BC)^2}{2(AB)(AC)}\right]$$

If the axes of the unit cell are orthogonal, the angle can be calculated from the direction cosines of the line segments *AB* and *AC*

$$\theta = \cos^{-1}(l_1 l_2 + m_1 m_2 + n_1 n_2)$$

where l_1, m_1, n_1 are the direction cosines of *AB* and l_2, m_2, n_2 are the direction cosines of *AC*.

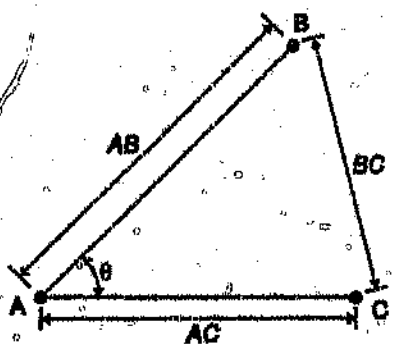


Figure 2.8: Bond angles

Torsion angles

For a sequence of four atoms A, B, C, D, the torsion angle ω(ABCD) is defined as the angle between the normals to the planes ABC and BCD (see Figure 2.9). By convention (Klyne and Prelog; 1960) ω is positive if the sense of rotation from BA to CD, viewed down BC, is clockwise, otherwise it is negative. From this definition and Figure 2.9 it can be shown that

$$\omega = \sin^{-1}\left(\frac{Vb}{ab^2c\,\sin\alpha\,\sin\gamma}\right)$$

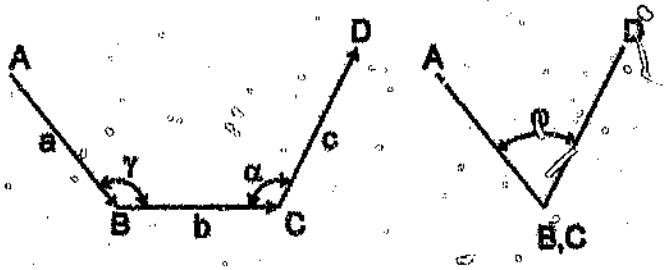


Figure 2.9 : Definition of the torsion angle ω

Mean planes

In discussing the geometry of a molecule, it may be desirable to test the planarity of a group of atoms. This is best done by fitting a least-squares plane through the atoms of interest, where a least-squares plane is that plane which minimises the function $\sum_m d_m^2$, where d_m are the perpendicular distances of the m atoms from the plane. The calculations involved in determining this plane have been illustrated by Schomaker *et al* in 1959.

Puckering parameters

A large number of compounds contain cyclic fragments and it is insightful to compare the observed conformations of these rings with the known preferred conformations of such rings. By using puckering parameters this comparison may be made quantitatively. These puckering parameters stem from the generalisation, in terms of cartesian coordinates, by Cremer and Pople (1975) of the expression derived by Kilpatrick and others in 1947, to describe the out-of-plane displacement of the j^{th} atom, perpendicular to the mean plane of a monocyclic ring. In general the N-3 puckering parameters derivable for an N membered ring consists of puckering amplitudes and phase angles. The puckering amplitudes relate to the extent of puckering while the phase angles refer to the nature of the puckering.

2.10 Graphical representation of structures

Following a small molecule crystallographic analysis, the results are generally represented in some graphical from. This is because a large amount of chemically meaningful information may be conveyed using a single picture. The exact nature of the representation will depend on the information that needs to be conveyed. Frequently, small molecules are represented in terms of ball-and-stick or ORTEP diagrams. These diagrams are mostly used to disseminate details about the molecular conformations as well as the numbering scheme employed. The latter having the advantage in that it also includes a representation of the anisotropic displacement of atoms about their mean positions. On the other hand, packing

diagrams can be used to show intermolecular interactions such as hydrogren bonding, or to illustrate some interesting packing features exhibited by the molecule. Lastly, various Fourier maps may be used to show interesting features, found in the electron density distribution within the molecule.

CHAPTER 3

Cryostat design, construction and testing

3.1 Introduction

As discussed earlier in this thesis, it is highly desirable to collect single-crystal diffraction data at low temperatures. To accomplish this a number of cryostats have been designed and built. A number are also available from commercial instrument manufacturers and suppliers.

In general cryostats suitable for use in the collection of 3-dimensional single-crystal diffraction data may be classified according to the presence of any windows though which the beam of X-rays have to travel as well as the cryogen used.

Liquid helium (LHe) cryostats generally contain windows (usually Be) to seperate the cold chamber from the room temperature enviroment. This reduces the precision of the diffractometer by absorption and parasitic x-ray scattering. This is the configuration generally encountered with continuous flow cryostats (Coppens *et al*, 1974; Albertsson *et al*, 1979) with flexible, low-loss transfer lines. In recent years, closed-cycle refrigerators or Displexes have also been used in designing cryostats for single-crystal diffraction studies (Hendriksen *et al*, 1986). The lower running cost of these designs make them particularly attractive for long term experiments. An alternative design, exemplified by that of Greubel *et al*, 1990, does not make use of any windows or a cold chamber, instead it employs the gas-flow principle also used in most liquid-nitrogen (LN2) cryostats. Examples of such cryostats include the Open Nitrogen Jet LT708 marketed by Oxford Instruments and the Liquid Nitrogen Cryostat manufactured by Enraf Nonius.

A gas flow cryostat operates on the principle of blowing a stream of cold gas over the crystal to be studied. To minimize condensation the cold stream is enveloped in a concentric stream of warmer gas (see Figure 3.1).

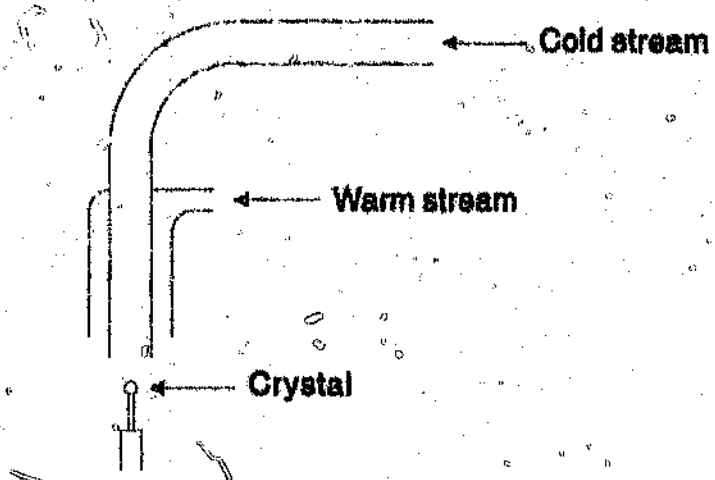


Figure 3.1:Gas flow cryostat nozzle

Considerable difficulty was experienced using an earlier version of the Nonius cryostat that operates on this principle. In this design, shown schematically in Figure 3.2, the cold and warm stream of gas is generated by evaporating the nitrogen in boiling units. The cold stream is then kept cold until it reaches the crystal in a silvered glass Dewar tube. The warm stream is warmed to approximately room temperature and conveyed to the nozzle of the cryostat by a piece of plastic tubing. The main problems were traced to the sensing of the cryogen level in the transfer Dewar. Transfers from the supply Dewar did not take place reliably resulting in an inability to keep the level of cryogen relatively constant. On at least two occasions this resulted in damages to the heating elements of the transfer Dewar. Problems were also experienced with the temperature stability as the cryostat had no facility for controlling the temperature. On speaking to other users of this and more recent models from Nonius, similar problems were reported. It was thus decided to extensively modify the cryostat.

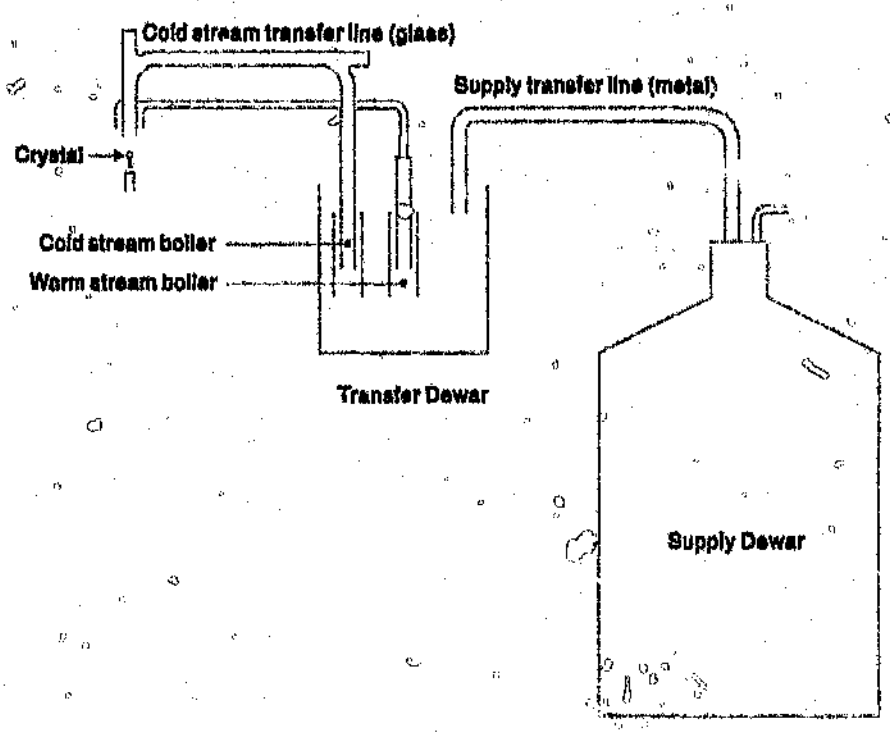


Figure 3.2 : Schematic diagram of Nonius cryostat

3.2 Modification concepts/criteria

In the original cryostat the level of the cryogen in the transfer Dewar was sensed by thermistors, that is resistors with a large negative temperature coefficient. Thus when submersed in LN2 they have an infinitely high resistance. Unfortunately repeated cooling to such low temperatures cause irreversible changes in the characteristics of the thermistors. Also they often cannot withstand the mechanical stresses placed on them and they break in two. The behaviour of thermocouples are well known and they have been widely used in cryogenics for the measuring of low temperatures. Thus it was decided that they could be used for the sensing of the cryogen levels. For the recording of the EMF's produced by the thermocouples, as well as the necessary decision making, it was decided to use a personal computer. This would allow for the greatest versatility in the recording and control necessary. Using a computer also allows for a number of possible future expansions. Level sensors were included in the supply Dewar to give an indication of the rate at which LN2 was consumed and to decide when next to refill the supply Dewar.

3.3 Prototype construction

To test these concepts a prototype was designed, built and tested. Copper-constantan thermocouples were installed in the cryostat as shown in Figure 3.3.

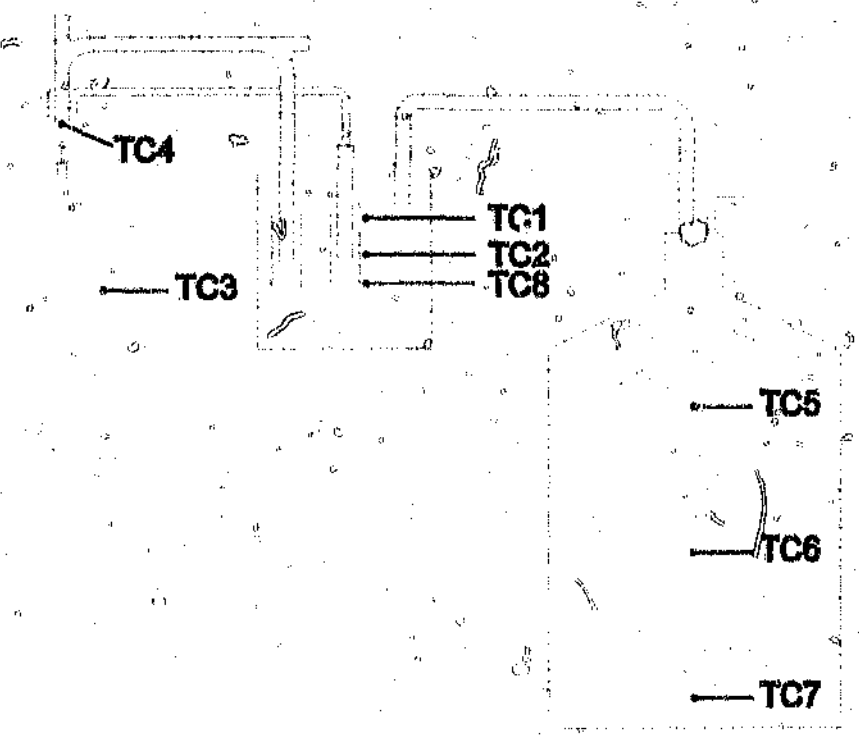


Figure 3.3: Thermocouple placements

All these thermocouples allowed for the monitoring of the cryogen levels in both the transfer and the supply Dewars, as well as the temperature of the cold stream near the crystal. Also included is a safety device which is used to sense the possibility of the system running out of cryogen. The thermocouples were connected to operational amplifiers which amplified the signals before sending it to a 12 bit A/D converter installed in an XT computer. The A/D convertor stores the EMF's from the thermocouples in specific memory locations within the computer from where they may be accessed by a control program. Control of additional electrical devices is also achieved via the A/D convertor. The basic logic required for the control of the

cryostat is depicted in the flow-diagram shown in Figure 3.4, and was implemented in the form of a BASIC program

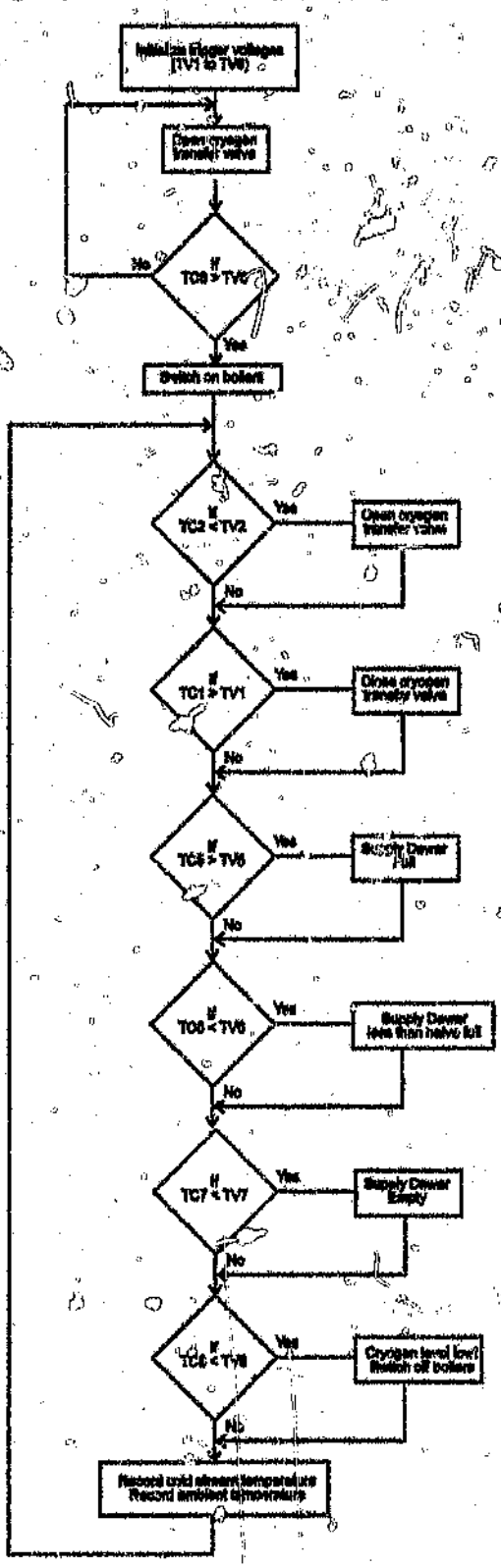


Figure 3.4: Flow-diagram of the logic operations of the cryostat

3.4 Discussion and conclusion

Initial testing of the prototype showed that even without the use of any temperature control facilities, temperature stabilities of the order of one degree could be achieved. The cryostat was then used to collect approximately five data sets, including those of ***17*** and ***18*** in this thesis. During these data collections the cryostat remained operational for extended periods of time. Overall, it could be concluded that this design overcomes the problems experienced prior to modification and holds promise of being both reliable and user friendly. Further improvements and expansions could include the addition of a temperature control facility. This could be accomplished by including a heating coil in the cold stream, and then controlling the power supplied to it from the computer. This would improve the temperature stability of the cryostat and also facilitate the choice of the temperature at which the analysis is done. This would greatly facilitate the study of different phases and phase transitions.

CHAPTER 4

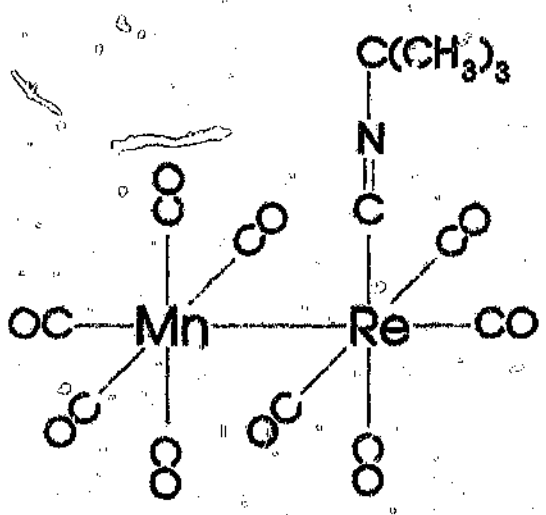
The metal-metal bond length in MnRe dimers

4.1 Introduction

While performing routine investigations into the structures of organometallic compunds, a value of 2.96Å was obtained for the Mn-Re bond length in ***1***, ($MnRe(CO)_9(CNBu^t)$). Although this analysis was based on relatively poor data, this value appeared "normal" because:

i. The value lay halfway between the reported metal-metal bond lengths for $Mn_2(CO)_{10}$ [2.9038(6)Å (Churchill *et al*; 1981), 2.895(1)Å (Martin *et al*; 1982)] and $Re_2(CO)_{10}$ [3.0413( )Å (Churchill *et al*; 1981)]

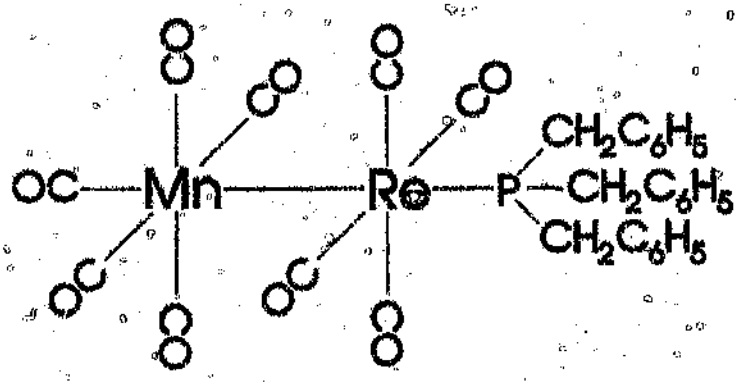
ii. An X-ray structure determination of $MnRe(CO)_{10}$ gave the value as 2.96Å (Struchkov *et al*; 1967).



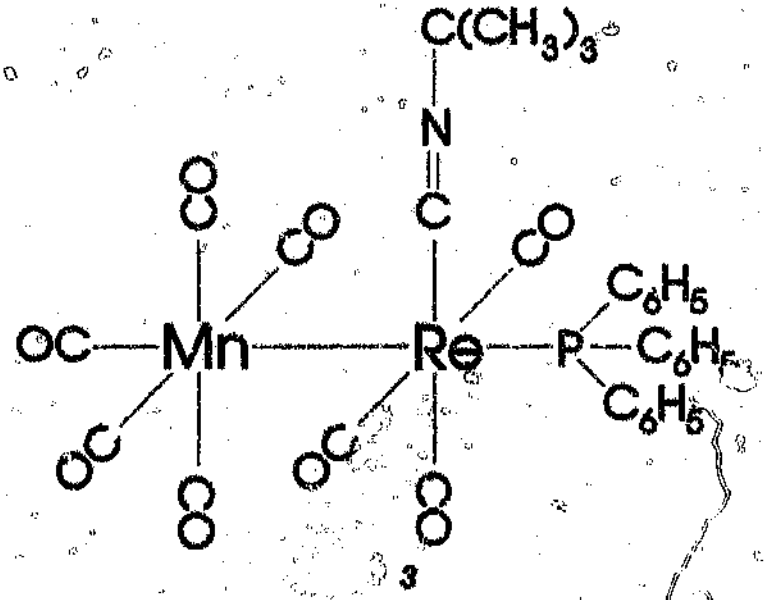
1

When the structure was, however, redetermined to correct for certain errors made in the assignment of the spacegroup (Rheingold *et al*; 1986) the authors reported a shorter bond length of 2.909(1)Å, a value nearly identical to the Mn-Mn bond length in $Mn_2(CO)_{10}$. This redetermined value suggests that the bond lengths of heteronuclear dimers may not be related in any intuitive manner to the bond lengths in the homonuclear dimers.

To obtain further information on the metal-metal bond length in heteronuclear MnRe dimers, it was decided to also determine the structures of the two related compounds ***2*** and ***3***. Because of the variety of substituents involved it should also be possible to assess the influence of different steric and electronic effects on the Mn-Re bond length.



2



3

4.2 Crystallographic analysis

Crystals of ***1***, ***2*** and ***3*** for analyses were grown from acetone/hexane solutions and suitable specimens mounted on glass fibres for the study. Cell determinations, using 25 high-order reflections, and data collections were done on Enraf-Nonius CAD4 four-circle diffractometers equipped with graphite monochromators. Crystals of ***1*** decayed excessively in the X-ray beam when using Mo-Kα radiation, and had to be collected using less energetic Cu-Kα radiation. Data reduction included corrections for Lorentz, polarization and background effects. Crystal decay was corrected linearly for compounds ***1*** and ***2*** , while a fifth-order polynomial was used for compound ***3***. Empirical absorption corrections (North *et al; 1968*) were applied to the intensity data of compounds ***1*** and ***2***. Analytical absorption corrections, calculated by the ABSORP routine of the NRCVAX set of programs were applied to the intensity data of compound ***3***. This routine requires that the faces of the crystals be indexed and measured. It then uses this information to calculate the necessary corrections by a Gaussian integration method.

Unit-cell parameters and details of the data collections are given in Table 4.1. Atomic coordinates for the structures are listed in Table 4.2, Table 4.3 and Table 4.4 respectively. The structures were solved using Patterson and difference-Fourier techniques, and refined by least-squares based on F^2. Hydrogen atom positions were generated geometrically and refined in riding mode in the final cycles of refinement. The SHELX suite of programs were used for structure solution and refinement.

Table 4.1 : Crystal and refinement data

Compound	***1***	***2***	***3***
Empirical formula	$C_{14}H_6MnNO_8Re$	$C_{30}H_{21}MnO_8PRe$	$C_{31}H_{24}MnNO_8PRe$
Formula weight / g.mol^{-1}	576.36	797.58	810.62
Wavelength/Å	1.5418	0.7107	0.7107
Crystal system	Monoclinic	Triclinic	Monoclinic
Space group	P $2_1/n$	P-1	P $2_1/c$
a/Å	12.0303(7)	12.314(7)	17.841(3)
b/Å	20.8343(8)	14.306(10)	9.615(2)
c/Å	15.2223(13)	19.198(6)	20.505(4)

α/°	-	68.40(5)	-
β/°	91.683(6)	78.39(4)	113.150(10)
γ/°	-	88.98(4)	-
Volume/Å^3	3813.7(4)	3074(5)	3234.6(11)
Z	8	4	4
ρ/ Mg.m^{-3}	2.008	1.723	1.665
Absorption coefficient/mm^{-1}	18.035	4 447	4.227
F(000)	2176	1552	1584
Range	3.60≤θ≤64.95	3≤θ≤23	2.5≤θ≤30
Index ranges : h k l	 -14→14 0→24 0→17	 -13→13 -14→15 0→15	 -22→20 0→12 0→26
Reflections collected	6450	6325	7025
Independent reflections	6190	6325	7025
Data/restraints/parameters	6190/0/461	6325/0/430	7025/0/389
Max shift, Δz	0	0.001	0
Residual density / e.Å^{-3} $(\Delta\rho)_{max}$ $(\Delta\rho)_{min}$	 4.026 -3.335	 1.295 -1.429	 1.1859 -0.623
Reliability indices R1 (I > 2σ(I)) wR2 (I > 2σ(I)) R1 (all data) wR2 (all data)	 0.069 0.175 0.081 0.180	 0.048 0.122 0.065 0.128	 0.034 0.083 0.064 0.087
S	1.047	1.065	0.95

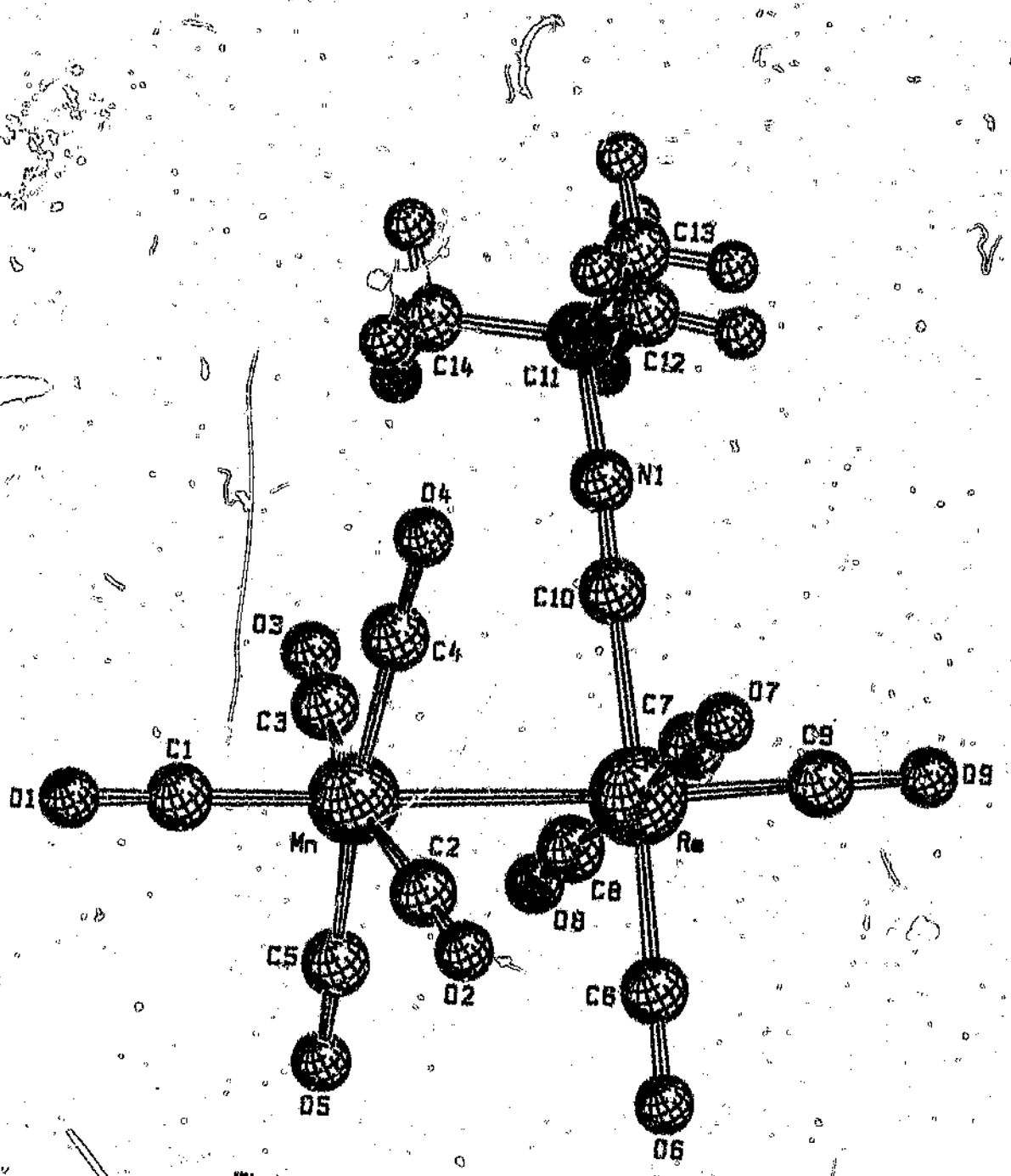


Figure 4.1: Labelled Schakal diagram of *1*

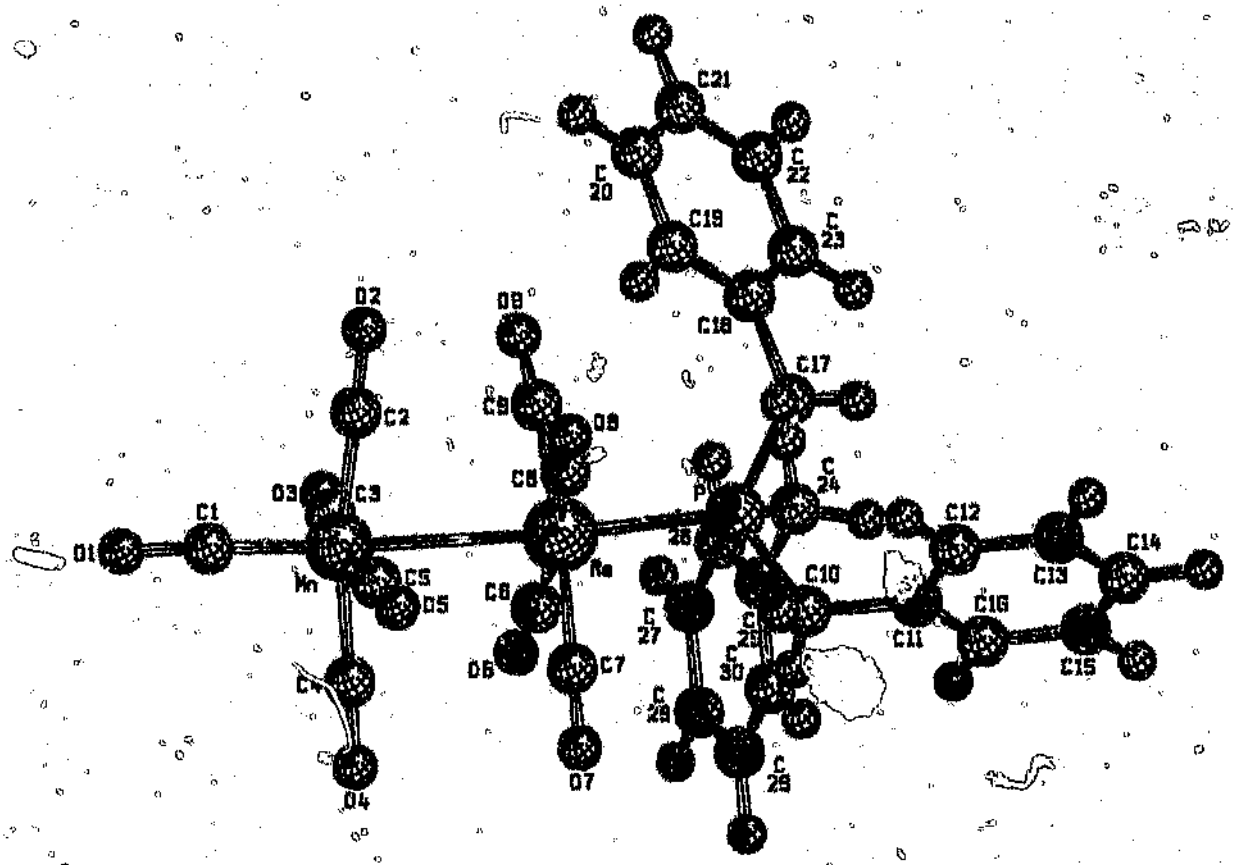


Figure 4.2: Labelled Schakal diagram of *2*

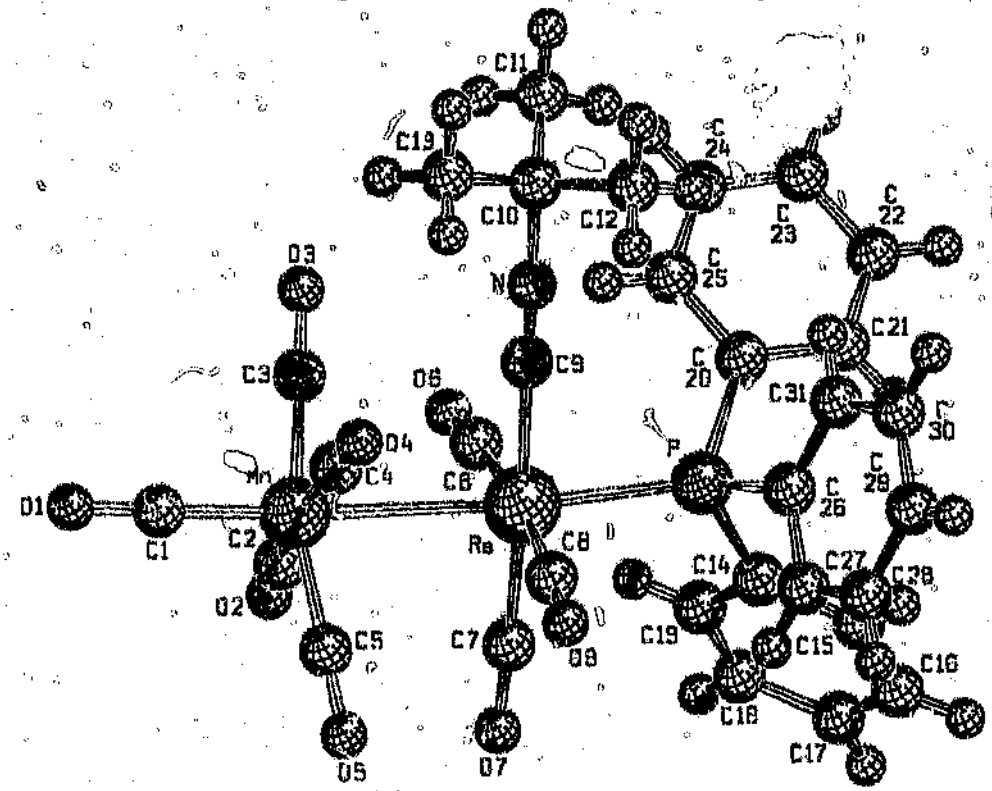


Figure 4.3: Labelled Schakal diagram of *3*

Table 4.2: Atomic coordinates (x 10^4) and equivalent isotropic displacement parameters ($Å^2$, x10^3) for *1*

	x/a	y/b	z/c	U_{eq}
Mn(A)	3083(1)	-3454(1)	1288(1)	41(1)
Re(A)	1895(1)	-4252(1)	2557(1)	38(1)
O(1A)	4236(10)	-2671(7)	-27(8)	111(4)
O(2A)	4252(9)	-2938(5)	2883(6)	86(3)
O(3A)	1560(8)	-4141(5)	-11(7)	70(2)
O(4A)	4685(9)	-4541(6)	1224(10)	103(4)
O(5A)	1309(8)	-2488(5)	1491(8)	90(3)
O(6A)	1541(10)	-3054(4)	3743(7)	82(3)
O(7A)	4172(8)	-4510(6)	3519(9)	93(4)
O(8A)	-296(7)	-3884(5)	1572(6)	66(2)
O(9A)	732(8)	-5134(4)	3823(6)	66(2)
N(1A)	2230(7)	-5462(4)	1280(6)	45(2)
C(1A)	3771(11)	-2981(7)	471(10)	66(4)
C(2A)	3793(10)	-3139(6)	2260(11)	60(3)
C(3A)	2152(9)	-3880(6)	465(9)	51(3)
C(4A)	4038(12)	-4124(7)	1222(11)	70(4)
C(5A)	1951(10)	-2846(6)	1413(9)	57(3)
C(6A)	1677(9)	-3494(6)	3303(7)	48(3)
C(7A)	3356(10)	-4430(6)	3157(9)	54(3)
C(8A)	501(8)	-4025(5)	1910(7)	41(2)
C(9A)	1171(9)	-4806(5)	3349(7)	41(2)
C(10A)	2121(8)	-5036(5)	1716(7)	41(2)
C(11A)	2365(10)	-6002(5)	663(8)	49(3)
C(12A)	1316(19)	-6374(10)	620(17)	133(9)
C(13A)	3301(17)	-6398(9)	979(14)	120(9)
C(14A)	2583(16)	-5707(8)	230(12)	101(6)
Mn(B)	1277(1)	-3520(1)	6984(1)	34(1)
Re(B)	3703(1)	-3778(1)	6947(1)	37(1)
O(1B)	-1155(7)	-3382(5)	6881(8)	83(3)
O(2B)	1668(9)	-2913(5)	8731(6)	75(3)
O(3B)	1291(8)	-4127(5)	5219(6)	66(2)
O(4B)	1189(7)	-4766(4)	7875(6)	63(2)
O(5B)	1786(10)	-2264(4)	6157(8)	89(3)
O(6B)	4115(8)	-2407(5)	7685(6)	73(3)
O(7B)	3641(9)	-4272(5)	8867(7)	72(3)
O(8B)	3692(9)	-3284(6)	5035(7)	86(3)
O(9B)	6197(7)	-4045(4)	6899(7)	63(2)
N(1B)	3066(7)	-5208(5)	6306(6)	46(2)
C(1B)	-206(9)	-3432(5)	6950(8)	47(2)
C(2B)	1512(10)	-3141(5)	8080(9)	51(3)
C(3B)	1314(10)	-3907(5)	5911(9)	49(3)

C(4B)	1226(9)	-4303(5)	7504(8)	45(3)
C(5B)	1611(9)	-2757(6)	6472(8)	50(3)
C(6B)	3968(10)	-2908(5)	7382(9)	57(3)
C(7B)	3643(8)	-4105(5)	8154(8)	45(3)
C(8B)	3697(9)	-3454(6)	5735(9)	53(3)
C(9B)	5243(8)	-3930(5)	6903(7)	42(2)
C(10B)	3308(9)	-4700(5)	6533(8)	46(3)
C(11B)	2745(9)	-5860(5)	6142(9)	52(3)
C(12B)	1477(13)	-5098(7)	5955(13)	89(5)
C(13B)	3372(19)	-6051(10)	5300(14)	118(8)
C(14B)	3020(16)	-6237(7)	6944(13)	97(6)

Table 4.3 : Atomic coordinates (x 10^4) and equivalent isotropic displacement parameters ($Å^2$, x10^3) for 2

	x/a	y/b	z/c	U_{eq}
Re(A)	2265(1)	1607(1)	1215(1)	43(1)
Mn(A)	1442(1)	-358(1)	1279(1)	42(1)
P(A)	2737(2)	3220(2)	1166(2)	42(1)
O(1A)	682(7)	-2284(7)	1259(5)	78(3)
O(2A)	-7(8)	912(7)	287(6)	82(3)
O(3A)	3296(9)	-53(7)	-56(6)	78(3)
O(4A)	2844(8)	-1318(7)	2402(6)	80(3)
O(5A)	-186(8)	-358(7)	2649(6)	82(3)
O(6A)	4626(6)	795(6)	949(5)	68(3)
O(7A)	2269(6)	593(7)	2948(6)	76(3)
O(8A)	-218(8)	2003(7)	1633(6)	82(3)
O(9A)	2482(9)	2373(7)	-554(6)	79(3)
C(1A)	959(10)	-1510(9)	1267(7)	58(3)
C(2A)	576(10)	435(9)	653(7)	56(3)
C(3A)	2591(11)	-154(9)	457(9)	58(4)
C(4A)	2350(10)	-935(8)	1947(8)	50(3)
C(5A)	417(10)	-342(9)	2123(9)	54(3)
C(6A)	3795(10)	1138(8)	1024(7)	48(3)
C(7A)	2259(10)	966(8)	2314(9)	51(3)
C(8A)	683(10)	1856(8)	1477(8)	55(3)
C(9A)	2357(9)	2127(8)	90(9)	52(4)
C(10A)	2636(10)	3258(8)	2132(7)	49(3)
C(12A)	1817(6)	4760(7)	2322(6)	80(2)
C(13A)	1909(6)	5694(6)	2386(6)	80(2)
C(14A)	2950(6)	6110(5)	2339(6)	80(6)
C(15A)	3898(6)	5592(7)	2227(6)	80(2)
C(16A)	3807(6)	4658(7)	2162(6)	80(2)
C(11A)	2765(6)	4242(5)	2210(6)	80(2)

C(17A)	1802(9)	4221(8)	805(6)	46(3)
C(19A)	702(7)	3978(6)	-112(5)	79(2)
C(20A)	540(6)	4188(7)	-852(6)	79(2)
C(21A)	1284(6)	4856(7)	-1480(4)	79(2)
C(22A)	2189(7)	5314(6)	-1359(5)	79(2)
C(23A)	2351(6)	5105(7)	-629(6)	79(2)
C(18A)	1607(8)	4437(7)	0(4)	79(2)
C(24A)	4061(8)	3858(8)	-607(7)	49(3)
C(26A)	5898(6)	3193(6)	-42(4)	66(1)
C(27A)	6664(6)	2668(6)	-47(4)	66(1)
C(28A)	7042(5)	2205(6)	631(5)	66(1)
C(29A)	6455(6)	2266(6)	1313(4)	66(1)
C(30A)	5489(6)	2790(6)	1317(4)	66(1)
C(25A)	5110(5)	3254(6)	640(5)	66(1)
Re(B)	3131(1)	2150(1)	6234(1)	51(1)
Mn(B)	4129(1)	1853(1)	7574(1)	46(1)
P(B)	2093(2)	2458(2)	5273(2)	49(1)
O(1B)	5181(9)	1655(8)	6867(6)	92(3)
O(2B)	3032(9)	3703(8)	7589(6)	96(3)
O(3B)	5924(10)	3196(9)	6396(7)	116(4)
O(4B)	5136(9)	96(8)	7267(7)	100(4)
O(5B)	2118(10)	541(8)	8549(7)	105(3)
O(6B)	5405(9)	1691(10)	5410(6)	116(5)
O(7B)	2662(8)	-180(7)	6870(7)	89(3)
O(8B)	1043(8)	2306(7)	7382(6)	85(3)
O(9B)	3903(8)	4404(8)	5634(7)	92(3)
C(1B)	-4741(12)	-1714(10)	1827(9)	67(4)
C(2B)	-3430(11)	-2990(11)	2405(11)	68(4)
C(3B)	5206(13)	2647(12)	6864(9)	85(4)
C(4B)	-4755(11)	-771(11)	2609(8)	65(4)
C(5B)	2903(12)	1067(11)	8148(9)	78(4)
C(6B)	4586(12)	1887(11)	5669(8)	72(4)
C(7B)	2810(10)	676(11)	6634(8)	64(4)
C(8B)	1801(10)	2262(9)	6939(8)	53(3)
C(9B)	3594(10)	3597(11)	5854(8)	59(3)
C(10B)	905(10)	3245(9)	5332(8)	61(4)
C(12B)	1563(9)	5068(8)	4691(5)	96(2)
C(13B)	1810(8)	5993(7)	4731(5)	96(2)
C(14B)	1607(9)	6102(8)	5438(7)	96(2)
C(15B)	1157(9)	5287(8)	6105(5)	96(2)
C(16B)	910(8)	4362(7)	6065(5)	96(2)
C(11B)	1113(9)	4253(8)	5359(7)	96(2)
C(17B)	1420(10)	1301(9)	5308(8)	61(4)
C(19B)	609(8)	1531(7)	4153(6)	84(2)

C(30B)	-305(8)	1551(7)	3822(4)	84(2)
C(21B)	-1377(7)	1390(7)	4270(6)	84(2)
C(22B)	-1536(6)	1210(7)	5050(5)	94(2)
C(23B)	-822(8)	1190(7)	5382(4)	84(2)
C(18B)	450(7)	1351(7)	4933(6)	84(2)
C(24B)	2770(10)	3107(10)	4281(7)	83(4)
C(26B)	4835(8)	3510(6)	3864(6)	83(2)
C(27B)	5889(7)	3298(6)	3570(6)	83(2)
C(28B)	6057(6)	2433(7)	3397(6)	83(2)
C(29B)	5149(8)	1781(6)	3518(6)	83(2)
C(30B)	4084(7)	1993(6)	3812(6)	83(2)
C(25B)	3927(6)	2858(7)	3986(6)	83(2)

Table 4.4 : Atomic coordinates (x 10^4) and equivalent isotropic displacement parameters ($Å^2$, x10^3) for *3*

	x/a	y/b	z/c	U_{eq}
Re	7381(1)	3779(1)	1933(1)	43(1)
Mn	6261(1)	2476(1)	591(1)	53(1)
P	8209(1)	4728(1)	3052(1)	46(1)
N	6769(3)	1451(4)	2739(2)	57(1)
O(1)	5045(3)	1261(5)	-715(3	104(2)
O(2)	5934(3)	5412(5)	68(3)	94(1)
O(3)	5096(2)	2666(5)	1304(2)	79(1)
O(4)	6849(3)	-270(4)	1281(3)	83(1)
O(5)	7712(2)	2481(5)	211(2)	90(1)
O(6)	5998(3)	5944(4)	1699(3)	89(1)
O(7)	8005(3)	5663(5)	1041(2)	94(1)
O(8)	8685(2)	1677(4)	1906(2)	78(1)
C(1)	5528(3)	1730(7)	-207(3)	69(2)
C(2)	6058(3)	4308(8)	285(3)	68(2)
C(3)	5547(3)	2620(6)	1037(3)	60(1)
C(4)	8823(3)	781(7)	1032(3)	62(1)
C(5)	7151(3)	2499(6)	356(3)	64(1)
C(6)	8498(3)	5127(6)	1800(3)	60(1)
C(7)	7771(3)	4993(6)	1388(3)	59(1)
C(8)	8212(3)	2438(5)	1933(3)	54(1)
C(9)	6967(3)	2302(5)	2448(2)	47(1)
C(10)	6482(4)	403(6)	3105(3)	84(1)
C(11)	5932(6)	1082(8)	3386(5)	131(4)
C(12)	7215(6)	-115(11)	3701(6)	160(4)
C(13)	6109(8)	-735(9)	2834(5)	182(6)
C(14)	8742(3)	6359(5)	3045(3)	51(1)
C(15)	9531(3)	6663(6)	3503(3)	65(1)

C(16)	9870(4)	7931(7)	3485(4)	75(2)
C(17)	9441(5)	8904(7)	3017(5)	96(2)
C(18)	8652(5)	8859(8)	2554(5)	102(2)
C(19)	8311(4)	7865(6)	2574(4)	79(2)
C(20)	7714(3)	5229(5)	3654(3)	52(1)
C(21)	8150(3)	5904(7)	4282(3)	75(2)
C(22)	7777(4)	6354(7)	4723(4)	83(2)
C(23)	6964(4)	6122(6)	4539(4)	79(2)
C(24)	6525(4)	5443(6)	3919(3)	72(2)
C(25)	6897(3)	4985(6)	3485(3)	61(1)
C(26)	9026(3)	3594(5)	3592(3)	53(1)
C(27)	9871(3)	3336(6)	3386(3)	64(1)
C(28)	10286(4)	2418(7)	3765(4)	81(2)
C(29)	10269(5)	1731(8)	4326(5)	99(2)
C(30)	9644(5)	1932(7)	4537(4)	91(2)
C(31)	9014(4)	2852(6)	4166(3)	75(2)

4.3 Results and Discussion

Compound ***1*** was synthesised from $MnRe(CO)_{10}$ and ^tBuNC using PdO as a catalyst, while compound ***2*** was synthesised from $MnRe(CO)_{10}$ and $P(CH_2C_6H_5)_3$. Compound ***3*** was obtained from the reaction of ***1*** with PPh_3. As can be seen in Figures 4.1 to 4.3, the crystal structure determination of the three complexes ***1*** - ***3*** reveal that substitution had taken place at the Re atom in every instance.

Selected bond length and bond angle data are given in Table 4.5. From the data the following conclusions can be drawn:

i. The Mn-Re bond lengths are all close to 2.96Å. This value is little affected by axial, equatorial or axial-equatorial substitution patterns.

ii. There are no bridging carbonyl groups. The ligands on the metal atoms are in a staggered arrangement with C-Mn-Re-C torsion angles in the range 45±5° for all three structures.

iii. Typical M-CO bond lengths are observed; ie., M-C(O) bonds that are *cis* to the Mn-Re bond and *trans* to a CO group are longer than M-C(O) bonds that are *trans* to a M-M bond or the ^tBuNC group.

iv. The position of the ligands in the coordination sphere is that expected from the steric/electronic properties of ^{t}BuNC and the phosphine ligand.

Table 4.5 : Selected bond lengths (Å)

	1		*2*		*3*
	A	B	A	B	
Mn-Re	2.959(2)	2.970(2)	2.956(2)	2.959(2)	2.9683(9)
Mn-C(1)	1.796(14)	1.792(11)	1.772(12)	1.79(2)	1.794(6)
Mn-C(2)	1.85(2)	1.832(13)	1.828(12)	1.838(14)	1.858(7)
Mn-C(3)	1.845(14)	1.824(13)	1.83(2)	1.76(2)	1.841(5)
Mn-C(4)	1.826(13)	1.815(11)	1.829(14)	1.83(2)	1.852(7)
Mn-C(5)	1.859(12)	1.819(12)	1.85(2)	1.80(2)	1.832(5)
Re-C(6)	1.968(13)	1.952(11)	1.998(12)	2.005(14)	1.974(6)
Re-C(7)	1.991(12)	1.964(12)	1.96(2)	1.98(2)	1.926(5)
Re-C(8)	1.977(9)	1.963(13)	1.972(13)	1.949(14)	1.969(5)
Re-C(9)	1.899(11)	1.883(11)	1.99(2)	1.98(2)	2.070(5)
Re-C(10)	2.098(11)	2.072(11)	-	-	-
C(10)-N(1)	1.117(13)	1.148(14)	-	-	-
Re-P	-	-	2.353(3)	2.359(3)	2.3691(13)

The crystallographic data indicates that in this case the M-M bond lengths give little information about the position or degree of subsititution on the dimers. Although it has been shown that bond lengthening can take place as steric crowding increases, the amount of steric crowding in complexes *1 - 3* is minimal. This of course provides strong evidence for a bond length of ±2.96Å for $MnRe(CO)_{10}$ as originally observed. (Struchkov *et al*; 1967) It should be noted that difficulties were experienced by Rheingold and co-workers in analyzing the $MnRe(CO)_{10}$ data (Rheingold *et al*; 1986). They dealt with the disorder associated with the Mn and Re positions by four different strategies, all giving a Mn-Re bond length of approximately 2.91 Å. No disorder was observed in our investigations, primarily because substitution had only taken place on the Re atom. Our data suggests that their bond length should be treated with caution.

CHAPTER 5

Bonding in heterapentalene type compounds

5.1 Introduction

If pentalene were to be reduced according to the scheme in figure 5.1 the product would be expected to have a planar aromatic structure.

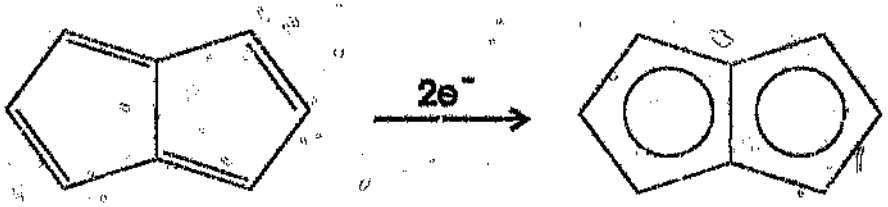


Figure 5.1 : Reduction of pentalene

Hypothetically this reduction could be achieved by replacing some of the carbon atoms in the pentalene framework by other atoms. The first structure of this nature reported was that of thio-thiophen, (Figure 5.2) [Bezzi *et al*; 1958] which was obtained by treating diacetyl-acetone with phosphorus pentasulphide.

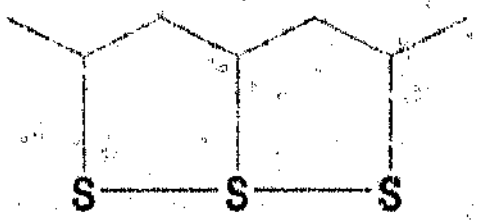


Figure 5.2 : Thio-thiophen

Bezzi *et al* reported the structure to be characterised by no-bond resonance which conferred upon it an aromatic character. The electronic structure of this compound was soon investigated [Giacometti *et al*; 1959] and this led to the structure being described in terms of the resonance hybrid between four structures (Figure 5.3) [Mammi *et al*; 1960]. When considering the stabilization of centers with six valence electrons through electron-rich three-center bonding, Gleiter and Hoffmann (1968), suggested that thio-thiophthene contains an electron rich three-center bond. This

bond being further stabilised by the fact that all three atoms form part of a π-electron system.

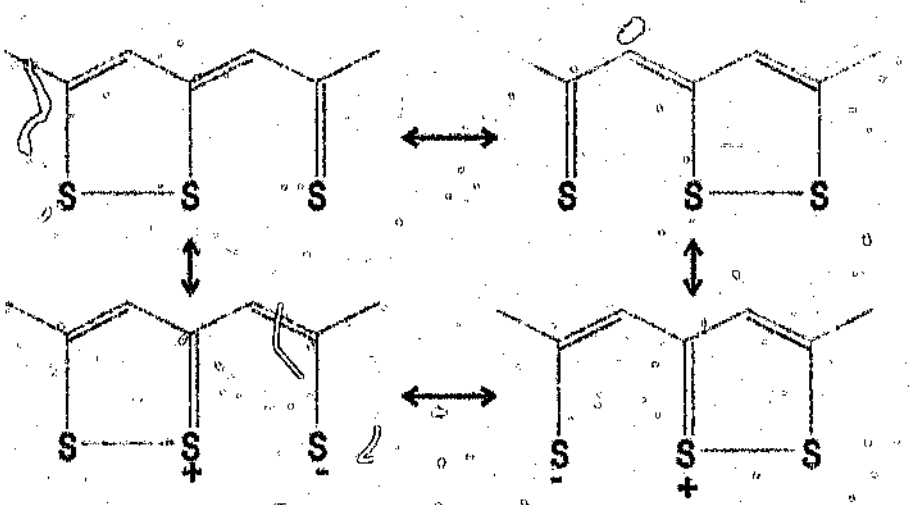


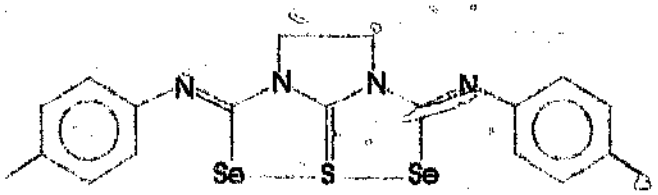
Figure 5.3 : Resonance scheme for thio-thiophen

Subsequent to this, a number of the structures of related molecules have been determined. These structures differed from thio-thiophen in substituents as well as the type and number of heteroatoms in the pentalene framework. All exhibited the linear tri-atomic sequence that is characteristic of this group of molecules.

Our interest in these structures started from collaboration with Reid and co-workers to characterize a number of reaction products, which, based on previous experience and NMR evidence, were expected to contain heterapentalene frameworks. We report here the results of these structural analyses. It also became clear that the nature of the bonding in these compounds is still not well understood and that no simple predictive method existed for predicting bond lengths in these compounds. Finally a clearer understanding was sought by comparing a number of new structures, with known structures from the literature. To facilitate this comparison, the bond order of each of the bonds in the pentalene framework was needed in order to compare structures containing different atom types.

5.2 Crystal structure of 5,6-Dihydro-1,4-bis-p-tolylimino-2aλ^4-thia-2,3, diselena-4a,6a-diazacyclopent[cd]pentalene.

The title compound ***4*** crystallises in the triclinic system and contains two molecules, A and B in the asymetric unit. These molecules differ conformationally in terms of the orientation of the aromatic rings relative to the rest of the molecule. Both molecules exhibit the characteristic structural features of heterapentalenes, with long Se-S bonds and wide Se-S-Se bond angle. All other bond lengths in the heterapentalene framework are intermediate between those of single and double bonds.



4

The Se-S bond lengths in molecule A, 2.5044(12)Å and 2.5309(12)Å, are greater by 14.1 and 15.3% respectively than (two-centre two-electron) covalent Se-S single bond lengths [2.195(15)Å, Allen *et al*;1987]. The Se-S bonds in molecule B are 2.5007(14)Å and 2.5639(14)Å in length and thus longer that the Se-S bond (2.195Å) by 13.9 and 16.8% respectively. The lengths of the corresponding bonds and the size of the corresponding bond angles in the two halves of the triheterapentalene framework in A and B are very similar, differing from one another by at most 0.063 Å and 1.42° respectively.

Compound ***4*** crystallized from dichloromethane-acetonitrile (1:3), as red needle-shaped crystals, m.p. 458-460K (decomposition). Cell determination, using 25 high-order reflections, and data collection were done on an Enraf-Nonius CAD4 four-circle diffractometer equipped with a graphite monochromator. Data reduction included correction for Lorentz and polarisation effects using standard Enraf Nonius routines, and absorption effects were corrected for empirically (North *et al; 1968*). Three standard reflections monitored every hour showed only random fluctuations. Unit cell parameters and details of the data collection are given in Table 5.1. The

structure was solved by direct methods using SHELXS[9] and refined using SHELXL93. All non-H atoms were refined with anisotropic displacement parameters. H atoms were placed geometrically in the final cycles of refinement and allowed to refine with a common isotropic displacement parameter.Figure 5.4 shows a labelled SCHAKAL diagram of the molecule and indicates the atomic numbering scheme used. Atomic coordinates and selected bond lengths are listed in Table 5.2 and Table 5.3 respectively. The selected torsion angles listed in Table 5.4 illustrate the conformational differences between the two molecules in the assymetric unit.

Table 5.1: Crystal and refinement data	
Compound	**4**
Empirical formula	$C_{18}H_{18}N_4SSe_2$
Formula weight / g.mol^{-1}	492.35
Temperature/K	295
Wavelength/Å	0.71069
Crystal system	Triclinic
Space group	P-1
a/Å	12.428(2)
b/Å	13.423(6)
c/Å	13.069(2)
α/°	112.35(2)
β/°	109.19(2)
γ/°	94.81(2)
Volume/Å^3	1934.0(10)
Z	4
ρ/ Mg.m^{-3}	1.691
Absorption coefficient/mm^{-1}	3.942
F(000)	976
Crystal size/mm^3	0.2 x 0.5 x 1.0
Range	3≤θ≤30
Index ranges : h k l	 0→17 -16→18 -19→12
Reflections collected	7999
Independent reflections	7784

R_{int}	0.018
Data/restraints/parameters	7784/0/473
Max shift, Δz	0.029
Residual density / e.Å^{-3}	
$(\Delta\rho)_{max}$	1.46
$(\Delta\rho)_{min}$	-1.200
Reliability indices	
R1 (I > 2σ(I))	0.052
wR2 (I > 2σ(I))	0.133
R1 (all data)	0.116
wR2 (all data)	0.145
S	0.922

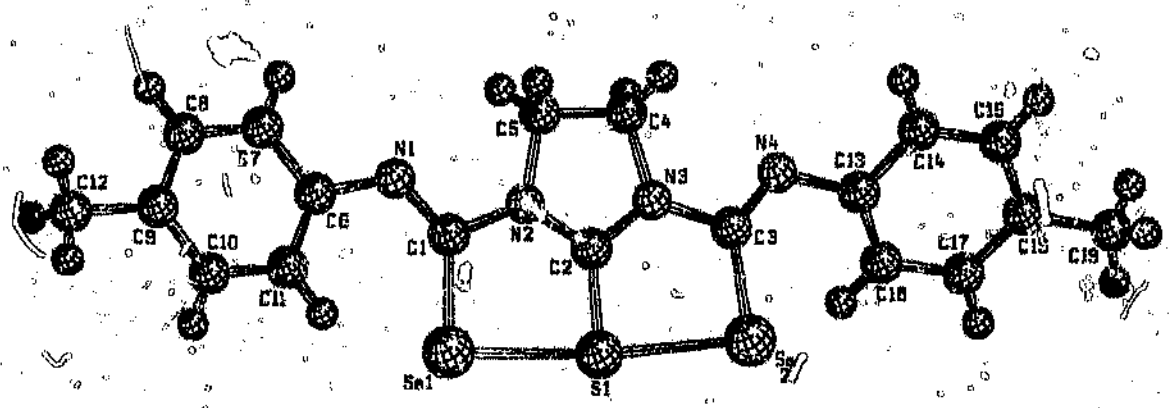


Figure 5.4: Labelled Schakal diagram of *4*

Table 5.2: Atomic coordinates (x 10^4) and equivalent isotropic displacement parameters (Å^2 , x 10^3) for *4*.

	x/a	y/b	z/c	U_{eq}
Se(1A)	4714(1)	2361(1)	4962(1)	56(1)
Se(2A)	6486(1)	2106(1)	2081(1)	52(1)
S(1A)	5637(1)	2341(1)	3562(1)	45(1)
N(1A)	3486(4)	96(3)	4252(3)	44(1)
N(2A)	4620(3)	352(3)	3329(3)	37(1)
N(3A)	5545(3)	240(3)	2196(3)	36(1)
N(4A)	6503(4)	-210(3)	995(3)	42(1)
C(1A)	4155(4)	813(4)	4174(4)	39(1)
C(2A)	5253(4)	921(3)	3020(4)	35(1)
C(3A)	6223(4)	573(4)	1674(4)	37(1)
C(4A)	5090(5)	-926(4)	1598(4)	48(1)

C(5A)	4365(5)	-858(4)	2818(4)	46(1)
C(6A)	2888(4)	350(4)	5003(4)	46(1)
C(7A)	2392(5)	-522(4)	5107(5)	61(2)
C(8A)	1748(5)	-386(5)	5799(5)	66(2)
C(9A)	1574(5)	631(5)	6377(5)	57(2)
C(10A)	2093(7)	1515(6)	6286(6)	87(2)
C(11A)	2730(7)	1383(5)	5607(6)	84(2)
C(12A)	868(6)	765(6)	7117(6)	84(2)
C(13A)	7185(4)	0(4)	413(4)	40(1)
C(14A)	6880(4)	-783(4)	-715(4)	41(1)
C(15A)	7512(5)	-664(4)	-1348(4)	49(1)
C(16A)	8471(5)	218(5)	-871(4)	49(1)
C(17A)	8787(5)	965(5)	261(5)	58(2)
C(18A)	8169(4)	847(4)	909(4)	48(1)
C(19A)	9153(6)	385(6)	-1657(5)	75(2)
Se(1B)	6294(1)	5296(1)	6040(1)	53(1)
Se(2B)	3305(1)	5021(1)	7766(1)	55(1)
S(1B)	4739(1)	5113(1)	6798(1)	45(1)
N(1B)	8475(4)	6661(4)	7952(3)	51(1)
N(2B)	6903(4)	6312(3)	8393(3)	43(1)
N(3B)	5599(4)	6207(3)	9123(3)	42(1)
N(4B)	4542(4)	6432(3)	10222(3)	43(1)
C(1B)	7401(5)	6177(4)	7576(4)	44(1)
C(2B)	5794(4)	5910(4)	8164(4)	36(1)
C(3B)	4507(4)	5971(4)	9205(4)	42(1)
C(4B)	6665(5)	6302(5)	10143(4)	49(1)
C(5B)	7604(5)	6873(5)	9633(4)	52(1)
C(6B)	9000(5)	6592(4)	7155(4)	52(1)
C(7B)	9978(5)	6176(5)	7208(5)	60(2)
C(8B)	10540(6)	6170(5)	6497(5)	68(2)
C(9B)	10150(6)	6591(5)	5710(6)	70(2)
C(10B)	9176(7)	7047(6)	5661(6)	80(2)
C(11B)	8599(6)	7031(6)	6382(6)	75(2)
C(12B)	10758(8)	6604(6)	4917(7)	98(3)
C(13B)	3554(4)	6366(4)	10511(4)	42(1)
C(14B)	3736(5)	6334(4)	11543(4)	49(1)

C(15B)	2845(6)	6330(4)	11934(5)	56(2)
C(16B)	1754(5)	6405(5)	11323(5)	58(2)
C(17B)	1582(6)	6473(5)	10291(5)	68(2)
C(18B)	2462(5)	6484(5)	9891(5)	61(2)
C(19B)	786(6)	6433(7)	11762(6)	93(2)

Table 5.3: Selected bond lengths (Å) for *4*

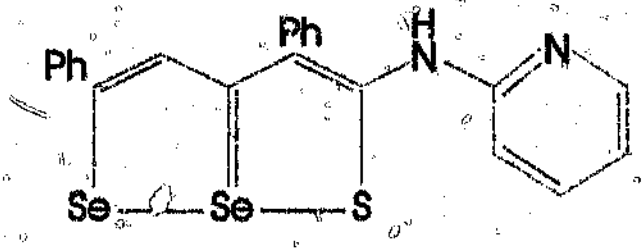
Se(1A)-C(1A)	1.877(5)	Se(1B)-C(1B)	1.900(5)
Se(1A)-S(1A)	2.5044(12)	Se(1B)-S(1B)	2.5007(14)
Se(2A)-C(3A)	1.884(5)	Se(2B)-C(3B)	1.889(5)
Se(2A)-S(1A)	2.5309(12)	Se(2B)-S(1B)	2.5639(14)
S(1A)-C(2A)	1.716(4)	S(1B)-C(2B)	1.728(5)
N(1A)-C(1A)	1.276(6)	N(1B)-C(1B)	1.262(6)
N(2A)-C(2A)	1.320(5)	N(2B)-C(2B)	1.323(6)
N(2A)-C(1A)	1.418(5)	N(2B)-C(1B)	1.407(6)
N(3A)-C(2A)	1.334(5)	N(3B)-C(2B)	1.329(5)
N(3A)-C(3A)	1.412(5)	N(3B)-C(3B)	1.417(6)
N(4A)-C(3A)	1.271(5)	N(4B)-C(3B)	1.272(6)

Table 5.4: Selected torsion angles (°) for *4*

C(7A)-N(1A)-C(6A)-C(7A)	-169.6(5)	C(1B)-N(1B)-C(6B)-C(7B)	-125.3(6)
C(1A)-N(1A)-C(6A)-C(11A)	13.4(9)	C(1B)-N(1B)-C(6B)-C(11B)	59.3(8)
C(3A)-N(4A)-C(13A)-C(14A)	44.6(7)	C(3B)-N(4B)-C(13B)-C(14B)	145.2(5)
C(3A)-N(4A)-C(13A)-C(18A)	-141.8(5)	C(3B)-N(4B)-C(13B)-C(18B)	-42.8(8)

5.3 Crystal structure of 3,5-Diphenyl-2,2'-pyridylamino-1-thia-6,6aλ^4-diselenapentalene.

The title compound **5** crystallises in the triclinic system and contains two independent molecules, A and B in the assymetric unit. These molecules differ conformationaly in terms of the orientation of the aromatic rings relative to the pentalene framework of the rest of the molecule. Both molecules exhibit the characteristic structural features of heterapentalenes, with long Se-Se and Se-S bonds and wide Se-Se-S bond angle. All other bond lengths in the heterapentalene framework are intermediate between those of single and double bonds.



5

The Se-Se and Se-S bond lengths in molecule A, 2.465(2)Å and 2.498(3)Å, are greater by 5.3% and 13.8% respectively than the (two-centre two-electron) covalent Se-Se and Se-S single bond lengths [2.195(15)Å and 2.340(24)Å, Allen *et al*, 1987]. The Se-Se and Se-S bonds in molecule B are 2.488(2)Å and 2.495(3)Å in length and thus greater than the Se-Se (2.340Å) and Se-S (2.195Å) by 6.3% and 13.7% respectively. The lengths of corresponding bonds and the size of the corresponding bond angles in molecule A and molecule B are very similar, differing from one another by at most 0.023Å and 0.9° respectively.

Compound **5** crystallized from cyclo-hexane, as red needle-shaped crystals, m.p. 482-483 K. Cell determination, using 25 high-order reflections, and data collection were done on an Enraf-Nonius CAD4 four-circle diffractometer equipped with a graphite monochromator. Data reduction included correction for Lorentz and polarisation effects using standard Enraf Nonius routines, and absorption effects were corrected for empirically (North *et al; 1968*). Three standard reflections monitored every hour showed only random fluctuations. Unit cell parameters and

details of the data collection are given in Table 5.5. The structure was solved by direct methods using SHELXS86 and refined using SHELXL93. All non-H atoms were refined with anisotropic displacement parameters. H atoms were placed geometrically in the final cycles of refinement and allowed to refine with a common isotropic displacement parameter. Figure 5.5 shows a labelled SCHAKAL diagram of the molecule and also indicates the numbering scheme used. Atomic coordinates and selected bond lengths are listed in Table 5.6 and Table 5.7 respectively. The selected torsion angles listed in Table 5.8 illustrate the conformational differences between the two molecules in the assymetric unit.

Table 5.5 : Crystal and refinement data	
Compound	*5*
Empirical formula	$C_{22}H_{16}N_2SSe_2$
Formula weight / g.mol^{-1}	498.35
Temperature/K	295(2)
Wavelength/Å	0.71069
Crystal system	Triclinic
Space group	P-1
a/Å	8.386(8)
b/Å	15.286(11)
c/Å	15.606(8)
α/°	94.57(4)
β/°	92.31(4)
γ/°	100.58(4)
Volume/Å^3	2004(3)
z	4
ρ / Mg.m^{-3}	1.652
Absorption coefficient/mm^{-1}	3.804
F(000)	984
Crystal size/mm^3	0.06 x 0.5 x 0.2
Range	2≤θ≤30
Index ranges : h k l	 -12→12 -21→21 -1→15
Reflections collected	11147

Independent reflections	9951
Data/restraints/parameters	9951/0/488
Max shift, Δz	0.007
Residual density / e.Å^{-3}	
$(\Delta\rho)_{max}$	-.733
$(\Delta\rho)_{min}$	0.512
Reliability indices	
R1 (I > 2σ(I))	0.055
wR2 (I > 2σ(I))	0.138
R1 (all data)	0.222
wR2 (all data)	0.158
S	0.895

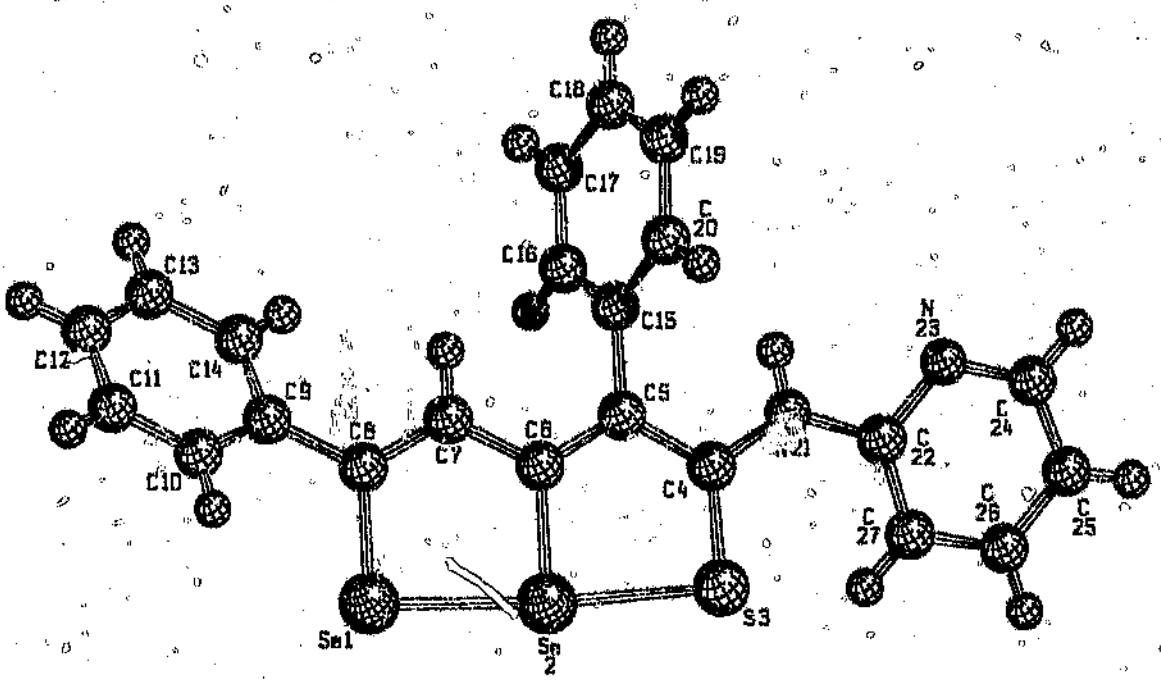


Figure 5.5 :Labelled Schakal diagram of ***5***

Table 5.6: Atom coordinates (x 10^4) and equivalent isotropic displacement parameters (Å^2 . x 10^3) for ***5***.

	x/a	y/b	z/c	U_{eq}
Se(1A)	4853(1)	-253(1)	2077(1)	65(1)
Se(2A)	6717(1)	1191(1)	2261(1)	50(1)
S(3A)	8539(2)	2668(1)	2273(1)	48(1)
C(4A)	7570(6)	2982(4)	1427(3)	38(1)
C(5A)	6144(7)	2423(4)	1061(3)	39(1)

C(6A)	5587(6)	1567(4)	1359(3)	34(1)
C(7A)	4228(6)	1001(4)	982(3)	37(1)
C(8A)	3714(7)	153(4)	1206(3)	35(1)
C(9A)	2337(6)	-474(3)	798(3)	36(1)
C(10A)	1409(7)	-1108(4)	1258(4)	49(2)
C(11A)	128(8)	-1683(4)	878(5)	57(2)
C(12A)	-255(8)	-1657(5)	22(5)	60(2)
C(13A)	604(7)	-1074(5)	-459(4)	54(2)
C(14A)	1893(7)	-483(4)	-68(4)	44(2)
C(15A)	5245(6)	2726(4)	337(3)	36(1)
C(16A)	5193(7)	2353(4)	-486(3)	43(2)
C(17A)	4361(7)	2653(5)	-1137(4)	56(2)
C(18A)	3630(7)	3357(5)	-975(4)	58(2)
C(19A)	3670(8)	3760(5)	-163(4)	59(2)
C(20A)	4454(7)	3442(4)	503(4)	46(2)
N(21A)	8086(6)	3764(3)	1068(3)	47(1)
C(22A)	9429(7)	4426(4)	1246(4)	46(2)
N(23A)	9228(7)	5200(4)	970(4)	60(2)
C(24A)	10458(10)	5859(5)	1086(5)	72(2)
C(25A)	11878(9)	5815(5)	1473(5)	68(2)
C(26A)	12084(8)	5019(6)	1726(4)	67(2)
C(27A)	10859(8)	4304(5)	1626(4)	58(2)
Se(1B)	-913(1)	-609(1)	2891(1)	59(1)
Se(2B)	1025(1)	785(1)	2726(1)	46(1)
S(3B)	2876(2)	2246(1)	2703(1)	50(1)
C(4B)	2171(7)	2700(4)	3589(3)	41(1)
C(5B)	873(7)	2215(4)	3991(3)	37(1)
C(6B)	226(6)	1325(4)	3590(3)	34(1)
C(7B)	-1041(6)	818(4)	4084(3)	39(1)
C(8B)	-1689(7)	-57(4)	3846(3)	37(1)
C(9B)	-2936(7)	-593(4)	4300(4)	38(1)
C(10B)	-3085(7)	-420(4)	5184(4)	42(2)
C(11B)	-4268(8)	-932(5)	5598(4)	56(2)
C(12B)	-5292(8)	-1616(5)	5154(5)	62(2)
C(13B)	-5164(8)	-1800(4)	4299(5)	60(2)
C(14B)	-4012(8)	-1308(4)	3874(4)	50(2)

C(15B)	219(6)	2668(4)	4747(3)	37(1)
C(16B)	407(7)	2423(4)	5557(4)	48(2)
C(17B)	-233(8)	2846(5)	6247(4)	66(2)
C(18B)	-1015(8)	3515(5)	6131(5)	61(2)
C(19B)	-1177(8)	3793(5)	5328(5)	64(2)
C(20B)	-590(7)	3359(4)	4624(4)	53(2)
N(21B)	2828(6)	3547(3)	3952(3)	54(1)
C(22B)	4085(7)	4167(4)	3732(4)	47(2)
N(23B)	3973(6)	5001(4)	4021(4)	59(2)
C(24B)	5169(10)	5545(5)	3882(5)	78(2)
C(25B)	6451(9)	5530(6)	3461(6)	83(2)
C(26B)	6596(9)	4691(6)	3185(5)	83(2)
C(27B)	5407(8)	3981(5)	3334(5)	70(2)

Table 5.7: Selected bond lengths (Å) for ***5***

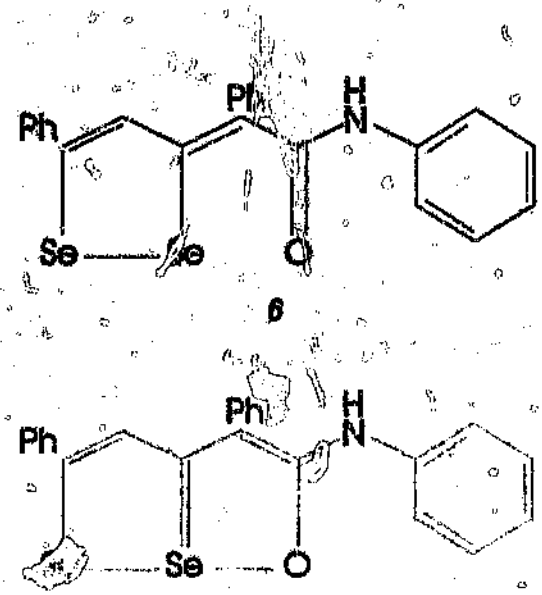
Se(1A)-Se(2A)	2.465(2)	Se(1B)-Se(2B)	2.488(2)
Se(1A)-C(6A)	1.854(5)	Se(1B)-C(6B)	1.861(5)
Se(2A)-C(6A)	1.879(5)	Se(2B)-C(6B)	1.873(5)
Se(2A)-S(3A)	2.496(3)	Se(2B)-S(3B)	2.495(3)
S(3A)-C(4A)	1.681(6)	S(3B)-C(4B)	1.682(6)
C(4A)-C(5A)	1.427(8)	C(4B)-C(5B)	1.417(8)
C(5A)-C(6A)	1.402(8)	C(5B)-C(6B)	1.408(8)
C(6A)-C(7A)	1.410(7)	C(6B)-C(7B)	1.409(8)
C(7A)-C(8A)	1.369(8)	C(7B)-C(8B)	1.366(8)

Table 5.8: Selected torsion angles (°) for ***5***

Se(1A)-C(6A)-C(9A)-C(10A)	32.8(7)	Se(1B)-C(6B)-C(9B)-C(10B)	150.1(4)
Se(1A)-C(6A)-C(9A)-C(14A)	-146.2(4)	Se(1B)-C(6B)-C(9B)-C(14B)	-29.0(7)
C(4A)-C(5A)-C(15A)-C(16A)	108.3(6)	C(4B)-C(5B)-C(15B)-C(16B)	-110.1(6)
C(4A)-C(5A)-C(15A)-C(20A)	-69.8(7)	C(4B)-C(5B)-C(15B)-C(20B)	69.3(7)
C(4A)-N(21A)-C(22A)-N(23A)	-158.2(6)	C(4B)-N(21B)-C(22B)-N(23B)	155.9(6)
C(4A)-N(21A)-C(22A)-C(27A)	25(1)	C(4B)-N(21B)-C(22B)-C(27B)	-

5.4 Crystal structure of N-Phenyl-2-phenyl-2-(5-phenyl-3H-1,2-diselenol-3-ylidine)acetamide,

The title compound **6** crystallises in the monoclinic system with one molecule in the asymmetric unit. Although the molecule contains a planar framework, and could be considered as the heterapentalene depicted in Figure 5.6, the Se-Se bond length of 2.3873(9)Å and the Se-O distance of 2.348 Å would seem to indicate that this structure should be considered to be monocyclic. As such the Se-Se bond length is only slightly longer that the covalent Se-Se bond length of 2.340(24)Å, (Allen *et al*; 1987).



6

Figure 5.6 : Possible heterapentalene equivalent to **6**

Compound **6** crystallised from a mixture of dichloromethane and hexane as orange crystals; m.p. 472-473K. Cell determination, using 25 high-order reflections, and data collection were done on an Enraf-Nonius CAD4 four-circle diffractometer equipped with a graphite monochromator. Data reduction included correction for Lorentz and polarisation effects using standard Enraf Nonius routines, and absorption effects were corrected for empirically (North *et al; 1968*). Three standard reflections monitored every hour showed an average decrease of 9.8% and this was corrected for linearly. Unit cell parameters and details of the data collection are given in Table 5.9. The structure was solved by direct methods using SHELXS86 and refined using SHELXL93 by least-squares methods, based on F^2. All non-H

atoms were refined with anisotropic displacement parameters. H atoms were placed geometrically in the final cycles of refinement and allowed to refine with a common isotropic displacement parameter. Figure 5.7 shows a labelled SCHAKAL diagram of the molecule and also indicates the numbering scheme used. Atomic coordinates and selected bond lengths are listed in Table 5.10 and Table 5.11 respectively.

Table 5.9: Crystal and refinement data	
Compound	**6**
Empirical formula	$C_{23}H_{17}NOSe_2$
Formula weight / g.mol^{-1}	481.3
Temperature/K	295(2)
Wavelength/Å	0.71069
Crystal system	Monoclinic
Space group	P $2_1/n$
a/Å	9.879(4)
b/Å	10.3395(8)
c/Å	19.346(6)
α/°	90
β/°	97.47(1)
γ/°	90
Volume/Å^3	1959.3(10)
z	4
ρ / Mg.m^{-3}	1.632
Absorption coefficient/mm^{-1}	3.786
F(000)	952
Crystal size/mm^3	0.1 x 0.2 x 0.3
Range	3≤θ≤30
Index ranges : h k l	 -13→13 -1→14 -1→27
Reflections collected	6772
Independent reflections	5693
R_{int}	0.058
Data/restraints/parameters	5693/0/245
Max shift, Δz	0
Residual density / e.Å^{-3} $(\Delta\rho)_{max}$ $(\Delta\rho)_{min}$	 0.813 -0.715

Reliability indices	
R1 (I > 2σ(I))	0.052
wR2 (I > 2σ(I))	0.102
R1 (all data)	0.206
wR2 (all data)	0.118
S	0.812

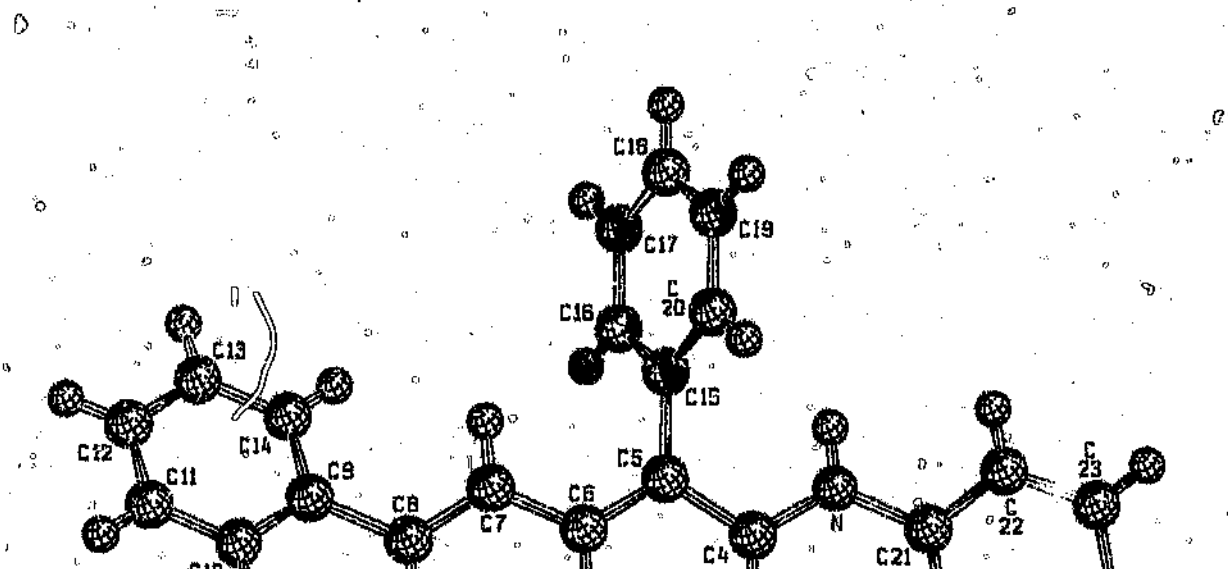


Figure 5.7 : Labelled Schakal diagram of *6*

Table 5.10: Atomic coordinates (x 10⁴) and equivalent isotropic displacement parameters (Å² x 10³) for *6*

	x/a	y/b	z/c	U_{eq}
Se(1)	2321(1)	1960(1)	-602(1)	55(1)
Se(2)	3757(1)	1289(1)	420(1)	47(1)
O(3)	4906(3)	211(3)	1398(2)	54(1)
C(4)	4455(4)	-908(4)	1387(2)	43(1)
C(5)	3462(4)	-1334(4)	806(2)	39(1)
C(6)	3012(4)	-419(4)	326(2)	36(1)
C(7)	2013(4)	-626(4)	-269(2)	39(1)
C(8)	1563(4)	305(4)	-736(2)	41(1)
C(9)	474(4)	108(5)	-1335(2)	46(1)
C(10)	441(5)	873(5)	-1938(2)	55(1)
C(11)	-580(6)	705(6)	-2479(2)	71(2)
C(12)	-1569(6)	-195(7)	-2438(3)	79(2)

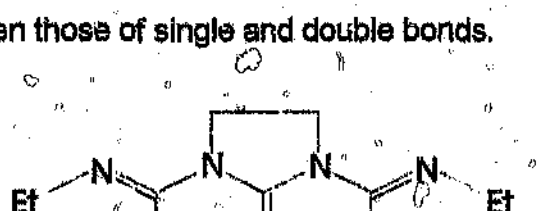
C(13)	-1554(5)	-943(6)	-1659(3)	88(2)
C(14)	-536(5)	-793(5)	-1300(2)	[illegible] (1)
C(15)	2907(4)	-2693(4)	758(2)	35(1)
C(16)	1617(4)	-2987(4)	805(2)	48(1)
C(17)	1155(5)	-4256(5)	753(2)	58(1)
C(18)	2020(6)	-5228(5)	658(2)	57(1)
C(19)	3357(5)	-4970(5)	611(2)	53(1)
C(20)	3826(4)	-3707(5)	652(2)	46(1)
N	4876(3)	-1770(3)	1896(2)	48(1)
C(21)	5891(4)	-1576(4)	2474(2)	40(1)
C(22)	6663(4)	-2617(5)	2709(2)	54(1)
C(23)	7647(5)	-2504(6)	3289(2)	62(1)
C(24)	7831(5)	-1347(6)	3627(3)	69(2)
C(25)	7045(6)	-319(6)	3401(3)	71(2)
C(26)	6072(5)	-413(5)	2815(3)	61(1)

Table 5.11: Selected bond lengths (Å) for 6

Se(1)-Se(2)	2.3877(9)
Se(1)-C(8)	1.872(4)
Se(2)-C(6)	1.894(4)
O(3)-C(4)	1.2[illegible]9(5)
C(4)-C(5)	1.461(6)
C(5)-C(6)	1.359(5)
C(6)-C(7)	1.432(5)
C(7)-C(8)	1.358(5)
Se(2)-O(3)	2.348

5.5 Crystal structure of 1,4-Bis(ethylimino)-5,6-dihydro-2,2aλ⁴,3-triselena-4a,6a-diazacyclopenta[cd]pentalene,

The title compound **7**, crystallises in the monoclinic crystal system and exhibits the characteristic structural features of heterapentalenes, with long Se-Se bonds and wide Se-Se-Se bond angle. All other bond lengths in the heterapentalene framework are intermediate between those of single and double bonds.



7

The Se-Se bond lengths in **7**, 2.5960(6)Å and 2.6560(6)Å are greater by 10.9% and 13.5% than the (two-centre two-electron) covalent Se-Se single bond length [2.340(24)Å, Allen *et al*, 1987]. The lengths of corresponding bonds and the size of corresponding bond angles in the two halves of the triheterapentalene framework are very similar, differing from one another by at most 0.06Å and 2.2° respectively.

Compound **7** crystallised from dichloromethane-hexane (1:3) as orange needle-shaped crystals; m.p. 448-451K. Cell determination, using 25 high-order reflections, and data collection were done on an Enraf-Nonius CAD4 four-circle diffractometer equipped with a graphite monochromator. Data reduction included correction for Lorentz and polarisation effects using standard Enraf Nonius routines, and absorption effects were corrected for empirically (North *et al; 1968*). Three standard reflections monitored every hour showed an average decrease of 2.8% and this was corrected for linearly. Unit cell parameters and details of the data collection are given in Table 5.12. The structure was solved by direct methods using SHELXS86 and refined using SHELXL93 by least-squares methods, based on F^2. All non-H atoms were refined with anisotropic displacement parameters. H atoms were placed geometrically in the final cycles of refinement and allowed to refine with a common isotropic displacement parameter. Figure 5.8 shows a labelled SCHAKAL

diagram of the molecule and also indicates the numbering scheme used. Atomic coordinates and selected bond lengths are listed in Table 5.13 and Table 5.14 respectively.

Table 5.12 : Crystal and refinement data	
Compound	**7**
Emprical formula	$C_9H_{14}N_4Se_3$
Formula weight / g.mol^{-1}	416.12
Temperature/K	295(2)
Wavelength/Å	0.71073
Crystal system	Monoclinic
Space group	P 2$_1$/a
a/Å	8.005(1)
b/Å	13.717(2)
c/Å	11.950(1)
α/°	90
β/°	93.42(1)
γ/°	90
Volume/Å^3	1309.8(3)
z	4
ρ / Mg.m^{-3}	2.105
Absorption coefficient/mm^{-1}	8.404
F(000)	792
Crystal size/mm^3	0.35 x 0.13 x 0.10
Range	2.3≤θ≤25
Index ranges ; h k l	 -9→9 0→16 -14→14
Reflections collected	4585
Independent reflections	2298
R_{int}	0.031
Data/restraints/parameters	2298/0/147
Max shift, Δz	0
Residual density / e.Å^{-3} $(\Delta\rho)_{max}$ $(\Delta\rho)_{min}$	 0.542 -0.441
Reliability indices R1 (I > 2σ(I)) wR2 (I > 2σ(I)) R1 (all data) wR2 (all data)	 0.026 0.059 0.052 0.063
S	0.977

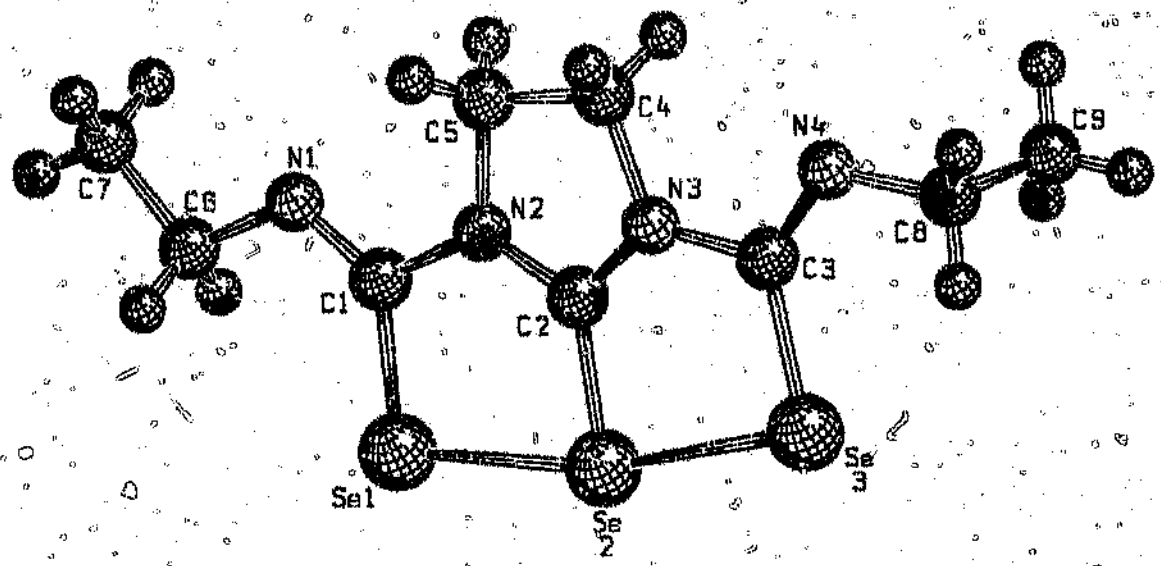


Figure 5.8: Labelled schakal diagram of **7**

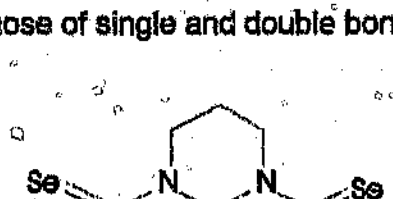
Table 5.13: Atomic coordinates (x 10^4) and equivalent isotropic displacement parameters ($Å^2$, x10^3) for **7**

	x/a	y/b	z/c	U_{eq}
Se(1)	268(1)	8446(1)	2022(1)	46(1)
Se(2)	1851(1)	8454(1)	3982(1)	37(1)
Se(3)	3445(1)	8048(1)	5940(1)	46(1)
N(1)	-151(4)	6486(2)	1212(3)	45(1)
N(2)	1086(3)	6641(2)	2961(2)	35(1)
N(3)	2456(3)	6476(2)	4590(2)	34(1)
N(4)	3558(4)	5968(2)	6265(2)	41(1)
C(1)	349(4)	7086(2)	1979(3)	36(1)
C(2)	1798(4)	7099(2)	3845(3)	31(1)
C(3)	3174(4)	6894(2)	5678(3)	36(1)
C(4)	2174(5)	5466(2)	4223(3)	41(1)
C(5)	1260(5)	5574(2)	3068(3)	44(1)
C(6)	-906(5)	6907(3)	175(3)	52(1)
C(7)	-1647(6)	6131(3)	-576(3)	70(1)
C(8)	4243(5)	6137(3)	7428(3)	50(1)
C(9)	291(5)	6012(3)	8245(3)	67(1)

Table 5.14: Selected bond lengths (Å) for 7	
Se(1)-Se(2)	2.5960(6)
Se(2)-Se(3)	2.6560(6)
Se(1)-C(1)	1.895(3)
Se(2)-C(2)	1.857(3)
Se(3)-C(3)	1.894(3)
N(2)-C(1)	1.408(4)
N(2)-C(2)	1.328(4)
N(3)-C(2)	1.321(4)
N(3)-C(3)	1.421(4)
N(1)-C(1)	1.261(2)
N(4)-C(3)	1.259(4)

5.6 Crystal structure of 2,3-Diethyl-6,7-dihydro-5H-2aλ⁴-selena-2,3, 4a,7a-tetraazacyclopent[cd]indene-1(2H),4(3H)-diselone.

The title compound ***8***, crystallises in the monoclinic crystal system, and exhibits the characteristic structural features of heterapentalenes, with long Se-N bonds and wide N-Se-N bond angle. All other bond lengths in the heterapentalene framework are intermediate between those of single and double bonds.



8

Compound ***8*** contains elongated Se-N bonds of length 2.030(5)Å and 2.042(5)Å which are greater by 8.6% and 9.2% respectively, than the two-centre two-electron Se-N covalent bond of length 1.87Å, based on the sum of the covalent radii of Se and N (Pauling; 1960). The lengths of corresponding bonds and the size of corresponding bond angles in the two halves of the triheterapentalene framework are very similar, differing from one another by at most 0.027Å and 1.2° respectively.

Compound ***8*** crystallised from dichloromethane-hexane (1:3) as yellow needle shaped crystals; m.p. 468-469K. Cell determination, using 25 high-order reflections, and data collection were done on an Enraf-Nonius CAD4 four-circle diffractometer equipped with a graphite monochromator. Data reduction included correction for Lorentz and polarisation effects using standard Enraf Nonius routines, and absorption effects were corrected for empirically (North *et al; 1968*). Three standard reflections monitored every hour showed only random fluctuations. Unit cell parameters and details of the data collection are given in Table 5.15. The structure was solved by direct methods using SHELXS86 and refined using SHELXL93 by least-squares methods, based on F^2. All non-H atoms were refined with anisotropic displacement parameters. H atoms were placed geometrically in the final cycles of

refinement and allowed to refine with a common isotropic displacement parameter. Figure 5.9 shows a labelled SCHAKAL diagram of the molecule and also indicates the numbering scheme used. Atomic coordinates and selected bond lengths are listed in Table 5.16 and Table 5.17 respectively.

Table 5.15: Crystal and refinement data	
Compound	8
Empirical formula	$C_{10}H_{16}N_4Se_2$
Formula weight / g.mol^{-1}	429.15
Temperature/K	293(2)
Wavelength/Å	0.71073
Crystal system	Monoclinic
Space group	$P2_1$
a/Å	5.322(2)
b/Å	10.531(3)
c/Å	12.939(2)
α/°	90
β/°	99.20(2)
γ/°	90
Volume/Å^3	715.8(4)
Z	2
ρ / Mg.m^{-3}	1.991
Absorption coefficient/mm^{-1}	7.693
F(000)	412
Crystal size/mm^3	1.72 x 0.12 x 0.12
Range	2.5≤Θ≤30
Index ranges : h k l	 -7→7 0→14 -18→18
Reflections collected	4379
Independent reflections	2193
R_{int}	0.076
Data/restraints/parameters	2193/0/154
Max shift, Δz	0.001
Residual density / e.Å^{-3} $(\Delta\rho)_{max}$ $(\Delta\rho)_{min}$	 0.733 -0.476
Reliability indices R1 (I > 2σ(I)) wR2 (I > 2σ(I)) R1 (all data) wR2 (all data)	 0.037 0.089 0.088 0.076
S	0.921

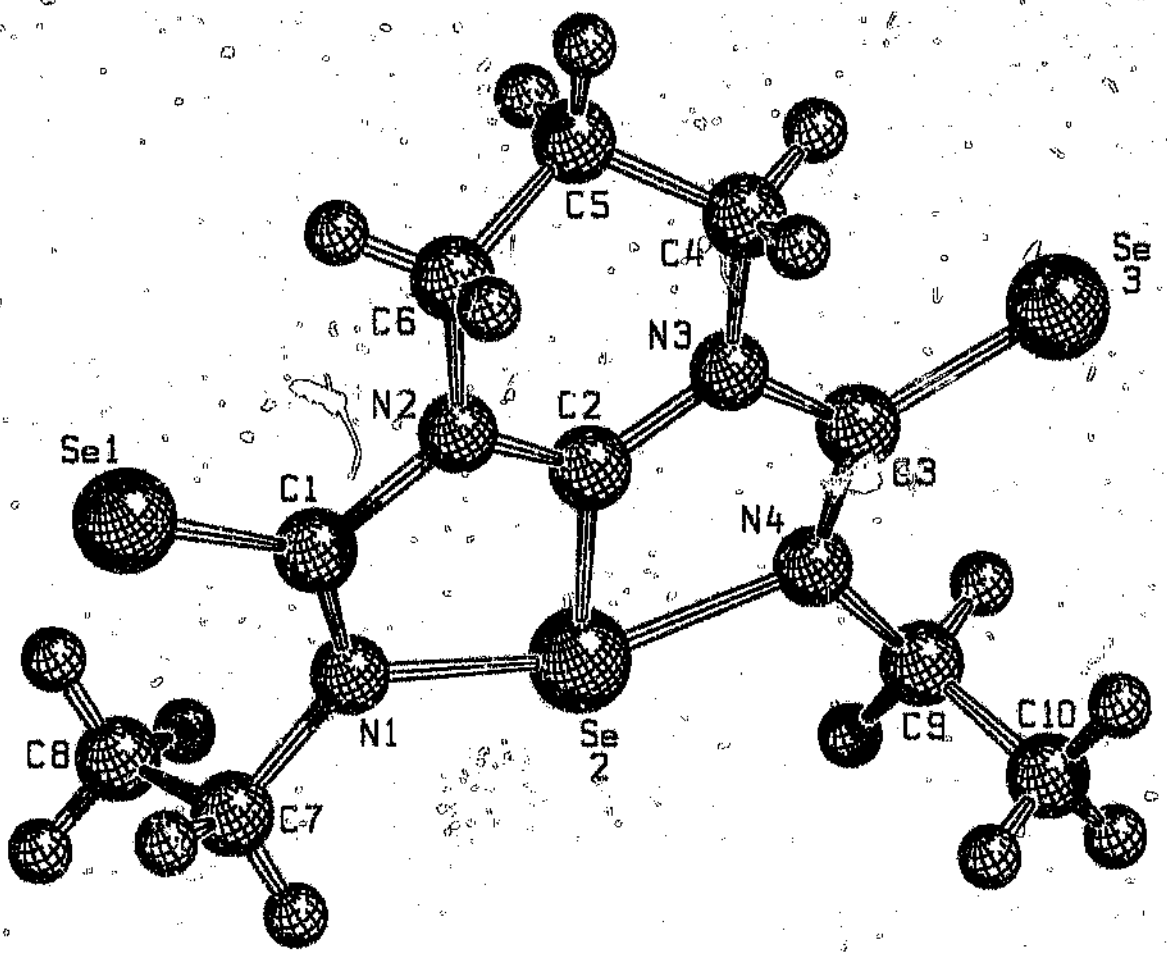


Figure 5.8 : Labelled Schakal diagram of *8*

Table 5.16: Atomic coordinates (x 10^4) and equivalent isotropic displacement parameters ($Å^2$, x10^3) for *8*

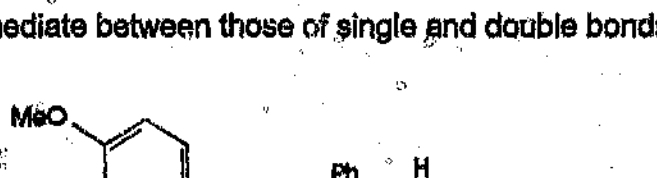
	x/a	y/b	z/c	U_{eq}
Se(1)	786(1)	-4869	6970(1)	57(1)
Se(2)	6465(1)	-1655(1)	8434(1)	43(1)
Se(3)	10360(1)	-1727(1)	5449(1)	64(1)
N(1)	3936(10)	-2686(5)	9105(4)	42(1)
N(2)	4136(9)	-3833(6)	7656(4)	43(1)
N(3)	6947(9)	-2915(6)	6629(4)	45(1)
N(4)	8687(10)	-1143(6)	7354(4)	45(1)
C(1)	3062(11)	-3716(7)	8605(5)	41(1)
C(2)	5771(11)	-2935(6)	7474(4)	39(1)
C(3)	8626(11)	-1889(7)	6562(7)	45(2)
C(4)	6385(13)	-3919(9)	5822(5)	56(2)
C(5)	5691(13)	-5129(8)	6307(5)	60(2)
C(6)	3474(12)	-4922(8)	6933(5)	54(2)

C(7)	3282(13)	2268(9)	10110(5)	58(2)
C(8)	5037(18)	-2917(10)	10978(6)	78(3)
C(9)	10143(13)	52(8)	7496(6)	57(2)
C(10)	8790(20)	1128(10)	6882(7)	83(3)

Table 5.17: Selected bond lengths (Å) for *8*	
Se(1)-C(1)	1.829(7)
Se(2)-C(2)	1.831(6)
Se(2)-N(1)	2.030(5)
Se(2)-N(4)	2.042(5)
Se(3)-C(3)	1.838(6)
N(1)-C(1)	1.310(9)
N(2)-C(2)	1.331(8)
N(2)-C(1)	1.440(8)
N(3)-C(2)	1.344(7)
N(3)-C(3)	1.413(9)
N(4)-C(3)	1.288(9)

5.7 Crystal structure of 5-p-methoxyphenyl-2-p-methoxyphenyl -imino-3,2-phenyl-1,6,6aλ^4-triselenapentalene.

The title compound ***9***, crystallises in the monoclinic crystal system, and exhibits the characteristic structural features of heterapentalenes, with the Se-Se bonds long and the Se-Se-Se bond angle wide. All other bond lengths in the heterapentalene framework are intermediate between those of single and double bonds.



9

The Se-Se bond lengths in ***9***, 2.542(2)Å and 2.598(2)Å are greater by 8.6% and 11.0% than the (two-centre two-electron) covalent Se-Se single bond [2.340(24)Å, Allen *et al*, 1987]. The lengths of corresponding bonds and the size of corresponding bond angles in the two halves of the triheterapentalene framework differ somewhat but this would be consistent with the assymetric substitution pattern on the pentalene framework.

Compound ***9*** crystallised from benzene as purple needle-shaped crystals; m.p. 506-507 K. Cell determination, using 25 high-order reflections, and data collection were done on an Enraf-Nonius CAD4 four-circle diffractometer equipped with a graphite monochromator. Data reduction included correction for Lorentz and polarisation effects using standard Enraf Nonius routines, and absorption effects were corrected for empirically (North *et al, 1968*). Three standard reflections monitored every hour showed an average increase of 3.2% and this was corrected for linearly. Unit cell parameters and details of the data collection are given in Table 5.18. The structure was solved by direct methods using SHELXS86 and refined using SHELXL93 by least-squares methods, based on F^2. All non-H atoms were refined with anisotropic displacement parameters. H atoms were placed geometrically in the final cycles of refinement and allowed to refine with a common

isotropic displacement parameter. Figure 5.10 shows a labelled SCHAKAL diagram of the molecule and also indicates the numbering scheme used. Atomic coordinates and selected bond lengths are listed in Table 5.19 and Table 5.20 respectively.

Table 5.18 : Crystal and refinement data	
Compound	**9**
Empirical formula	$C_{25}H_{21}NO_2Se_2$
Formula weight / g.mol^{-1}	604.31
Temperature/K	293(2)
Wavelength/Å	0.71069
Crystal system	Monoclinic
Space group	P 2$_1$/c
a/Å	7.394(7)
b/Å	18.295(2)
c/Å	17.487(1)
α/°	90
β/°	90.12(4)
γ/°	90
Volume/Å^3	2365(2)
z	4
ρ / Mg.m^{-3}	1.697
Absorption coefficient/mm^{-1}	4.687
F(000)	11.84
Crystal size/mm^3	0.35 x 0.5 x 1.0
Range	2.5≤θ≤30
Index ranges : h k l	 -10→10 -1→25 -1→24
Reflections collected	7913
Independent reflections	6873
R_{int}	0.056
Data/restraints/parameters	6873/3/0/281
Max shift, Δz	-0.001
Residual density / e.Å^{-3} $(\Delta\rho)_{max}$ $(\Delta\rho)_{min}$	 0.931 -0.464
Reliability indices R1 (I > 2σ(I)) wR2 (I > 2σ(I)) R1 (all data) wR2 (all data)	 0.052 0.099 0.196 0.111
S	0.833

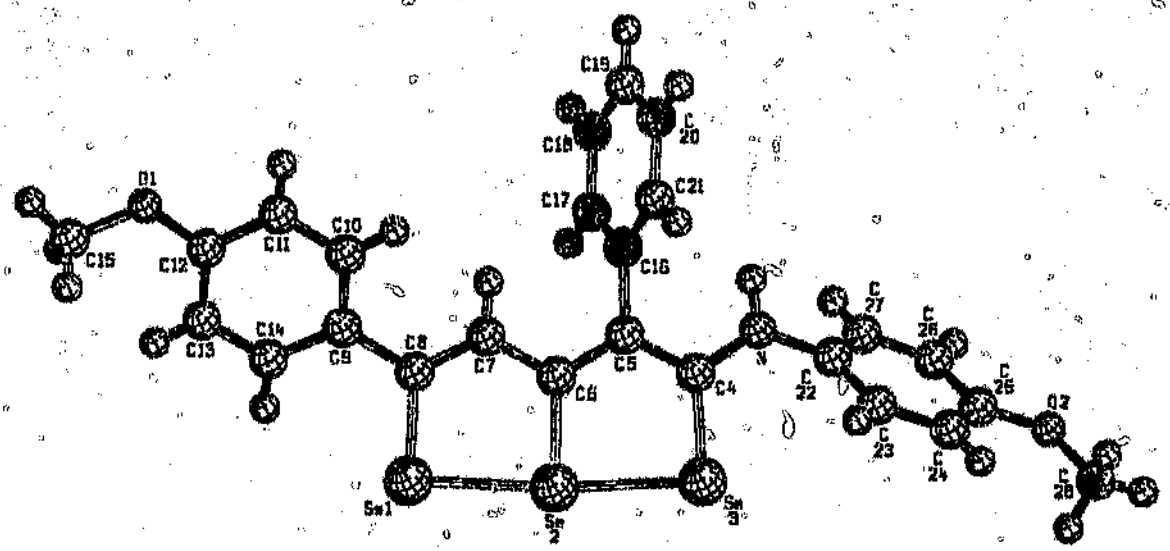


Figure 5.10: Labelled Schakal diagram of **9**

Table 5.19: Atomic coordinates (x 10^4) and equivalent isotropic displacement parameters ($Å^2$, x10^3) for **9**

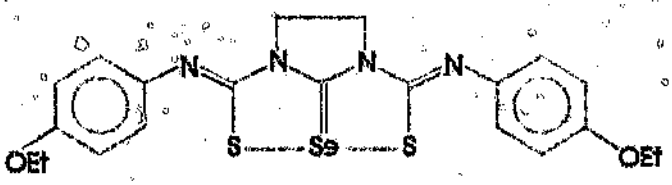
	x/a	y/b	z/c	U_{eq}
Se(1)	3441(1)	6195(1)	5321(1)	44(1)
Se(2)	6393(1)	5747(1)	4742(1)	40(1)
Se(3)	9316(1)	5352(1)	4031(1)	48(1)
O(1)	-1080(5)	9222(2)	5183(2)	62(1)
O(2)	15635(5)	4406(2)	1760(2)	68(1)
N	10125(5)	6223(2)	2772(2)	50(1)
C(4)	9037(6)	6145(2)	3381(3)	42(1)
C(5)	7617(6)	6648(2)	3500(2)	38(1)
C(6)	8333(5)	6565(2)	4080(2)	37(1)
C(7)	4927(6)	7067(2)	4193(2)	39(1)
C(8)	3548(6)	7029(2)	4704(2)	36(1)
C(9)	2124(6)	7565(2)	4804(2)	40(1)
C(10)	2405(6)	8307(3)	4801(3)	48(1)
C(11)	1115(6)	8837(3)	4724(3)	54(1)
C(12)	-514(7)	8660(3)	5072(3)	46(1)
C(13)	-841(7)	7940(3)	5254(3)	59(1)
C(14)	458(6)	7416(3)	5127(3)	55(1)
C(15)	-3321(7)	9072(4)	5566(4)	85(2)
C(16)	7421(6)	7247(2)	2930(2)	37(1)
C(17)	6130(7)	7201(3)	2357(3)	51(1)
C(18)	5988(7)	7734(3)	1807(3)	62(2)
C(19)	7116(8)	8316(3)	1815(3)	61(2)
C(20)	8397(8)	8384(3)	2378(3)	65(2)

C(21)	8534(7)	7848(3)	2935(3)	56(1)
C(22)	11567(8)	5755(3)	2534(3)	44(1)
C(23)	12984(8)	5592(2)	3026(3)	44(1)
C(24)	14373(8)	5149(3)	2780(3)	45(1)
C(25)	14336(8)	4862(3)	2053(3)	48(1)
C(26)	12928(7)	5028(3)	1569(3)	61(1)
C(27)	11554(7)	5476(3)	1808(3)	59(1)
C(28)	17115(7)	4210(4)	2249(3)	75(2)

Table 5.20: Selected bond lengths (Å) for *8*	
Se(1)-C(8)	1.872(4)
Se(1)-Se(2)	2.542(2)
Se(2)-C(6)	1.893(4)
Se(2)-Se(3)	2.598(2)
Se(3)-C(4)	1.855(4)
C(4)-C(5)	1.411(6)
C(5)-C(8)	1.399(5)
C(6)-C(7)	1.426(6)
C(7)-C(8)	1.361(6)

5.8 Crystal structure of 1,4-Bis-p-ethoxyphenylimino-5,6-dihydro-2, 3-dithia-2aλ⁴-selena-4a,6a-diazacyclopenta[cd]pentalene.

The title compound ***10*** crystallises in the triclinic system and contains two molecules, A and B in the asymmetric unit. These molecules differ conformationally in terms of the orientation of the aromatic rings relative to the pentalene framework of the rest of the molecule. Both molecules exhibit the characteristic structural features of heterapentalenes, with long S-Se bonds and wide S-Se-S bond angle. All other bond lengths in the heterapentalene framework are intermediate between those of single and double bonds.



10

The Se-S bond lengths in molecule A 2.478(4)Å and 2.493(4)Å are greater by 12.9% and 13.6% respectively than the (two-centre two-electron) covalent Se-S single bond length [2.195(15)Å, Allen *et al*;1987]. The Se-S bonds in molecule B are 2.467(4)Å and 2.518(4)Å in length and thus longer that the Se-S bond (2.195Å) by 12.4 and 14.7% respectively. The lengths of the corresponding bonds and the size of the corresponding bond angles in the two halves of the triheterapentalene framework in A and B are very similar, differing from one another by at most 0.015 Å and 0.6° , and 0.051Å and 0.76° respectively.

Compound ***10*** crystallised from dichloromethane as bright yellow needle shaped crystals; m.p. 465-466K. Cell determination, using 25 high-order reflections, and data collection were done on an Enraf-Nonius CAD4 four-circle diffractometer equipped with a graphite monochromator. Data reduction included correction for Lorentz and polarisation effects using standard Enraf Nonius routines, and absorption effects were corrected for empirically (North *et al; 1968*). Three standard reflections monitored every hour showed an average decrease of 5.7% and this was

corrected for linearly. Unit cell parameters and details of the data collection are given in Table 5.21. The structure was solved by direct methods using SHELXS86 and refined using SHELXL93 by least-squares methods, based on F^2. All non-H atoms were refined with anisotropic displacement parameters. H atoms were placed geometrically in the final cycles of refinement and allowed to refine with a common isotropic displacement parameter. Figure 5.11 shows a labelled SCHAKAL diagram of the molecule and also indicates the numbering scheme used. Atomic coordinates and selected bond lengths are listed in Table 5.22 and Table 5.23 respectively. The selected torsion angles listed in Table 5.24 illustrate the conformational differences between the two molecules in the assymetric unit.

Table 5.21 : Crystal and refinement data	
Compound	***10***
Empirical formula	$C_{21}H_{22}N_4O_2S_2Se$
Formula weight / g.mol^{-1}	505.51
Temperature/K	293(2)
Wavelength/Å	0.71073
Crystal system	Triclinic
Space group	P-1
a/Å	13.675(10)
b/Å	14.11(2)
c/Å	14.399(8)
α/°	94.49(6)
β/°	118.25(3)
γ/°	111.51(5)
Volume/Å^3	2167(4)
z	4
ρ / Mg.m^{-3}	1.55
Absorption coefficient/mm^{-1}	1.952
F(000)	1032
Crystal size/mm^3	0.15 x 0.2 x 1.1
Range	2.5≤θ≤30
Index ranges : h k l	 -19→16 -19→19 0→20
Reflections collected	13044
Independent reflections	12576

R_{int}	0.021
Data/restraints/parameters	12578/0/382
Max shift, Δz	0.182
Residual density / e.Å^{-3} $(\Delta\rho)_{max}$ $(\Delta\rho)_{min}$	 1.257 -0.911
Reliability indices R1 (I > 2σ(I)) wR2 (I > 2σ(I)) R1 (all data) wR2 (all data)	 0.058 0.165 0.121 0.173
S	1.072

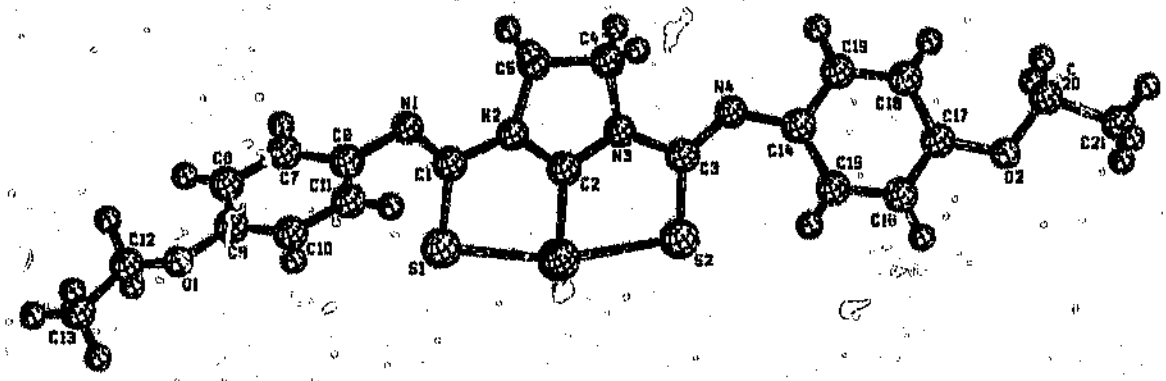


Figure 5.11: Labelled Schakal diagram of ***10***

Table 5.22: Atomic coordinates (x 10^4) and equivalent isotropic displacement parameters (Å^2, x10^3) for ***10***

	x/a	y/b	z/c	U_{eq}
Se(A)	4625(1)	8037(1)	4613(1)	47(1)
S(1A)	5807(1)	9778(1)	6077(1)	57(1)
S(2A)	3529(1)	6095(1)	3574(1)	59(1)
N(1A)	6531(3)	9731(2)	8172(3)	57(1)
N(2A)	5826(3)	8141(2)	6861(2)	47(1)
N(3A)	4543(3)	6488(2)	5733(2)	45(1)
N(4A)	3430(3)	4712(2)	4821(2)	48(1)
O(1A)	2621(6)	6009(4)	785(4)	158(2)
O(2A)	147(3)	823(2)	1455(2)	70(1)
C(1A)	6040(3)	9247(3)	7172(3)	48(1)
C(2A)	4954(3)	7517(3)	5811(3)	44(1)
C(3A)	3763(3)	5455(3)	4719(3)	46(1)
C(4A)	4971(4)	6330(3)	6825(3)	57(1)
C(5A)	5716(4)	7472(3)	7611(3)	62(1)
C(6A)	6821(4)	10624(3)	8432(3)	54(1)
C(7A)	8017(5)	11636(4)	8962(4)	86(1)

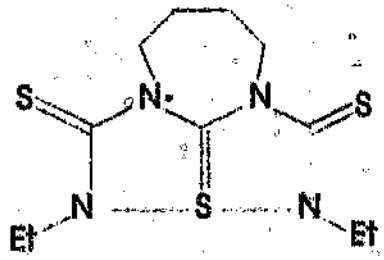
C(8A)	8270(6)	12699(5)	9248(5)	100(2)
C(9A)	7317(4)	12949(4)	8968(4)	73(1)
C(10A)	6165(5)	12177(4)	8495(4)	81(1)
C(11A)	5905(4)	11111(4)	8225(4)	72(1)
C(12A)	8306(7)	14722(6)	9519(7)	147(3)
C(13A)	8111(6)	15768(5)	9636(5)	100(2)
C(14A)	2634(3)	3773(3)	3628(3)	45(1)
C(15A)	1594(4)	3628(3)	2911(3)	60(1)
C(16A)	811(4)	2649(3)	2116(4)	63(1)
C(17A)	1013(3)	1757(3)	2297(3)	52(1)
C(18A)	2012(3)	1882(3)	3302(3)	51(1)
C(19A)	2791(3)	2865(3)	4105(3)	48(1)
C(20A)	257(4)	-126(4)	1645(4)	74(1)
C(21A)	-867(5)	-1059(4)	643(4)	87(2)
Se(B)	1570(1)	8076(1)	3989(1)	56(1)
S(1B)	2396(1)	9948(1)	5027(1)	60(1)
S(2B)	410(1)	6066(1)	3196(1)	69(1)
N(1B)	1428(2)	10278(2)	6262(2)	45(1)
N(2B)	724(2)	8568(2)	5308(2)	43(1)
N(3B)	-160(2)	6845(2)	4488(2)	44(1)
N(4B)	-1241(3)	5047(2)	3818(2)	48(1)
O(1B)	3983(3)	14702(2)	8224(2)	61(1)
O(2B)	-3338(2)	694(2)	1717(2)	58(1)
C(1B)	1503(3)	9871(3)	5614(3)	43(1)
C(2B)	641(3)	7808(3)	4630(3)	44(1)
C(3B)	-441(3)	5872(3)	3823(3)	47(1)
C(4B)	-729(3)	6904(3)	5130(3)	47(1)
C(5B)	-124(3)	8104(3)	5691(3)	48(1)
C(6B)	2099(3)	11392(3)	6701(3)	45(1)
C(7B)	3107(3)	12081(3)	6649(3)	55(1)
C(8B)	3696(4)	13174(3)	7152(3)	57(1)
C(9B)	3317(3)	13618(3)	7742(3)	48(1)
C(10B)	2331(3)	12950(3)	7793(3)	52(1)
C(11B)	1739(3)	11886(3)	7279(3)	50(1)
C(12B)	3700(4)	15171(3)	8925(3)	56(1)
C(13B)	4535(4)	16362(3)	9363(4)	68(1)
C(14B)	-1700(3)	3977(3)	3234(3)	45(1)
C(15B)	-2367(3)	3208(3)	3540(3)	48(1)
C(16B)	-2903(3)	2127(3)	3020(3)	51(1)
C(17B)	-2787(3)	1775(3)	2172(3)	48(1)
C(18B)	-2133(3)	2534(3)	1850(3)	56(1)
C(19B)	-1595(4)	3619(3)	2374(3)	57(1)
C(20B)	-3145(4)	306(3)	906(4)	66(1)
C(21B)	-3862(4)	-897(3)	506(4)	70(1)

Table 5.23: Selected bond lengths (Å) for *10*			
Se(A)-C(2A)	1.850(4)	Se(B)-C(2B)	1.849(3)
Se(A)-S(1A)	2.478(4)	Se(B)-S(1B)	2.497(4)
Se(A)-S(2A)	2.493(4)	Se(B)-S(2B)	2.518(4)
S(1A)-C(1A)	1.741(4)	S(1B)-C(1B)	1.742(3)
S(2A)-C(3A)	1.732(4)	S(2B)-C(3B)	1.745(4)
N(1A)-C(1A)	1.259(5)	N(1B)-C(1B)	1.284(4)
N(2A)-C(2A)	1.337(5)	N(2B)-C(2B)	1.326(4)
N(2A)-C(1A)	1.400(5)	N(2B)-C(1B)	1.409(5)
N(3A)-C(2A)	1.324(5)	N(3B)-C(2B)	1.320(4)
N(3A)-C(3A)	1.412(5)	N(3B)-C(3B)	1.417(5)
N(4A)-C(3A)	1.284(5)	N(4B)-C(3B)	1.268(4)

Table 5.24: Selected torsion angles (°) for *10*			
C(1A)-N(1A)-C(6A)-C(7A)	-105.2(5)	C(1B)-N(1B)-C(6B)-C(7B)	-8.8(6)
C(1A)-N(1A)-C(6A)-C(11A)	79.2(5)	C(1B)-N(1B)-C(6B)-C(11B)	173.0(3)
C(3A)-N(4A)-C(14A)-C(15A)	-38.6(5)	C(3B)-N(4B)-C(14B)-C(15B)	167.2(4)
C(3A)-N(4A)-C(14A)-C(19A)	149.6(6)	C(3B)-N(4B)-C(14B)-C(19B)	-15.3(6)

5.9 Crystal structure of 2,3-Diethyl-5,6,7,8-tetrahydro-2aλ⁴- thia-2,3,4a,8a-tetraazacyclopent[cd]azulene-1(2H),4(3H)-diselone.

The title compound ***11***, crystallises in the monoclinic crystal system, and exhibits the characteristic structural features of heterapentalenes, with long S-N bonds and wide N-S-N bond angle. All other bond lengths in the heterapentalene framework are intermediate between those of single and double bonds.



11

Compound ***11*** contains elongated N-S bonds [1.8765(13)Å and 1.9032(14)Å] which are greater by 9.7% and 11.3% respectively, than the two-center, two-electron N-S bond [1.710(19); Allen *et al*;1987]. The lengths of the corresponding bonds and the size of the corresponding bond angles in the two halves of the heterapentalene framework are very similar, differing from one another by at most 0.027 Å and 0.83° respectively.

The title compound was recrystallised from a mixture of dichloromethane and hexane (1:2) as clear crystals, m.p. 413-414 K. Cell determination, using 25 high-order reflections, and data collection were done on Enraf-Nonius CAD4 four-circle diffractometer equipped with a graphite monochromator, using standard Enraf-Nonius routines. Data reduction was done using the PC version of NRCVAX and included correction for Lorentz and polarisation effects. Absorption effects were corrected for analytically, using the ABSORP routine from the NRCVAX suite of programs.This routine required that the faces of the crystal be indexed and measured. It then used this information to calculate the necessary corrections by a Gaussian integration method. Three standard reflections monitored every hour showed only random fluctuations. Unit cell parameters and details of the data

collection are given in Table 5.25. The structure was solved by direct methods using SHELXS86 and refined using SHELXL93 by least-squares methods, based on F^2. All non-H atoms were refined with anisotropic displacement parameters. H atoms were placed geometrically in the final cycles of refinement and allowed to refine with a common isotropic displacement parameter. Figure 5.12 shows a labelled SCHAKAL diagram of the molecule and also indicates the numbering scheme used. Atomic coordinates and selected bond lengths are listed in Table 5.26 and Table 5.27 respectively.

Table 5.25: Crystal and refinement data	
Compound	*11*
Empirical formula	$C_{11}H_{18}N_4S_4$
Formula weight / g.mol^{-1}	302.47
Temperature/K	293(2)
Wavelength/Å	0.7107
Crystal system	Monoclinic
Space group	$P2_1$
a/Å	5.615(2)
b/Å	10.0865(10)
c/Å	13.0482(10)
α/°	90
β/°	100.13(2)
γ/°	90
Volume/Å^3	726.0(3)
z	2
ρ / Mg.m^{-3}	1.384
Absorption coefficient/mm^{-1}	0.499
F(000)	320
Crystal size/mm^3	0.37 x 0.45 x 0.9
Range	2.5≤Θ≤40
Index ranges : h k l	 -10→10 -1→18 -23→23
Reflections collected	5043
Independent reflections	5043
Data/restraints/parameters	5043/0/165
Max shift, Δz	0.009
Residual density / e.Å^{-3} $(\Delta\rho)_{max}$ $(\Delta\rho)_{min}$	 0.266 -0.241

Reliability Indices	
R1 (I > 2σ(I))	0.030
wR2 (I > 2σ(I))	0.086
R1 (all data)	0.058
wR2 (all data)	0.094
S	0.946

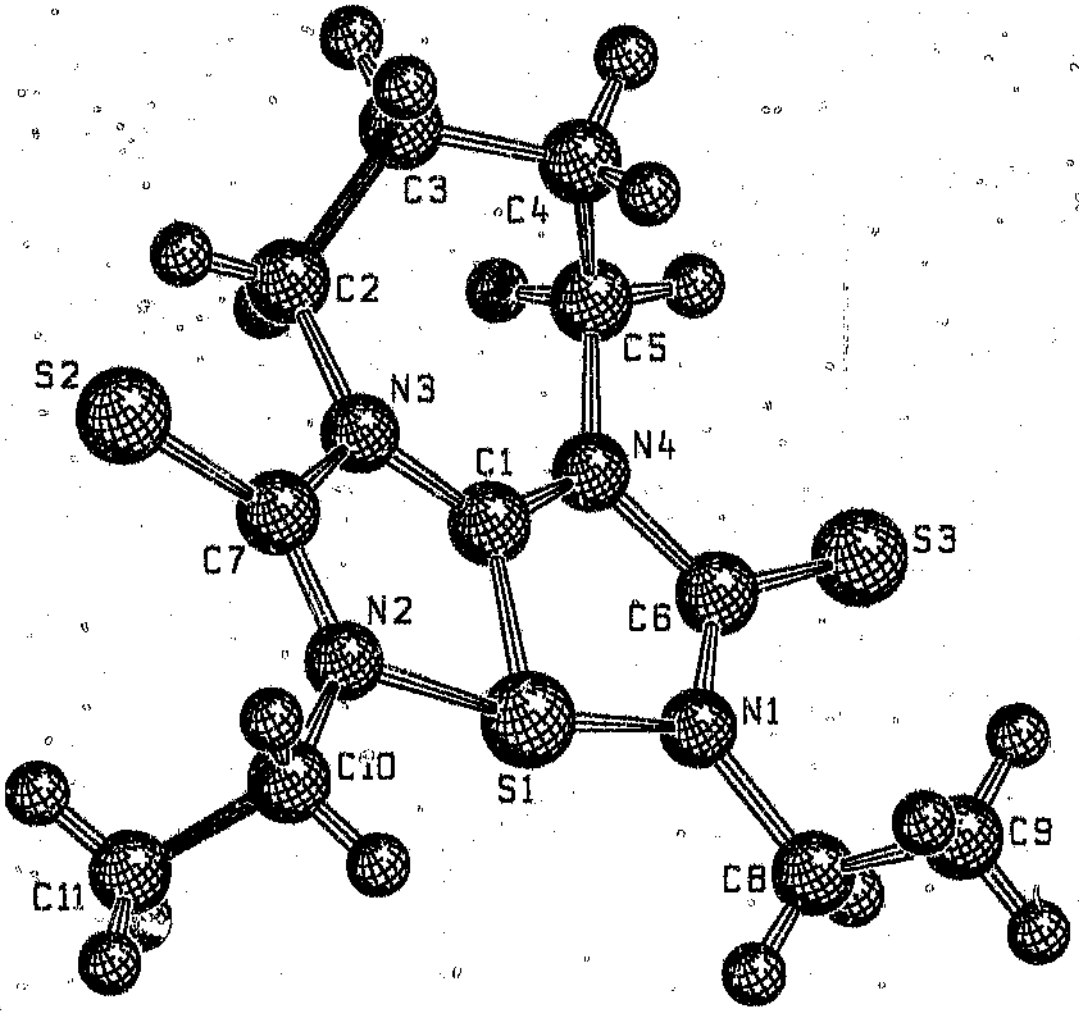


Figure 5.12: Labelled Schakal diagram of *11*

Table 5.26: Atomic coordinates (x 10^4) and equivalent isotropic displacement parameters ($Å^2$, x10^3) for *11*

	x/a	y/b	z/c	U_{eq}
S(1)	3882(1)	374	1650(1)	46(1)
S(2)	90(1)	386(1)	4312(1)	63(1)
S(3)	9326(1)	-2501(1)	1069(1)	62(1)
N(1)	6201(2)	-464(2)	997(1)	51(1)

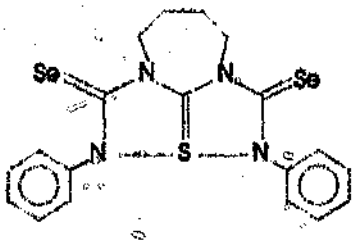
N(2)	1745(2)	820(2)	2551(1)	51(1)
N(3)	3819(2)	-785(1)	3424(1)	45(1)
N(4)	5368(2)	-1709(1)	2408(1)	44(1)
C(1)	4712(2)	-816(1)	2585(1)	42(1)
C(2)	4465(3)	-1544(2)	4382(1)	58(1)
C(3)	4008(3)	-3011(2)	4270(2)	68(1)
C(4)	4918(3)	-3618(2)	3336(2)	66(1)
C(5)	7085(3)	-2897(2)	3050(1)	56(1)
C(6)	7255(2)	-1507(2)	1459(1)	47(1)
C(7)	1803(2)	217(2)	3383(1)	48(1)
C(8)	6482(4)	-20(2)	-40(1)	65(1)
C(9)	4791(5)	-771(3)	-862(2)	89(1)
C(10)	155(3)	2059(2)	2284(1)	60(1)
C(11)	1037(4)	3286(2)	2873(2)	84(1)

Table 5.27: Selected bond lengths (Å) for *11*

S(1)-C(1)	1.7149(13)
S(1)-N(1)	1.8765(13)
S(1)-N(2)	1.9032(14)
S(2)-C(7)	1.6819(13)
S(3)-C(6)	1.6797(14)
N(1)-C(6)	1.300(2)
N(2)-C(7)	1.291(2)
N(3)-C(1)	1.348(2)
N(3)-C(7)	1.428(2)
N(4)-C(1)	1.342(2)
N(4)-C(6)	1.426(2)

5.10 Crystal structure of 5,6,7,8 - Tetrahydro - 2,3-diphenyl - 2aλ^4 - thia - 2,3,4a,8a - tetraazacyclopent[cd]azulene -1[2H],4[3H] - diselone.

The title compound ***12*** crystallises in the triclinic system and contains two molecules, A and B in the assymetric unit. These molecules differ conformationally in terms of the orientation of the aromatic rings relative to the pentalene framework of the rest of the molecule. Both Molecules exhibit the characteristic structural features of heterapentalenes. with long S-Se bonds and wide S-Se-S bond angle. All other bond lengths in the heterapentalene framework are intermediate between those of single and double bonds.



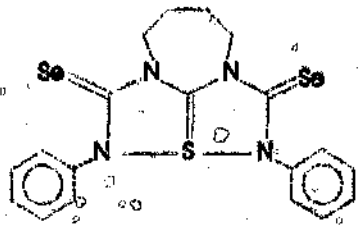
12

The N-S bond lengths in molecule A 1.910(3)Å and 1.900(3)Å are greater by 11.7% and 11.1% respectively than the (two-centre two-electron) covalent N-S single bond length [1.710(19)Å, Allen *et al*,1987]. The N-S bonds in molecule B are1.90734)Å and 1.901(3)Å in length and thus longer that the N-S bond (1.710Å) by 11.5% and 11.2% respectively. The lengths of the corresponding bonds and the size of the corresponding bond angles in the two halves of the heterapentalene framework in A and B are very similar, differing from one another by at most 0.010 Å and 0.3° , and 0.009Å and 0.3° respectively.

Compound ***12*** crystallised from MeCN-CH_2Cl_2 as light yellow crystals; m.p. 419-420K. Cell determination, using 25 high-order reflections, and data collection were done on an Enraf-Nonius CAD4 four-circle diffractometer equipped with a graphite monochromator. Data reduction included correction for Lorentz and polarisation effects using standard Enraf Nonius routines, and absorption effects

5.10 Crystal structure of 5,6,7,8 - Tetrahydro - 2,3-diphenyl - 2aλ^4 - thia - 2,3,4a,8a - tetraazacyclopent[cd]azulene -1[2H],4[3H] - diselone.

The title compound ***12*** crystallises in the triclinic system and contains two molecules, A and B in the assymetric unit. These molecules differ conformationally in terms of the orientation of the aromatic rings relative to the pentalene framework of the rest of the molecule. Both Molecules exhibit the characteristic structural features of heterapentalenes. with long S-Se bonds and wide S-Se-S bond angle. All other bond lengths in the heterapentalene framework are intermediate between those of single and double bonds.



12

The N-S bond lengths in molecule A 1.910(3)Å and 1.900(3)Å are greater by 11.7% and 11.1% respectively than the (two-centre two-electron) covalent N-S single bond length [1.710(19)Å, Allen *et al*,1987]. The N-S bonds in molecule B are1.90734)Å and 1.901(3)Å in length and thus longer that the N-S bond (1.710Å) by 11.5% and 11.2% respectively. The lengths of the corresponding bonds and the size of the corresponding bond angles in the two halves of the heterapentalene framework in A and B are very similar, differing from one another by at most 0.010 Å and 0.3° , and 0.009Å and 0.3° respectively.

Compound ***12*** crystallised from MeCN-CH_2Cl_2 as light yellow crystals; m.p. 419-420K. Cell determination, using 25 high-order reflections, and data collection were done on an Enraf-Nonius CAD4 four-circle diffractometer equipped with a graphite monochromator. Data reduction included correction for Lorentz and polarisation effects using standard Enraf Nonius routines. and absorption effects

were corrected for empirically (North *et al; 1968*). Three standard reflections monitored every hour showed only random fluctuations. Unit cell parameters and details of the data collection are given in Table 5.28. The structure was solved by direct methods using SHELXS86 and refined using SHELXL93 by least-squares methods, based on F^2. All non-H atoms were refined with anisotropic displacement parameters. H atoms were placed geometrically in the final cycles of refinement and allowed to refine with a common isotropic displacement parameter. Figure 5.13 shows a labelled SCHAKAL diagram of the molecule and also indicates the numbering scheme used. Atomic coordinates and selected bond lengths are listed in Table 5.29 and Table 5.30 respectively. The selected torsion angles listed in Table 5.31 illustrate the conformational differences between the two molecules in the asymmetric unit.

Table 5.28 : Crystal and refinement data	
Compound	***12***
Empirical formula	$C_{14}H_{18}N_4SSe_2$
Formula weight /g.mol^{-1}	492.35
Temperature / K	293(2)
Wavelength / Å	0.71069
Crystal system	Triclinic
Space group	P -1
a/Å	9.395(7)
b/Å	14.373(8)
c/Å	14.530(5)
α/°	89.11(4)
β/°	88.27(4)
γ/°	86.79(4)
Volume/Å^3	1958(2)
z	4
ρ / Mg.m^{-3}	1.670.
Absorption coefficient/mm^{-1}	3.894
F(000)	976
Crystal size/mm^3	0.5 x 0.7 x 1.1
Range	2≤θ≤30
Index ranges : h k l	 -1→11 -18→18 -20→18
Reflections collected	9942

Independent reflections	8411
R_{int}	0.02
Data/restraints/parameters	8411 / 0 / 469
Max shift, Δz	-0.003
Residual density / e.Å^{-3} $(\Delta\rho)_{max}$ $(\Delta\rho)_{min}$	 1.169 -0.800
Reliability indices R1 (I > 2σ(I)) wR2 (I > 2σ(I)) R1 (all data) wR2 (all data)	 0.036 0.099 0.079 0.105
S	1.07

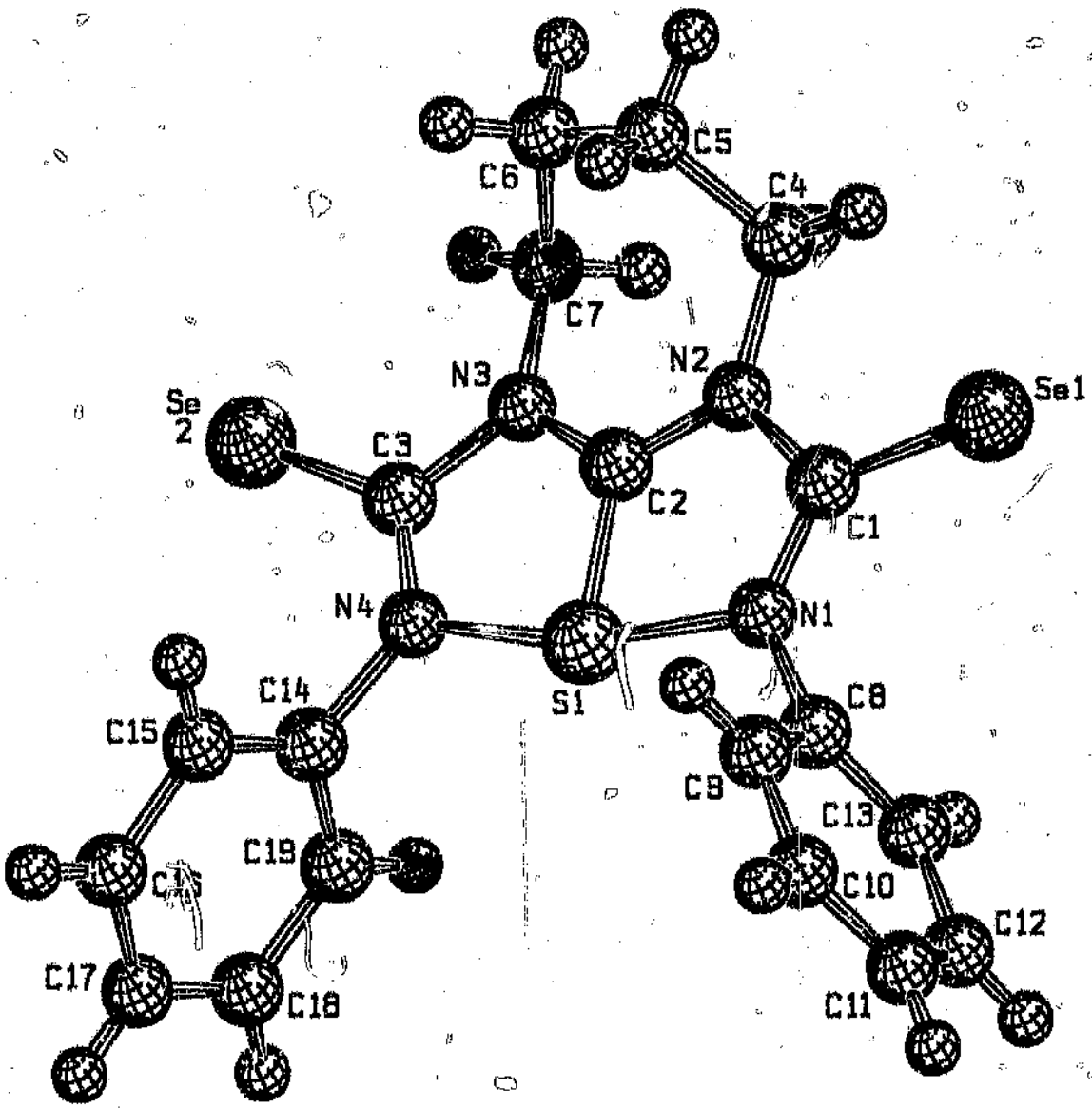


Figure 5.13: Labelled Schakal diagram of ***12***

Table 5.29: Atomic coordinates (x 10^4) and equivalent isotropic displacement parameters ($Å^2$, x10^3) for *12*

	x/a	y/b	z/c	U_{eq}
Se(1A)	1969(1)	8489(1)	10261(1)	66(1)
Se(2A)	2019(1)	7106(1)	4882(1)	53(1)
S(1A)	4121(1)	7627(1)	7586(1)	38(1)
N(1A)	3836(3)	7999(2)	8830(2)	42(1)
N(2A)	1611(3)	8053(2)	8357(2)	37(1)
N(3A)	1674(3)	7670(2)	6760(2)	36(1)
N(4A)	3914(3)	7289(2)	6333(2)	40(1)
C(1A)	2516(3)	8161(2)	9108(2)	39(1)
C(2A)	2297(3)	7794(2)	7506(2)	34(1)
C(3A)	2622(3)	7359(2)	6030(2)	36(1)
C(4A)	39(4)	8162(3)	8494(3)	57(1)
C(5A)	-698(4)	7343(3)	8149(3)	61(1)
C(6A)	-844(4)	7332(3)	7131(3)	58(1)
C(7A)	157(4)	7924(3)	6604(2)	54(1)
C(8A)	5068(3)	8038(2)	9377(2)	39(1)
C(9A)	5648(4)	7226(3)	9762(2)	47(1)
C(10A)	6879(4)	7253(3)	10253(3)	59(1)
C(11A)	7510(4)	8070(4)	10359(3)	63(1)
C(12A)	6960(5)	8862(3)	9975(3)	69(1)
C(13A)	5718(4)	8860(3)	9470(3)	57(1)
C(14A)	5180(3)	6976(2)	5832(2)	39(1)
C(15A)	5566(5)	6054	5810(3)	63(1)
C(16A)	6883(5)	5758(4)	5410(3)	78(1)
C(17A)	7760(4)	6388(4)	5048(2)	74(1)
C(18A)	7367(4)	7305(4)	5058(3)	68(1)
C(19A)	6064(4)	7612(3)	5457(3)	54(1)
Se(1B)	-3113(1)	15269(1)	8414(1)	63(1)
Se(2B)	-2800(1)	9860(1)	6997(1)	53(1)
S(1B)	-761(1)	12591(1)	7484(1)	35(1)
N(1B)	-1081(3)	13849(2)	7857(2)	41(1)
N(2B)	-3290(3)	13396(2)	7821(2)	38(1)
N(3B)	-3183(3)	11779(2)	7475(2)	34(1)
N(4B)	-938(3)	11318(2)	7177(2)	37(1)
C(1B)	-2415(3)	14131(2)	8010(2)	39(1)
C(2B)	-2580(3)	12589(2)	7598(2)	33(1)
C(3B)	-2223(3)	11025(2)	7218(2)	36(1)
C(4B)	-4847(3)	13602(2)	7724(3)	47(1)
C(5B)	-5443(4)	13107(3)	6918(3)	50(1)
C(6B)	-5730(4)	12097(2)	7134(3)	51(1)
C(7B)	-4665(3)	11641(2)	7781(2)	43(1)
C(8B)	112(3)	14406(2)	7965(3)	44(1)

C(9B)	797(4)	14741(3)	7195(3)	67(1)
C(10B)	1994(5)	15229(3)	7266(5)	95(2)
C(11B)	2516(5)	15392(3)	8117(6)	101(2)
C(12B)	1819(6)	15054(3)	8890(5)	93(2)
C(13B)	630(4)	14554(3)	8809(3)	66(1)
C(14B)	327(3)	10771(2)	6928(2)	37(1)
C(15B)	677(4)	10615(3)	6007(3)	50(1)
C(16B)	1971(5)	10142(3)	5785(3)	65(1)
C(17B)	2890(4)	9864(3)	6461(4)	62(1)
C(18B)	2536(4)	10035(3)	7367(3)	63(1)
C(19B)	1238(4)	10485(2)	7609(3)	49(1)

Table 5.30: Selected bond lengths (Å) for *12*

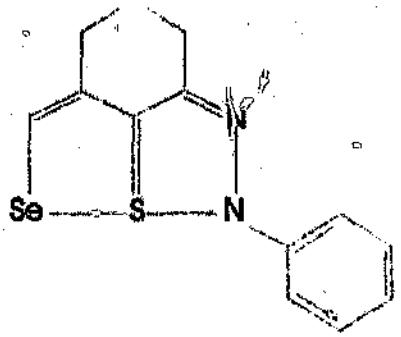
Se(1A)-C(1A)	1.824(3)	Se(1B)-C(1B)	1.826(3)
Se(2A)-C(3A)	1.828(3)	Se(2B)-C(3B)	1.825(3)
S(1A)-C(2A)	1.719(3)	S(1B)-C(2B)	1.712(3)
S(1A)-N(1A)	1.900(3)	S(1B)-N(1B)	1.901(3)
S(1A)-N(4A)	1.910(3)	S(1B)-N(4B)	1.907(3)
N(1A)-C(1A)	1.304(4)	N(1B)-C(1B)	1.309(4)
N(2A)-C(2A)	1.348(4)	N(2B)-C(2B)	1.344(4)
N(2A)-C(1A)	1.419(4)	N(2B)-C(1B)	1.410(4)
N(3A)-C(2A)	1.344(4)	N(3B)-C(2B)	1.340(4)
N(3A)-C(3A)	1.425(4)	N(3B)-C(3B)	1.418(4)
N(4A)-C(3A)	1.302(4)	N(4B)-C(3B)	1.300(4)

Table 5.31: Selected torsion angles (°) for *12*

S(1A)-N(4A)-C(14A)-C(15A)	92.1(4)	S(1B)-N(4B)-C(14B)-C(15B)	-99.7(3)
S(1A)-N(4A)-C(14A)-C(19A)	-81.4(4)	S(1B)-N(4B)-C(14B)-C(19B)	74.3(5)
S(1A)-N(1A)-C(8A)-C(9A)	-81.0(3)	S(1B)-N(1B)-C(8B)-C(9B)	75.7(4)
S(1A)-N(1A)-C(8A)-C(13A)	94.8(3)	S(1B)-N(1B)-C(8B)-C(13B)	-99.9(4)

5.11 Crystal structure of 6,7-Dihydro-2-phenyl-5H-2aλ⁴-thia-3-selena-1,2-diazacyclopent[cd]indene

The title compound ***13***, crystallises in the triclinic crystal system, and exhibits the characteristic structural features of heterapentalenes, with elongated Se-S and S-N bonds and wide Se-S-N bond angle. All other bond lengths in the heterapentalene framework are intermediate between those of single and double bonds.



13

The Se-S and S-N bond lengths in ***13***, 2.5891(10)Å and 1.817(3)Å, are greater by 18.0% and 6.3% respctively than the (two-centre two-electron) covalent Se-S and S-N single bond lengths (2.195(15)Å and 1.710(19)Å, Allen *et al*,1987].

Compound ***13*** crystallised from hexane as green crystals; m.p. 368-370K. Cell determination, using 25 high-order reflections, and data collection were done on an Enraf-Nonius CAD4 four-circle diffractometer equipped with a graphite monochromator. Data reduction included correction for Lorentz and polarisation effects using standard Enraf Nonius routines, and absorption effects were corrected for empirically (North *et al; 1968*). Three standard reflections monitored every hour showed only random fluctuations. Unit cell parameters and details of the data collection are given in Table 5.32. The structure was solved by direct methods using SHELXS86 and refined using SHELXL93 by least-squares methods, based on F^2. All non-H atoms were refined with anisotropic displacement parameters. H atoms were placed geometrically in the final cycles of refinement and allowed to refine with a common isotropic displacement parameter. Figure 5.14 shows a labelled SCHAKAL diagram of the molecule and also indicates the numbering scheme used.

Atomic coordinates and selected bond lengths are listed in Table 5.33 and Table 5.34 respectively.

Table 5.32 : Crystal and refinement data	
Compound	*13*
Empirical formula	$C_{13}H_{12}N_2SSe$
Formula weight / g.mol^{-1}	307.27
Temperature/K	293(2)
Wavelength/Å	0.71069
Crystal system	Triclinic
Space group	P -1
a/Å	7.698(2)
b/Å	7.818(4)
c/Å	11.684(2)
α/°	90.24(2)
β/°	97.89(2)
γ/°	117.60(3)
Volume/Å^3	615.4(4)
z	2
ρ / Mg.m^{-3}	1.658
Absorption coefficient/mm^{-1}	3.197
F(000)	308
Crystal size/mm^3	0.45 x 0.45 x 0.85
Range	3≤θ≤30
Index ranges : h k l	 -10→10 -10→10 0→16
Reflections collected	3736
R_{int}	0.023
Independent reflections	3573
Data/restraints/parameters	3573 / 0 / 155
Max shift, Δz	-0.001
Residual density / e.Å^{-3} $(\Delta\rho)_{max}$ $(\Delta\rho)_{min}$	 1.017 -1.026
Reliability indices R1 (I > 2σ(I)) wR2 (I > 2σ(I)) R1 (all data) wR2 (all data)	 0.049 0.129 0.123 0.143
S	0.914

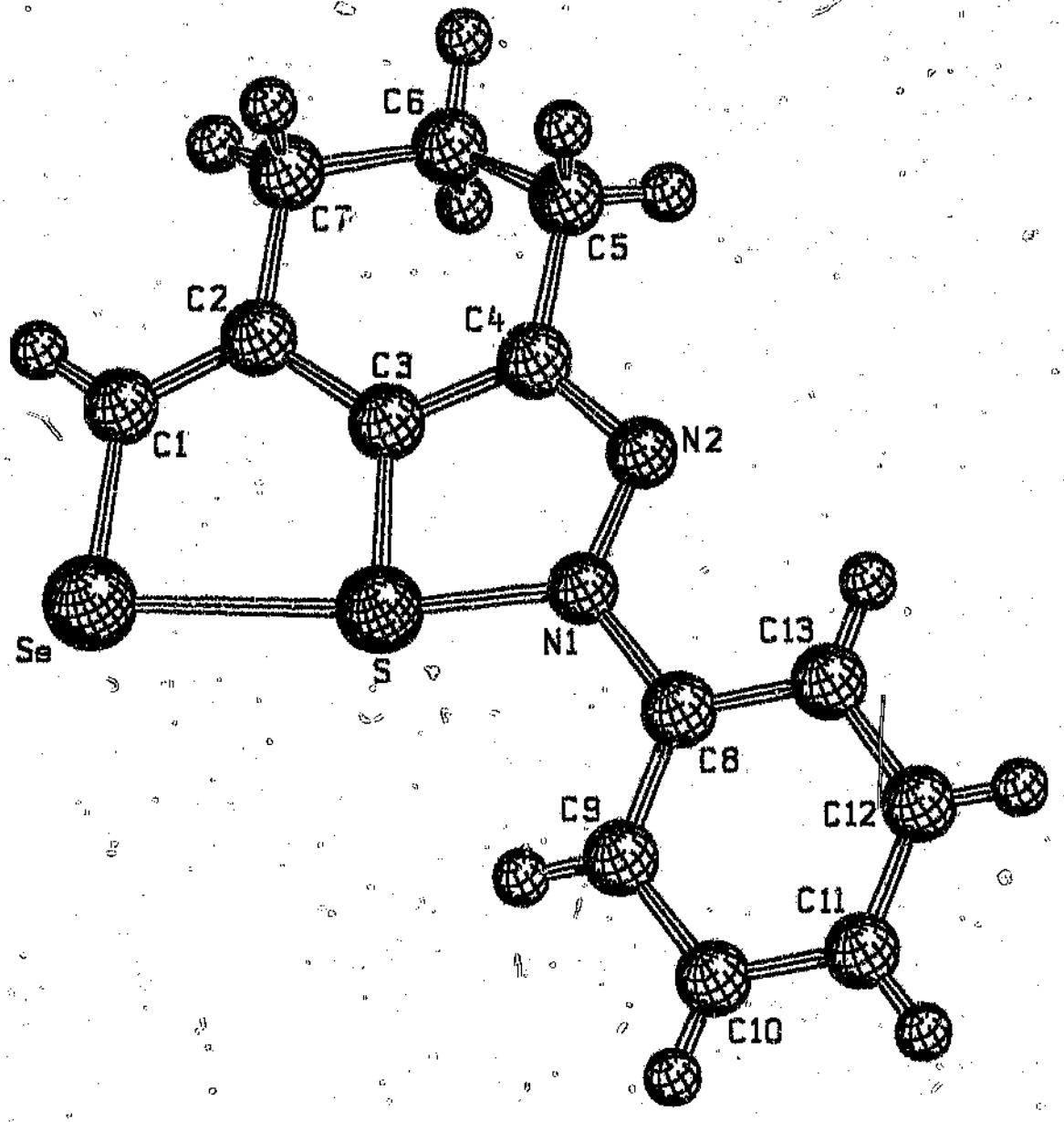


Figure 5.14: Labelled SCHAKAL diagram of ***13***

Table 5.33: Atomic coordinates (x 10^4) and equivalent isotropic displacement parameters ($Å^2$, x10^3) for ***13***

	x/a	y/b	z/c	U_{eq}
Se	1404(1)	3023(1)	1173(1)	74(1)
S	855(1)	2674(1)	3277(1)	50(1)
N(1)	-201(4)	2203(4)	4672(2)	43(1)
N(2)	-2037(4)	816(4)	4656(2)	50(1)
C(1)	-1120(5)	1099(5)	738(3)	61(1)
C(2)	-2334(5)	227(4)	1531(3)	49(1)
C(3)	-1658(4)	854(4)	2721(3)	45(1)

C(4)	-2831(5)	57(4)	3591(3)	47(1)
C(5)	-4916(5)	-1547(5)	3299(3)	58(1)
C(6)	-5769(5)	-1477(5)	2050(3)	58(1)
C(7)	-4395(5)	-1426(5)	1213(3)	58(1)
C(8)	929(5)	3299(4)	5722(3)	47(1)
C(9)	2674(5)	4976(5)	5689(3)	57(1)
C(10)	3809(6)	6047(5)	6715(3)	64(1)
C(11)	3175(6)	5496(6)	7745(3)	65(1)
C(12)	1434(6)	3844(6)	7775(3)	64(1)
C(13)	301(5)	2710(5)	6769(3)	58(1)

Table 5.34: Selected bond lengths (Å) for *13*	
Se-S	2.5891(10)
S-N(1)	1.617(3)
Se-C(1)	1.819(3)
S-C(3)	1.715(3)
N(1)-N(2)	1.321(3)
N(2)-C(4)	1.314(4)
C(1)-C(2)	1.350(5)
C(2)-C(3)	1.416(4)
C(3)-C(4)	1.406(4)

5.12 Discussion

The characteristic structural features of heterapentalenes include a planar bicyclic system and a linear tri-atomic sequence with elongated bonds. These features have been observed in the heterpentalene structures (listed in Table 5.35) that have been determined during the course of this work, as well as in the known structures listed in Table 5.36. The lengths of the bonds in the heterapentalene framework in these structures are listed in Table 5.37 using the labelling set out in Figure 5.15.

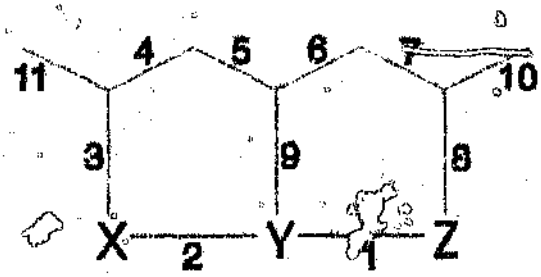
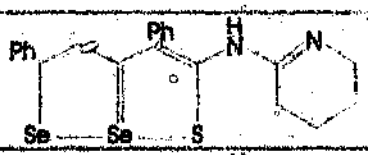
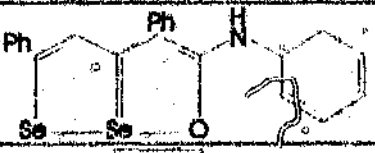
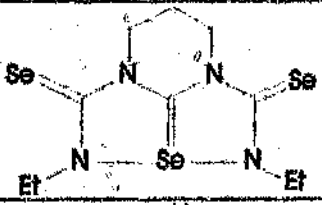
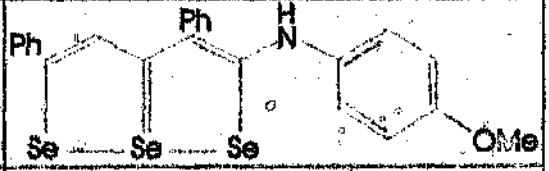
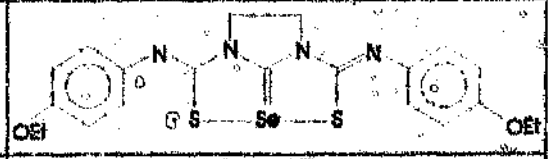
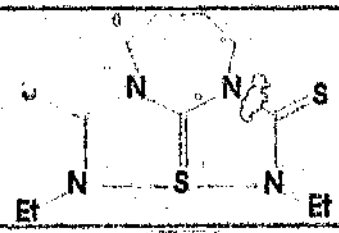
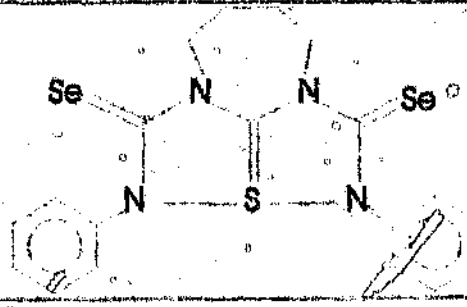


Figure 5.15 : Bond labels used.

A convenient way of looking at the bonding in these heterapentalene systems is in terms of a σ skeleton consisting of both localised and delocalised bonds; where the σ system in the tri-heteraatom sequence is equivalent to that in trihalide ions and may be referred to as a three-center four-electron bond. Futhermore, there is also a delocalised π system comprising the ten electrons in *p* orbitals perpendicular to the plane of the two fused rings, that is, a π system analogous to that in naphthalene. Hence the partial bonds in the linear tri-heteraatom sequence are both σ and π in character, but weaker than the other bonds in the molecule and therefore more susceptable to changes in bond length when the σ system or the π system is perturbed to some degree.

This dependence of the bond lengths, on the substitution pattern in the molecule has been discussed extensively in the case of 6a-thio-thiophenes (Hordvik and Saethre; 1972), and can also be seen in the bond lengths listed in Table 5.37.

Table 5.35 : New heterapentalene structures

Structure Code	
4	
5	
6	
7	
8	
9	
10	
11	
12	

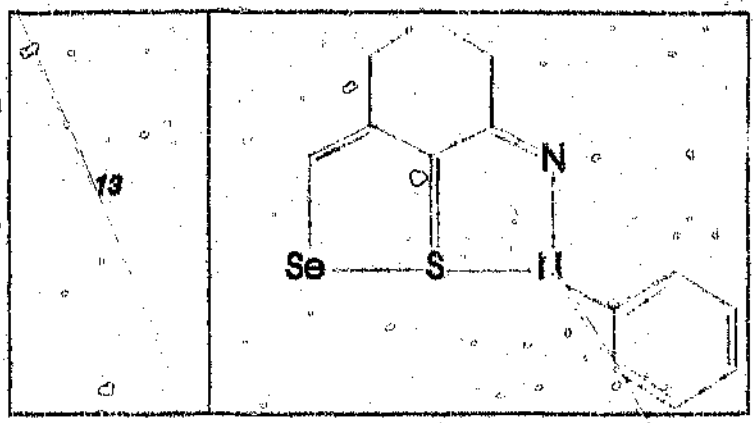
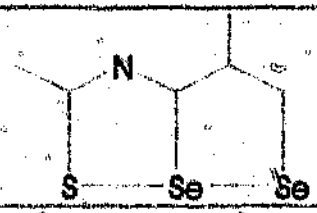
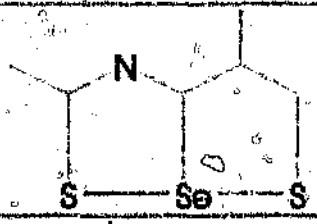
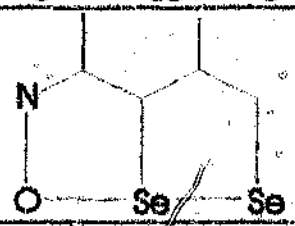
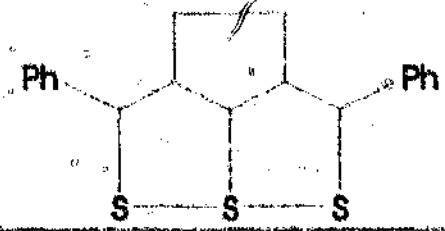
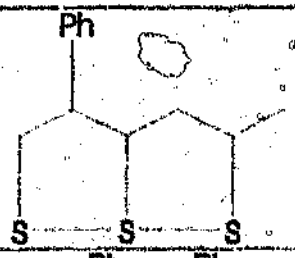
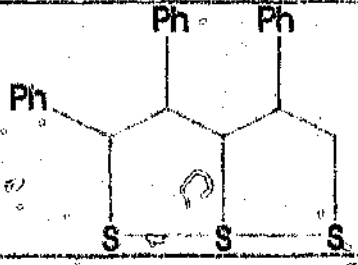
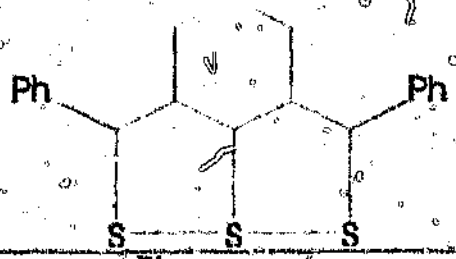
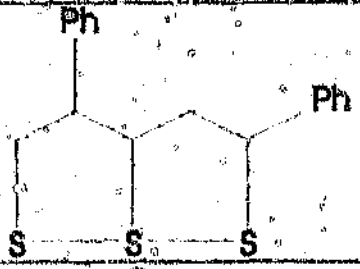
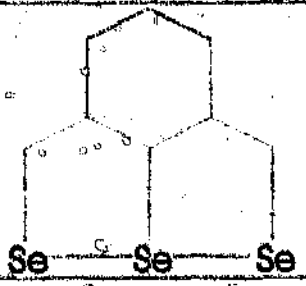


Table 5.36 : Known heterapentalene structures.

Identification code	Structure	Reference
(i)		Allen *et al*; 1987
(ii)		Allen *et al*; 1987
(iii)		Allen *et al*; 1987
(iv)		Birknes *et al*; 1982
(v)		Hordvik and Julshamn; 1971a

(vi)		Hordvik and Julshamn, 1971b
(vii)		Hordvik; 1971
(viii)		Birkness *et al*; 1975
(ix)		Hordvik *et al*; 1969
(x)		Hordvik and Porten; 1973
(xi)		Hansen and Hordvik; 1973

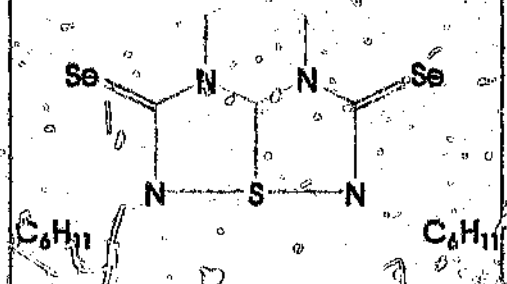
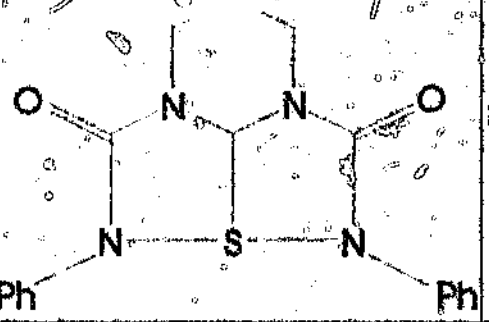
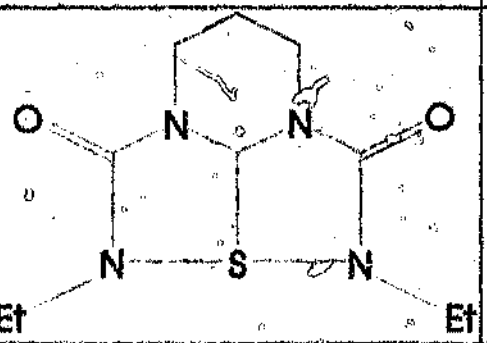
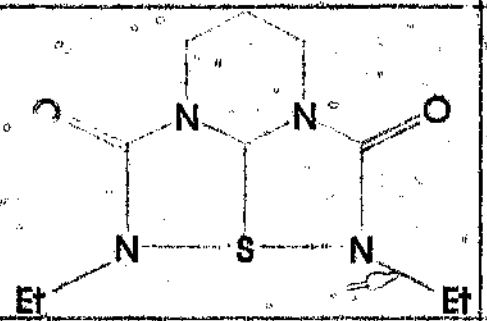
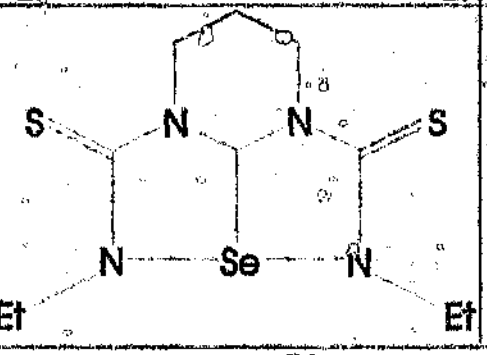
(xii)		Billing *et al*; 1991
(xiii)		Iwasaki *et al*; 1991
(xlv)		Iwasaki *et al*; 1991
(xv)		Iwasaki *et al*; 1991
(xvi)		Iwasaki *et al*; 1991

Table 5.37 : Observed heterapentalene bond lengths.

Structure	Linear hetero sequence	Bond										
		1	2	3	4	5	6	7	8	9	10	11
(i)	Se-Se-S	2.473(1)	2.507(2)	1.681(3)	1.302(3)	1.350(9)	1.402(10)	1.337(11)	1.830(8)	1.906(6)		
(ii)	S-Se-S	2.467(2)	2.372(2)	1.689(5)	1.310(6)	1.340(5)	1.393(6)	1.360(7)	1.687(6)	1.899(4)		
(iii)	Se-Se-O	2.444(2)	2.043(8)	1.318(12)	1.307(14)	1.442(14)	1.391(14)	1.39(2)	1.821(13)	1.858(10)		
(iv)	S-S-S	2.349(1)	2.349(1)	1.726(4)	1.372(5)	1.406(4)	1.406(4)	1.372(5)	1.720(4)	1.711(5)		
(v)	Se-Se-Se	2.579(3)	2.586(3)	1.856(29)	1.374(31)	1.427(31)	1.395(30)	1.371(28)	1.811(2[illegible]	1.904(23)		
(vi)	S-S-S	2.475(2)	2.237(2)	1.693(5)	1.362(6)	1.439(5)	1.393(6)	1.385(6)	1.688(5)	1.747(4)		
(vii)	S-S-S	2.371(4)	2.267(4)	1.676(8)	1.377(12)	1.430(11)	1.412(12)	1.367(12)	1.666(10)	1.755(8)		
(viii)	S-S-S	2.528(1)	2.287(1)	1.659(2)	1.378(3)	1.423(3)	1.423(3)	1.375(3)	1.698(2)	1.744(2)		
(ix)	S-S-S	2.499(3)	2.218(3)	1.669(7)	1.360(9)	1.448(11)	1.398(9)	1.374(11)	1.696(5)	1.741(5)		
(x)	Se-Se-Se	2.543(3)	2.563(3)	1.771(23)	1.375(24)	1.432(23)	1.414(22)	1.397(23)	1.811(22)	1.899(20)		
(xi)	S-S-S	2.350(1)	2.350(1)	1.673(3)	1.347(3)	1.401(2)	1.401(2)	1.347(3)	1.673(2)	1.737(3)		
(xii)	N-S-N	1.935(7)	1.931(7)	1.307(10)	1.414(10)	1.352(10)	1.345(10)	1.375(11)	1.724(9)	1.726(8)	1.844(9)	1.826(9)
(xiii)	N-S-N	1.969(6)	1.949(6)	1.318(9)	1.441(9)	1.329(9)	1.318(9)	1.432(9)	1.337(9)	1.717(7)	1.220(9)	1.217(9)
(xiv)	N-S-N	1.934(6)	1.920(6)	1.316(8)	1.446(7)	1.334(7)	1.329(7)	1.414(7)	1.337(8)	1.720(6)	1.223(7)	1.217(7)
(xv)	N-S-N	1.932(5)	1.943(5)	1.330(8)	1.439(7)	1.334(7)	1.334(7)	1.434(8)	1.311(3)	1.713(6)	1.225(6)	1.221(7)
(xvi)	N-Se-N	2.045(6)	2.022(6)	1.293(9)	1.419(9)	1.326(9)	1.331(9)	1.445(13)	1.294(13)	1.852(7)	1.676(12)	1.702(8)
4a	Se-S-Se	2.5909(12)	2.5044(12)	1.877(5)	1.418(5)	1.320(5)	1.334(5)	1.412(5)	1.884(5)	1.716(4)	1.271(5)	1.276(6)
4b	Se-S-Se	2.5239(14)	2.5007(14)	1.900(5)	1.407(5)	1.323(6)	1.329(5)	1.417(6)	1.889(5)	1.728(5)	1.272(6)	1.262(6)
5a	S-Se-Se	2.438(3)	2.465(2)	1.854(5)	1.369(8)	1.410(7)	1.402(8)	1.427(8)	1.681(6)	1.879(5)		
5b	S-Se-Se	2.435(3)	2.468(2)	1.861(5)	1.366(8)	1.409(8)	1.403(8)	1.417(8)	1.662(6)	1.873(5)		
6	O-Se-Se	2.348	2.3877(9)	1.872(4)	1.358(5)	1.432(5)	1.359(5)	1.461(6)	1.239(5)	1.894(4)		
7	Se-Se-Se	2.6560(8)	2.5360(6)	1.895(3)	1.408(4)	1.328(4)	1.321(4)	1.421(4)	1.694(3)	1.867(3)	1.259(4)	1.261(2)
8	N-Se-N	2.042(5)	2.030(5)	1.310(9)	1.440(8)	1.331(8)	1.344(7)	1.413(9)	1.298(9)	1.831(6)	1.838(6)	1.829(7)
9	Se-Se-Se	2.598(2)	2.542(2)	1.872(4)	1.361(6)	1.426(6)	1.399(5)	1.411(6)	1.855(4)	1.893(4)		
10a	S-Se-S	2.493(4)	2.478(4)	1.741(4)	1.400(5)	1.337(5)	1.324(5)	1.412(5)	1.732(4)	1.850(4)	1.284(5)	1.253(5)
10b	S-Se-S	2.516(4)	2.497(4)	1.742(3)	1.409(5)	1.326(4)	1.320(4)	1.417(5)	1.745(4)	1.849(3)	1.268(4)	1.284(4)
11	N-S-N	1.8765(13)	1.9032(14)	1.291(2)	1.428(2)	1.346(2)	1.342(2)	1.428(2)	1.300(2)	1.7149(13)	1.6797(14)	1.6819(13)
12a	N-S-N	1.900(3)	1.910(3)	1.302(4)	1.425(4)	1.344(4)	1.343(4)	1.419(4)	1.304(4)	1.719(3)	1.624(3)	1.826(3)
12b	N-S-N	1.901(3)	1.907(3)	1.300(4)	1.418(4)	1.340(4)	1.344(4)	1.410(4)	1.[illegible](4)	1.712(3)	1.826(3)	1.825(3)
13	N-S-Se	1.817(3)	2.5891(10)	1.819(3)	1.360(5)	1.416(4)	1.406(4)	1.314(4)	1.321(3)	1.715(3)		

When considering the bond lengths listed in Table 5.37, it is clear that the bond lengths within related heterapentalene fragments are similar. What is not clear, however, is whether the bonding in molecules containing different types of atoms within the heterapentalene structure is comparable. This question may be addressed by determining the orders of the bonds that make up the heterapentalene fragment.

The orders of bonds can be evaluated by using the empirically derived relation (Pauling; 1960)

$$\log_{10} n = \frac{(r_0 - r)}{c}$$

where n is the order of the bond of length r, r_0 represents the sum of the covalent radii of the atoms involved and c is an empirically derived constant. Table 5.38 lists the orders of the bonds listed in Table 5.37, as evaluated using this relation. The values used for the constant c and the covalent radii are those suggested by Pauling (1960), and may be in need of some refining. The results are nevertheless very informative. For example, if one looks at the sum of the bond orders of bonds 1 and 2, it is consistently close to unity. This result is consistent with what would be expected for three-center four-electron bonds. Another interesting observation relates to the order of bonds 4 and 7. It is clear that two different amounts of delocalisation are present. The two extreme cases are illustrated in Figure 5.16 with the average bond orders for the two cases are shown in Figure 5.17. The asymmetry observed in the bond orders can be ascribed to the asymmetric substitution pattern found in most of the studied compounds.



Figure 5.16.: Types of delocalisation observed in heterapentalenes

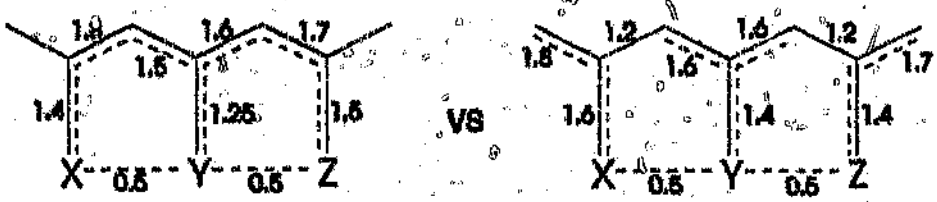


Figure 5.17 : Average bond orders.

Table 5.38 : Calculated orders of heterapentalene bonds.

	Bond										
Structure	1	2	3	4	5	6	7	8	9	10	11
(I)	0.7	0.4	1.5	1.7	1.5	1.6	1.8	1.4	1.1		
(II)	0.6	0.4	1.5	1.7	1.5	1.6	1.8	1.5	1.2		
(III)	0.7	0.5	1.2	1.7	1.4	1.6	1.7	1.5	1.3		
(IV)	0.4	0.4	1.4	1.8	1.6	1.6	1.8	1.4	1.4		
(V)	0.5	0.5	1.3	1.7	1.5	1.6	1.8	1.5	1.1		
(VI)	0.3	0.6	1.5	1.6	1.4	1.6	1.7	1.5	1.2		
(VII)	0.4	0.5	1.5	1.7	1.4	1.5	1.6	1.8	1.2		
(VIII)	0.5	0.5	1.4	1.7	1.5	1.5	1.7	1.7	1.3		
(IX)	0.3	0.6	1.6	1.8	1.4	1.6	1.7	1.7	1.3		
(X)	0.5	0.5	1.7	1.7	1.4	1.5	1.6	1.6	1.2		
(XI)	0.4	0.4	1.6	1.9	1.6	1.6	1.9	1.9	1.3		
(XII)	0.5	0.5	1.7	1.2	1.5	1.5	1.4	1.4	1.3	1.4	1.5
(XIII)	0.5	0.5	1.7	1.1	1.6	1.7	1.1	1.1	1.4	2	2
(XIV)	0.6	0.6	1.7	1.1	1.6	1.6	1.2	1.2	1.4	2	2
(XV)	0.5	0.5	1.6	1.1	1.6	1.6	1.1	1.1	1.4	2	2
(XVI)	0.6	0.6	1.6	1.2	1.6	1.6	1.1	1.1	1.3	1.6	1.4
4a	0.4	0.4	1.2	1.2	1.6	1.6	1.2	1.2	1.4	1.9	1.9
4b	0.3	0.4	1.2	1.2	1.6	1.6	1.2	1.2	1.3	1.9	2
5a	0.4	0.7	1.3	1.8	1.5	1.6	1.5	1.5	1.2		
5b	0.4	0.6	1.3	1.8	1.6	1.6	1.5	1.5	1.3		
7	0.4	1.4	1.2	1.2	1.6	1.6	1.2	1.2	1.3	2	2
8	0.6	0.6	1.7	1.1	1.6	1.5	1.2	1.6	1.4	1.4	1.4
9	0.4	0.5	1.3	1.8	1.5	1.6	1.5	1.3	1.2		
10a	0.4	0.4	1.3	1.3	1.6	1.6	1.2	1.3	1.4	1.8	2
10b	0.4	0.4	1.3	1.2	1.6	1.6	1.2	1.3	1.4	1.9	1.8
11	0.6	0.6	1.8	1.2	1.5	1.5	1.2	1.8	1.4	1.5	1.5
12a	0.6	0.6	1.7	1.2	1.5	1.5	1.2	1.7	1.4	1.5	1.5
12b	0.6	0.6	1.8	1.2	1.6	1.5	1.2	1.7	1.4	1.5	1.5
13	0.8	0.3	1.5	1.8	1.5	1.6	1.7	1.3	1.4		

These average bond orders may be used to predict the expected bond lengths in other related compounds. The bond order calculations may also be refined by improved estimates of the empirical constant as well as the covalent radii of the atoms. It would be interesting to see if the calculated bond orders could be used to predict the bond lengths in tellurium containing heterapentalenes. The advantage of considering these structures in terms of the observed bond orders, instead of bond lengths, lies therein that structures containing different types of atoms may readily be compared.

CHAPTER 6

Conformational preferences in single *ortho*, N-substituted acetanilide derivatives.

The relative spatial disposition of the moieties attached to the nitrogen atom in single-*ortho*, N-substituted acetanilide derivatives has long been of interest (Staskun; 1980 and Baert *et al*; 1984). The dispositions of particular interest is the preferred conformation of the amide carbonyl group (Figure 6.1) as well as that of the alkyl substituent on the methylene bridge (Figure 6.2).

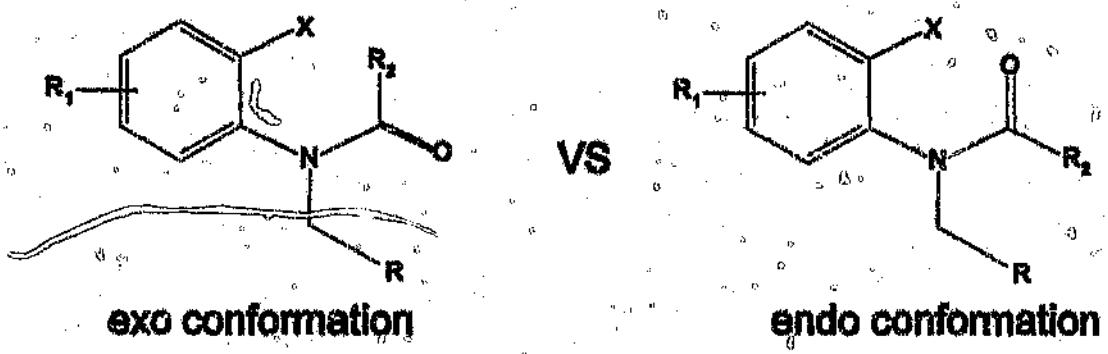


Figure 6.1: Possible orientations of the carbonyl group

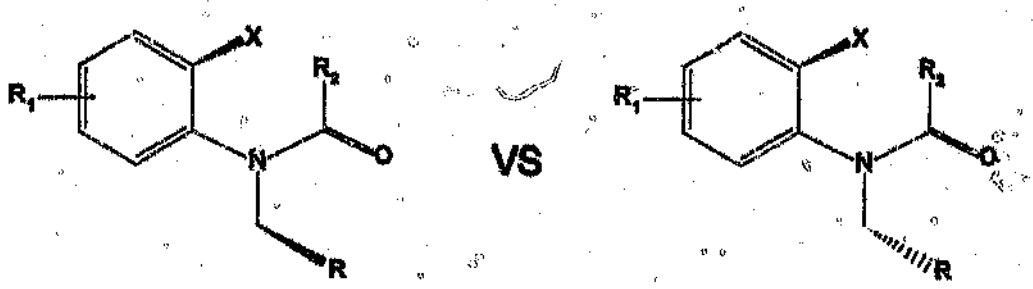
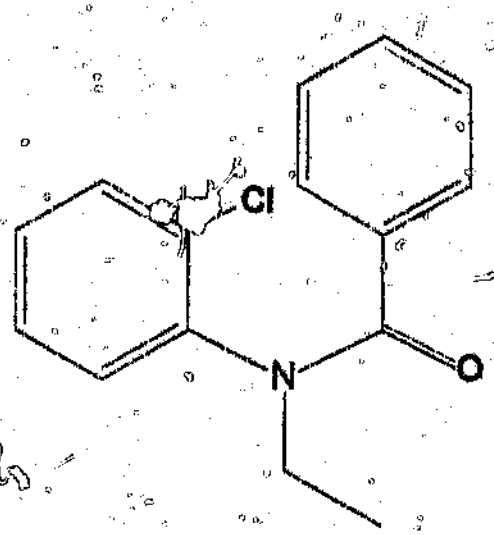
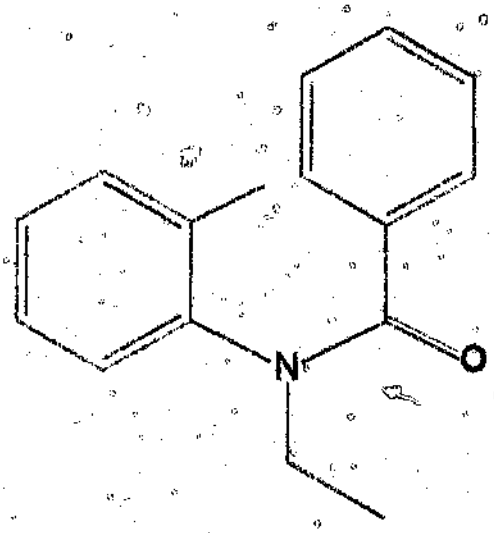


Figure 6.2 : Possible orientations of the alkyl group

Previous studies have included investigations into the preferred conformation in the solid state as well as in solution. The determination of the crystal structures of ***14*** and ***15***, contributes to this growing body of knowledge. The observed conformations may be compared by referring to the torsion angles defined in Figure 6.3.



14



15

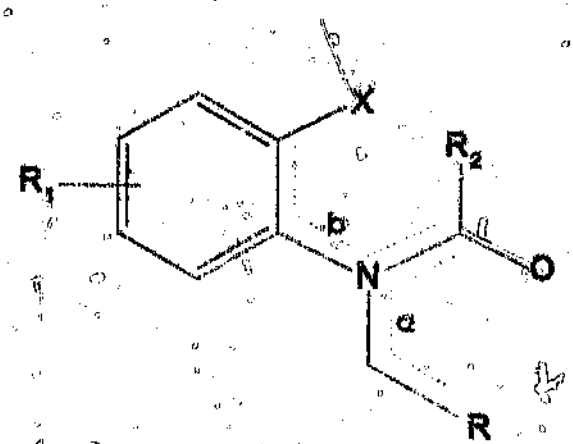
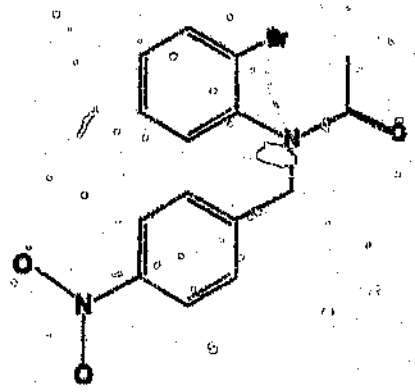
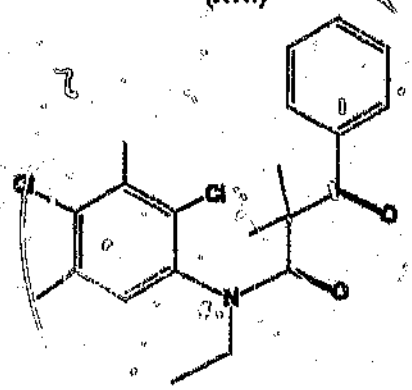


Figure 6.3 : Torsion angles used to describe conformation

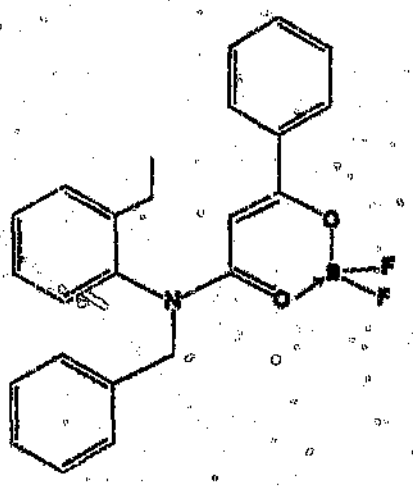
When the crystal structures of compounds ***14*** and ***15*** were determined, the amide carbonyl group was found in the *exo*-conformation in both structures. Further, the *ortho* substituent,X, on the phenyl ring, and the R group attached to the nitrogen atom via the methylene bridge were found on the same side of the amide plane. This is clear from the fact that the torsion angles (a and b in Figure 6.3) listed in Table 6.1 have the same sign. This result differs from that of Boeyens and co-workers (1987), who in their investigation into the structures of three single-*ortho*, N-substituted amide derivatives, (xvii), (xviii) and (xix), found the *ortho* substituent and the R group on opposite sides of the amide plane. (The torsion angles a and b for (xvii), (xviii) and (xix) listed in Table 6.1 have opposite signs). In all five structures considered, the amide carbonyl group is found in the *exo* conformation. It would thus appear that while the conformation of the amide carbonyl group is independent of the nature of the acyl group, the preferred conformation of the alkyl substituent, R, may not be. A molecular mechanics study should be able to reveal if the conformation adopted by ***14*** and ***15***, is indeed a low-energy conformation, or merely their preferred conformation in the solid state.



(xvii)



(xviii)



(xix)

Table 6.1 : Torsion angles define in figure 6.1		
Compound	Torsion angle a	Torsion angle b
14	102.0(2)	-63.5(2)
15	104.3(3)	-65.6(3)
(xvii)	-91(2)	-91(2)
(xviii)	93.5(3)	106.7(3)
(xix)	101.6(8)	100.2(9)

The crystal structures of ***14*** and ***15*** were determined from data collected on Enraf Nonius diffractometers, using graphite monochromated Mo-Kα radiation. In each case the cell was detemined from 25 accurately measured high-order reflections. Data reduction included corrections for Lorentz and polarisation effects using standard Enraf Nonius routines. Standard reflections monitored hourly showed only random fluctuations. Unit cell parameters and the details of the data collections are given in Table 6.2. The structures were solved by direct methods using SHELXS86, and refined by least-squares methods, based on F^2, using SHELXL93. All non-hydrogen atoms were refined with anisotropic displacement parameters, while H atoms were refined in riding mode with a common isotropic displacement parameter. Figure 6.4 and Figure 6.5 show SCHAKAL diagrams of the compounds and indicate the labelling schemes used. Atomic coordinates are listed in Tables 6.3 and 6.4 respectively.

Table 6.2 : Crystal and refinement data		
Compound	*14*	*16*
Empirical formula	$C_{15}H_{14}ClNO$	$C_{15}H_{17}NO$
Formula weight / g.mol^{-1}	259.72	239.31
Temperature / K	293(2)	293(2)
Wavelength / Å	0.71069	0.71069
Crystal system	Monoclinic	Monoclinic
Space group	P $2_1/n$	P $2_1/n$
a / Å	9.387(3)	9.393(4)
b / Å	13.5896(9)	13.627(2)
c / Å	10.589(4)	10.69(2)
α / °	90	90
β / °	101.81(2)	102.42(9)
γ / °	90	90
Volume / Å^3	1322.2(7)	1366(3)
z	4	4
ρ / Mg.m^{-3}	1.305	1.19
Absorption coefficient / mm^{-1}	0.276	0.074
F(000)	544	512
Range	$2.5 \leq \theta \leq 30$	$3 \leq \theta \leq 30$
Index ranges : h k l	 -13 → 13 -1 → 19 -1 → 14	 -13→13 -1→19 -1→15
Reflections collected	4738	4789
Independent reflections	3831	3883
R_{int}	0.013	0.0393
Data/restraints/parameters	3831/0/164	3883/0/164
Max shift, Δz	0	0.001
Residual density / e.Å^{-3} $(\Delta\rho)_{max}$ $(\Delta\rho)_{min}$	 0.249 -0.302	 0.500 -0.572
Reliability indices R1 (I > 2σ(I)) wR2 (I > 2σ(I)) R1 (all data) wR2 (all data)	 0.0411 0.1284 0.0662 0.1357	 0.1076 0.3348 0.1495 0.3704
S	1.084	1.056

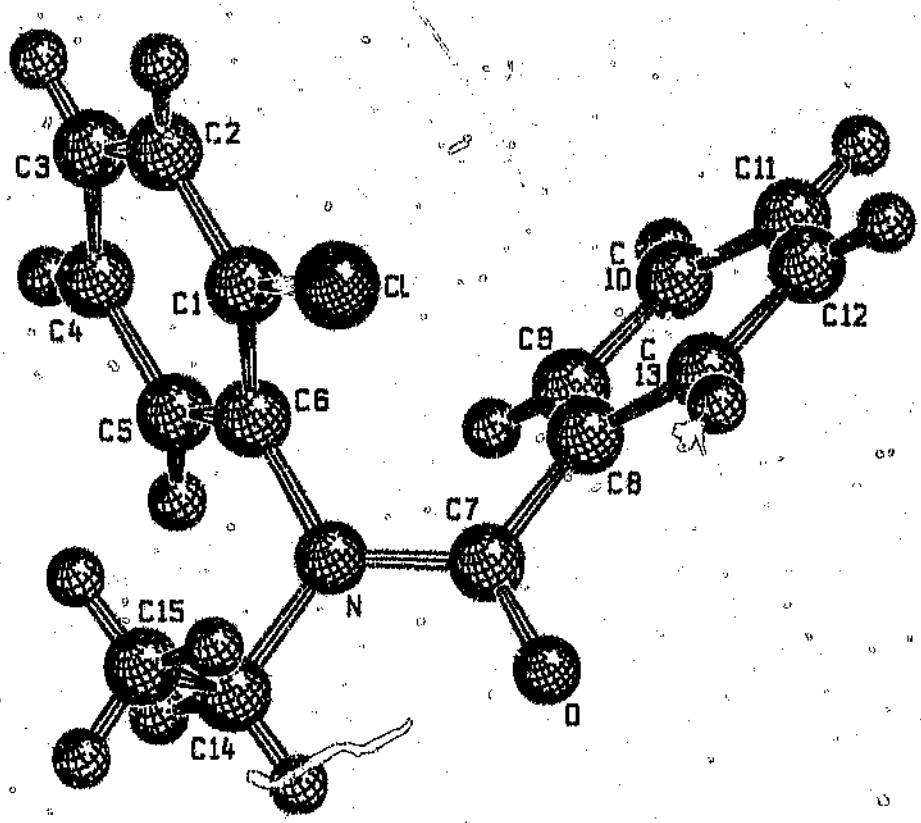


Figure 6.4 : Labelled SCHAKAL diagram of ***14***

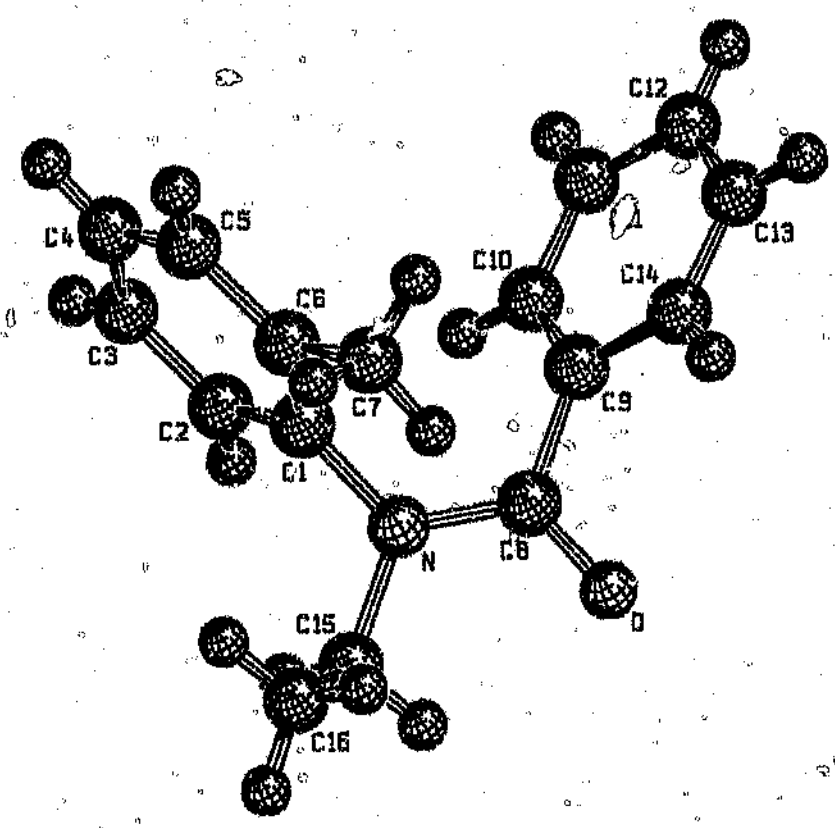


Figure 6.5: Labelled SCHAKAL diagram of ***15***

Table 6.2 : Atomic coordinates (x 10^4) and equivalent isotropic displacement parameters ($Å^2$, x10^3) for *14*

	x/a	y/b	z/c	U_{eq}
Cl	1698(1)	6211(1)	3689(1)	58(1)
O	916(1)	5552(1)	7060(1)	63(1)
N	2455(1)	6705(1)	6543(1)	45(1)
C(1)	2426(1)	7316(1)	4349(1)	41(1)
C(2)	2710(1)	8055(1)	3530(1)	49(1)
C(3)	3288(2)	8936(1)	4035(2)	57(1)
C(4)	3587(2)	9088(1)	5346(2)	58(1)
C(5)	3305(1)	8350(1)	6168(1)	52(1)
C(6)	2706(1)	7459(1)	5678(1)	41(1)
C(7)	1096(2)	6336(1)	6542(1)	44(1)
C(8)	-190(1)	6944(1)	5939(1)	42(1)
C(9)	-277(2)	7945(1)	6195(1)	50(1)
C(10)	-1540(2)	8462(1)	5714(2)	63(1)
C(11)	-2721(2)	7986(1)	4971(1)	66(1)
C(12)	-2643(2)	7006(1)	4719(2)	63(1)
C(13)	-1394(2)	6476(1)	5196(1)	53(1)
C(14)	3748(2)	6199(1)	7295(2)	61(1)
C(15)	4523(2)	5583(2)	6489(2)	77(1)

Table 6.3 : Atomic coordinates (x 10^4) and equivalent isotropic displacement parameters ($Å^2$, x10^3) for *15*

	x/a	y/b	z/c	U_{eq}
O	909(2)	561(2)	1950(2)	72(1)
N	2455(2)	1686(2)	1442(2)	51(1)
C(1)	2734(2)	2448(2)	618(2)	45(1)
C(2)	3287(3)	3345(2)	1144(2)	58(1)
C(3)	3587(3)	4092(2)	390(3)	66(1)
C(4)	3336(3)	3964(2)	-924(3)	65(1)
C(5)	2794(3)	3086(2)	-1462(2)	57(1)
C(6)	2478(2)	3211(2)	-718(2)	46(1)
C(7)	1928(3)	1350(2)	-1331(2)	59(1)
C(8)	1097(3)	1326(2)	1439(2)	50(1)
C(9)	-192(2)	1950(2)	839(2)	45(1)
C(10)	-265(3)	2943(2)	1074(2)	55(1)
C(11)	-1528(3)	3461(2)	614(3)	64(1)
C(12)	-2735(3)	2995(3)	-120(3)	71(1)
C(13)	-2662(3)	1994(3)	-366(3)	71(1)
C(14)	-1411(3)	1485(2)	108(2)	59(1)
C(15)	3736(3)	1203(2)	2251(3)	67(1)
C(16)	4562(4)	582(3)	1501(4)	88(1)

CHAPTER 7

X-ray diffraction study of TGS

Due to its electro-optic properties triglycine sulphate (TGS) has been studied extensively. Of particular interest has been the effect that doping the crystals with impurities has on its ferroelectric properties. (Ravi *et al* ; 1993). The influence of laser light on its X-ray diffraction pattern has also been investigated (Zhukov *et al*, 1991). In this study it was found that the intensities of some of the Bragg reflections increased significantly when TGS was irradiated with laser light perpendicular to its b-axis.

The aim of this study was to try and reproduce the results obtained by Zhukov and co-workers in 1991, and also to investigate the H-bonding network present in TGS by means of a low temperature diffraction study. It was hoped that this could lead to some understanding of the influence of laser light on the diffraction pattern.

Very large crystals of the title complex were grown from aqueous solutions containing stoichiometric amounts of glycine (NH_2CH_2COOH) and sulphuric acid (H_2SO_4) by slow evaporation. Crystals selected for analysis were ground into spheres with radii in the range 0.2 to 0.3 mm, using a Nonius crystal grinder. Cell determinations, using 25 high-order reflections, and data collections were done on Enraf-Nonius CAD4 four-circle diffractometers equipped with graphite monochromators and Mo-Kα radiation. The low temperature data was collected using the cryostat described in chapter 4. Because of the shape of the crystals used and the relatively light elements present in the crystals, no absorption corrections were applied to the data.

Unit cell parameters and details of the data collections are given in Table 7.1. Atomic coordinates for the structures are listed in Table 7.2 and 7.3 respectively. The structures were refined, starting with coordinates retrieved from the Cambridge Crystallographic Database for a previous analysis (Solans *et al*, 1985), by least-squares methods based on F^2 using SHELXL93. The ORTEP diagrams shown

in Figures 7.1 and 7.2 show the numbering scheme used in the analysis. In both structures, the positions of the hydrogen atoms not involved in hydrogen bonding were calculated geometrically, and refined riding on the atom to which it is bonded.

The remaining two hydrogen atoms are both involved in hydrogen bonding and their positions were inferred from the difference Fourier maps, calculated using the low-temperature data, shown in Figures 7.3 and 7.4. These positions were refined isotropically using a common isotropic displacement parameter for all the hydrogen atoms. Table 7.4 lists the coordinates of all the hydrogen atoms as determined from the low-temperature data. The hydrogen bonds present in the crystal are illustrated in Figure 7.5, whilst the stacking of the molecules along the c-axis is shown in the packing diagram in Figure 7.6. It is interesting to note that at a first glance all the glycine molecules in TGS are present in the zwitterionic form of glycine ($H_3N^+CH_2CO_2^-$).

Table 7.1 : Crystal and refinement data

Compound	*16*	*17*
Empirical formula	$C_6H_{17}N_3O_{10}S$	$C_6H_{17}N_3O_{10}S$
Formula weight / g.mol^{-1}	323.29	323.29
Temperature / K	293(2)	100(2)
Wavelength / Å	0.71069	0.71069
Crystal system	Monoclinic	Monoclinic
Space group	P 2_1	P 2_1
a / Å	9.1669(8)	9.1508(4)
b / Å	12.649(1)	12.5890(5)
c / Å	5.731(6)	5.6047(2)
β / °	105.554(8)	105.180(4)
Volume / Å^3	640.1(7)	632.08(4)
z	2	2
ρ / Mg.m^{-3}	1.677	1.699
Absorption coefficient / mm^{-1}	0.311	0.315
F(000)	340	340
Crystal diameter / mm	0.6	0.4
Range	$2.8 \leq \theta \leq 35$	$2.3 \leq \theta \leq 62$
Index ranges : h k l	 -14 → 14 -1 → 20 -7 → 9	 -22 → 21 -1 → 31 -10 → 13
Reflections collected	3066	6552
Independent reflections		9283

R_{int}		0.048
Data/restraints/parameters	3066 / 0 / 182	9283 / 0 / 190
Max shift, Δz		
Residual density / e.Å^{-3} $(\Delta\rho)_{max}$ $(\Delta\rho)_{min}$	 0.549 -0.380	 1.032 -1.064
Reliability indices R1 ($I > 2\sigma(I)$) wR2 ($I > 2\sigma(I)$) R1 (all data) wR2 (all data)	 0.0295 0.0993 0.0299 0.0999	 0.0281 0.0885 0.0317 0.0914
S	0.915	1.069

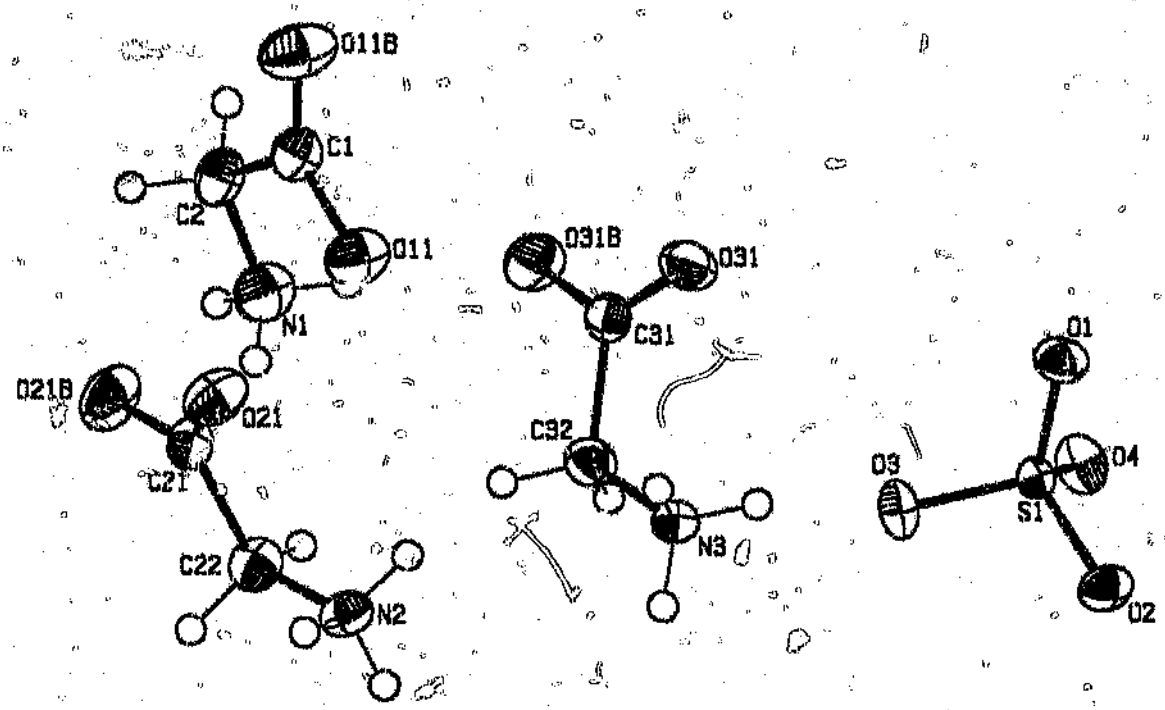


Figure 7.1 : Labelled ORTEP diagram of ***16***

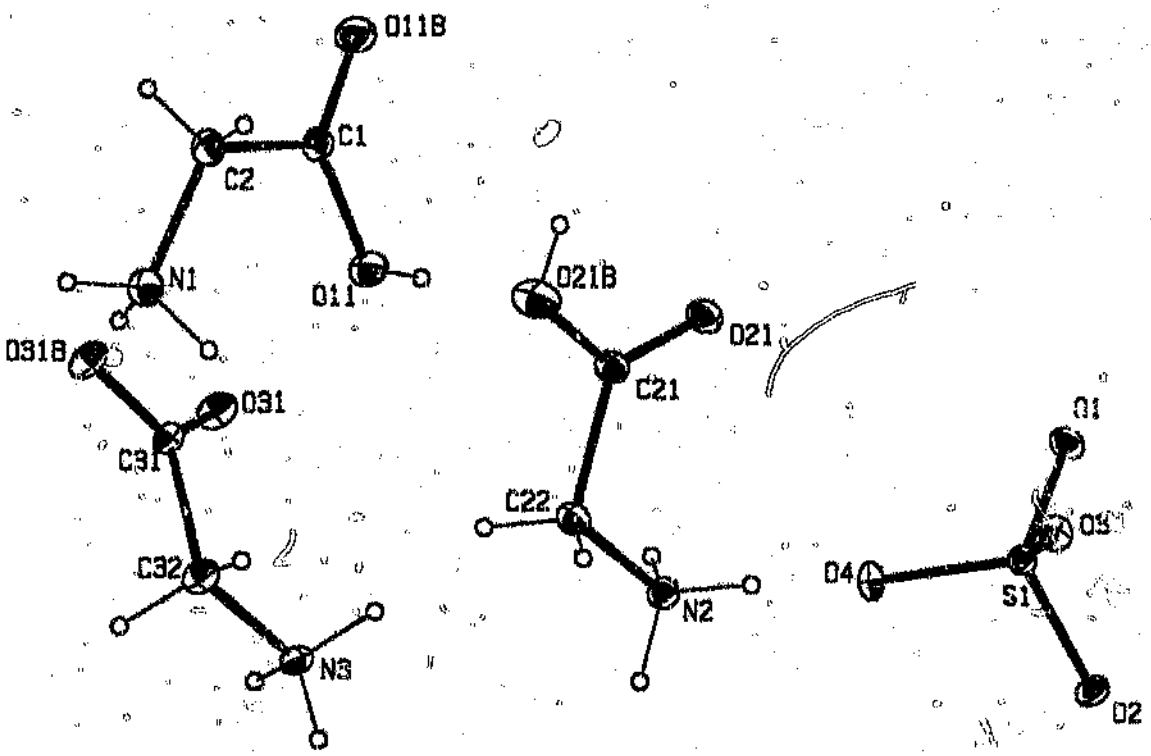


Figure 7.2 : Labelled ORTEP diagram of ***17***

Table 7.2: Atomic coordinates (x 10^4) and equivalent isotropic displacement parameters ($Å^2$, x10^3) for ***16***

	x/a	y/b	z/c	U_{eq}
S(1)	9997(1)	2500	2735(1)	17(1)
O(1)	9655(1)	2517(1)	85(2)	30(1)
O(2)	8574(1)	2494(1)	3507(2)	28(1)
O(3)	10874(1)	1559(1)	3745(3)	30(1)
O(4)	10849(1)	3463(1)	3764(2)	29(1)
O(11)	6068(1)	2423(2)	10287(2)	36(1)
O(11B)	4953(2)	2328(2)	13288(2)	48(1)
C(1)	4894(1)	2401(2)	11170(3)	28(1)
C(2)	3401(1)	2446(2)	9248(3)	30(1)
N(1)	3583(2)	2874(2)	6939(2)	40(1)
O(21)	2137(2)	4982(1)	-480(3)	36(1)
O(21B)	4484(2)	5192(2)	1925(3)	45(1)
C(21)	3019(2)	5238(1)	1424(3)	28(1)
C(22)	2485(2)	5685(2)	3500(3)	30(1)
N(2)	831(2)	5732(1)	2887(2)	26(1)
O(31)	7793(2)	4951(1)	10553(3)	36(1)
O(31B)	5392(1)	4682(2)	8405(3)	39(1)
C(31)	6832(2)	4678(1)	8710(3)	25(1)
C(32)	7295(2)	4301(2)	6508(3)	30(1)
N(3)	8946(2)	4295(1)	6964(3)	26(1)

Table 7.3: Atomic coordinates (x 10^4) and equivalent isotropic displacement parameters ($Å^2$, x10^3) for *17*

	x/a	y/b	z/c	U_{eq}
S(1)	9988(1)	2500	2707(1)	6(1)
O(1)	9675(1)	2525(1)	27(1)	10(1)
O(2)	8547(1)	2486(1)	3447(1)	10(1)
O(3)	10878(1)	1553(1)	3709(1)	10(1)
O(4)	10828(1)	3474(1)	3752(1)	10(1)
O(11)	6081(1)	2873(1)	10144(1)	13(1)
O(11B)	4969(1)	2244(1)	13209(1)	15(1)
C(1)	4905(1)	2335(1)	11054(1)	10(1)
C(2)	3404(1)	2408(1)	9139(1)	11(1)
N(1)	3573(1)	2887(1)	6845(1)	11(1)
O(21)	2097(1)	4971(1)	-466(1)	13(1)
O(21B)	4432(1)	5108(1)	2073(1)	17(1)
C(21)	2962(1)	5204(1)	1500(1)	10(1)
C(22)	2412(1)	5858(1)	3580(1)	11(1)
N(2)	747(1)	5738(1)	2888(1)	9(1)
O(31)	7769(1)	4907(1)	10611(1)	12(1)
O(31B)	5374(1)	4660(1)	8474(1)	12(1)
C(31)	6811(1)	4652(1)	8746(1)	9(1)
C(32)	7272(1)	4302(1)	6483(1)	11(1)
N(3)	8937(1)	4294(1)	6939(1)	9(1)

Table 7.4: Hydrogen coordinates (x 10^4) and isotropic displacement parameters ($Å^2$, x10^3) for *17*

	x/a	y/b	z/c	U_{eq}
H(2A)	3036(7)	1799(11)	8879(5)	24(1)
H(2B)	2802(11)	2774(7)	9879(10)	24(1)
H(1A)	2611(11)	3042(10)	5823(15)	24(1)
H(1B)	4073(13)	2406(7)	6058(15)	24(1)
H(1C)	4141(14)	3515(9)	7201(5)	24(1)
H(22A)	2718(5)	5233(7)	4910(22)	24(1)
H(22B)	2821(7)	6312(11)	3974(6)	24(1)
H(2C)	442(4)	5994(10)	4121(17)	24(1)
H(2D)	351(5)	5104(8)	2503(24)	24(1)
H(2E)	453(4)	6165(10)	1626(22)	24(1)
H(32A)	6893(6)	3823(10)	8029(7)	24(1)
H(32B)	6855(5)	4766(7)	5199(20)	24(1)
H(3A)	9188(3)	4048(10)	5817(20)	24(1)
H(3B)	9340(5)	3873(11)	8216(22)	24(1)
H(3C)	9294(5)	4956(9)	7261(23)	24(1)
H(1)	7069(20)	2516(21)	11269(33)	24(1)
H(2)	4647(21)	4877(20)	1003(34)	24(1)

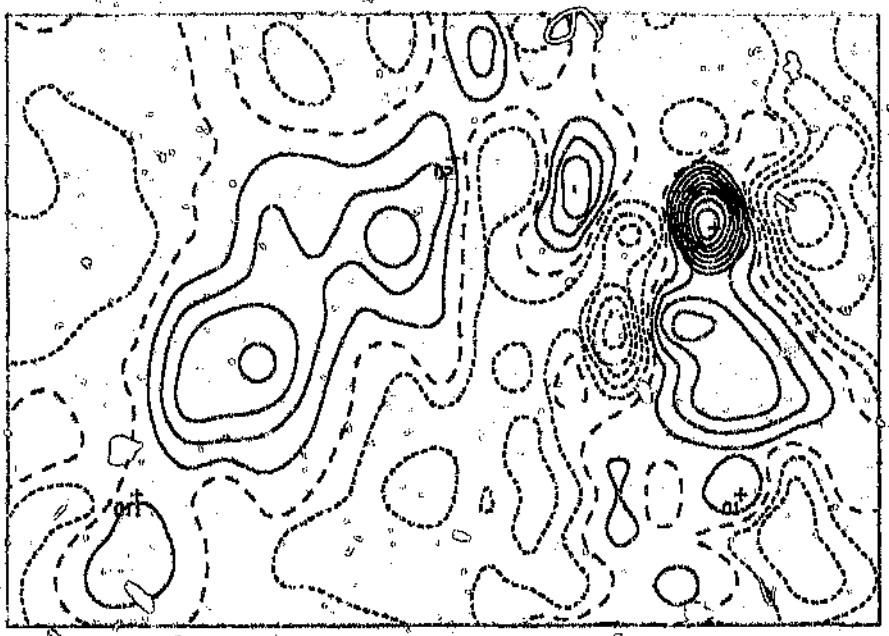


Figure 7.3 : Difference Fourier map through O(11), O(1) and O(2)

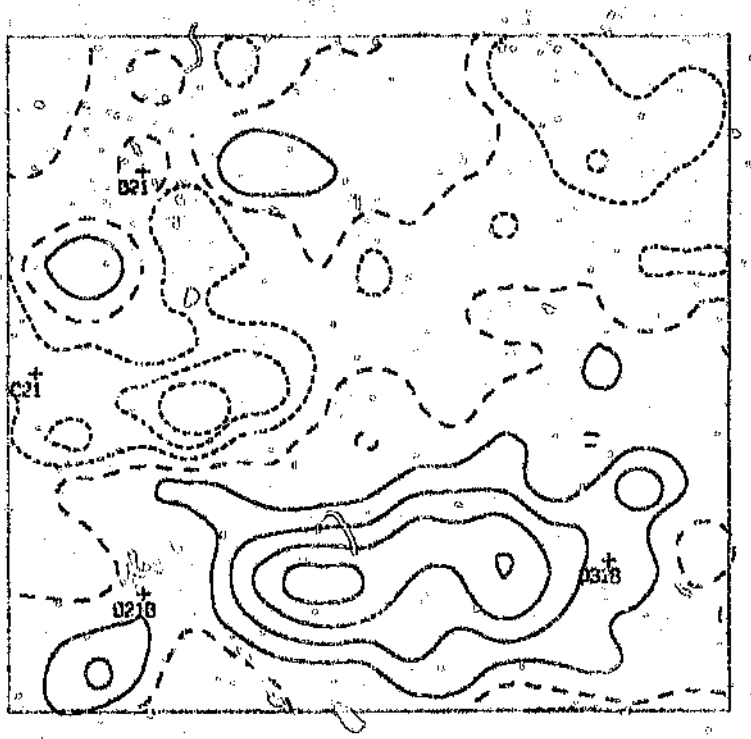


Figure 7.4 : Difference Fourier map through O(21), O(21B) and O(31B)

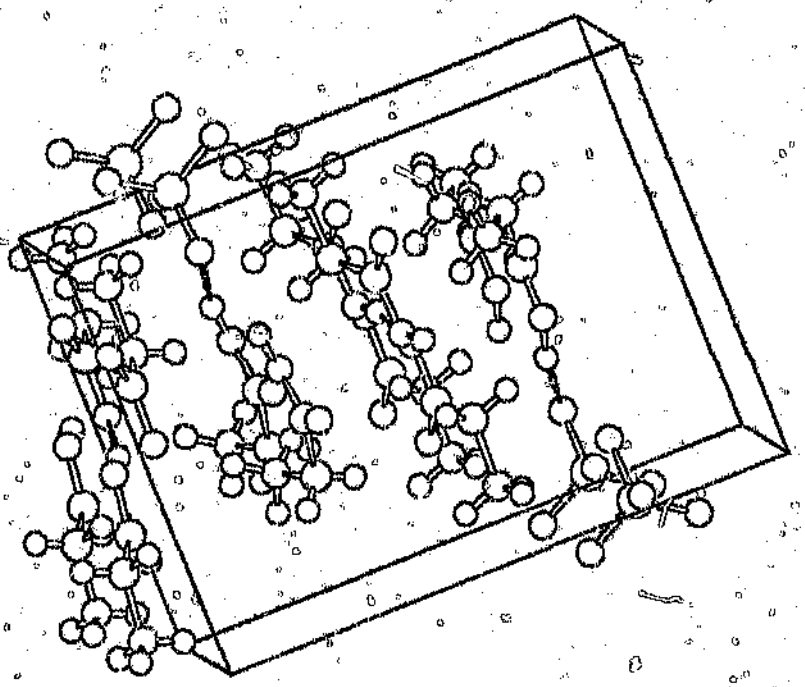


Figure 7.5 : Packing diagram showing the hydrogen bonds.

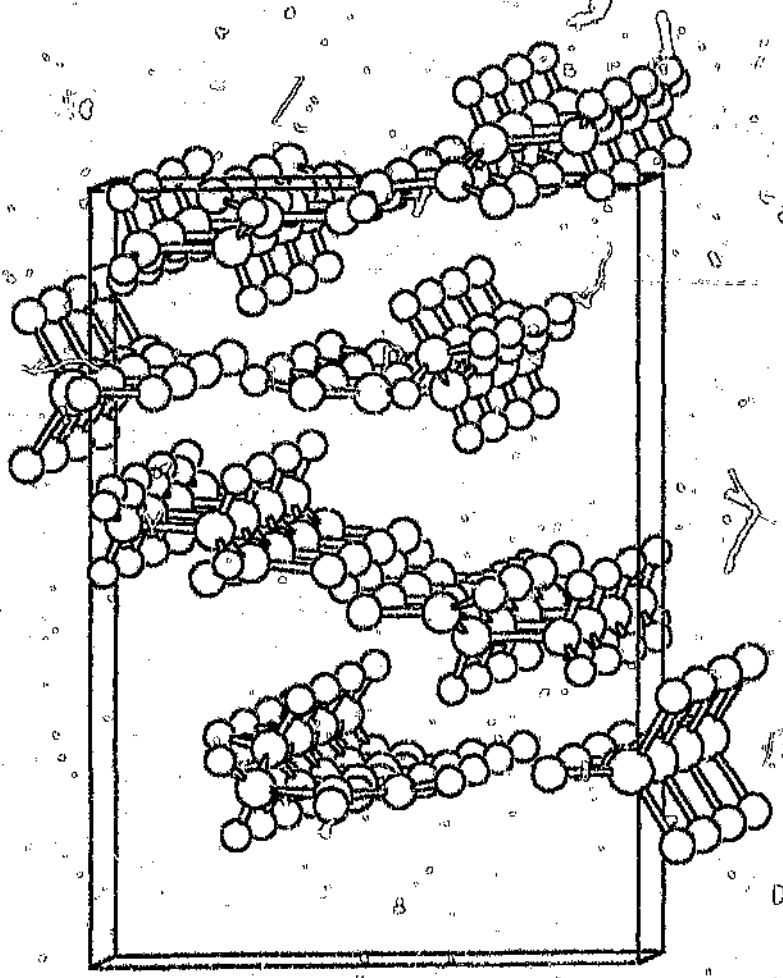


Figure 7.6 : Packing diagram showing the stacking of the molecules

In a previous investigation, increases of up to 30% in the integrated intensities of the Bragg reflections of TGS, when irradiated by laser light (λ = 630 nm) perpendicular to the b-axis have been reported. (Zhukov *et al*, 1991) It was also reported that the intensity maximum was reached just after switching the laser radiation on and that the most noticeable changes where observed for low-angle reflections.

In our analysis TGS crystals were irradiated with laser light from a battery-powered solid state diode laser (λ = 670 nm) mounted on the goniometer head as shown in Figure 7.7. Before any measurements were made it was ensured that the additional strain placed on goniometerhead by the mounted laser did not cause the centered crystal to move within the X-ray beam. Care also had to be taken throughout the study to ensure that the laser and its mount did not cause any collisions between the various diffractometer arms.

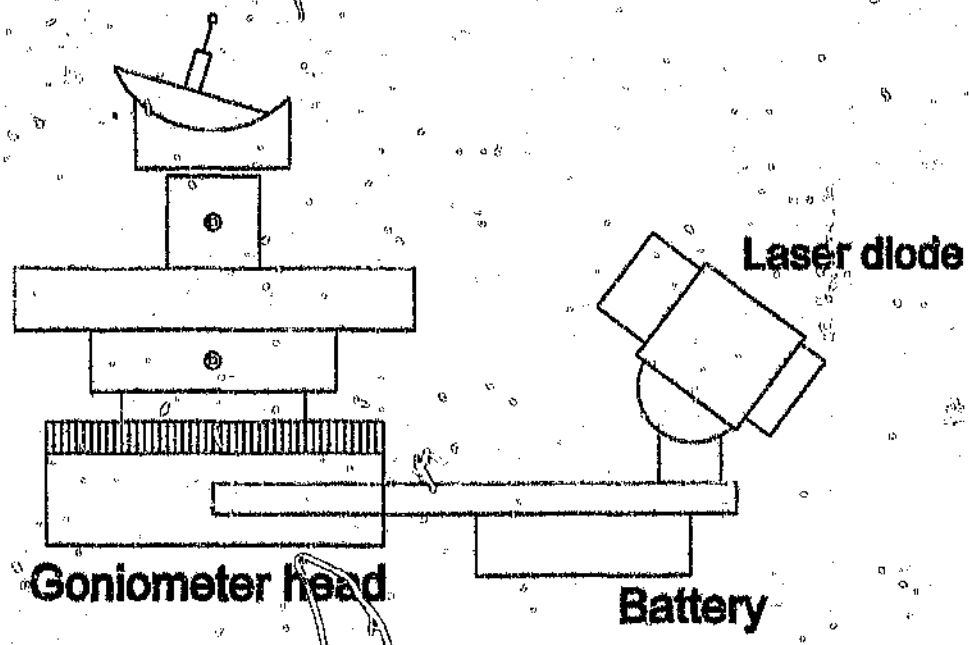


Figure 7.7: Laser diode mounted on goniometerhead

To establish if the effect of the laser on the diffraction pattern is isotropic or not, the directions from which the crystals were irradiated were chosen at random. In all the effect of the laser radiation on the X-ray diffraction of three randomly oriented spherical crystals were investigated. Although no detailed measurements were recorded it was established that laser light does significantly alter the observed intensities of some of the reflections. However, it was observed that the extent to which individual reflections are affected depends on the orientation of the laser beam with respect to the unit cell of the crystal. That is the observed phenomenon is anisotropic. It was also noted that the observed phenomenon does not remain reversible indefinitely. In other words, after some period the diffracted intensity becomes insensitive to laser light.

The crystal structure of TGS is characterised by the presence of the two hydrogen bonded complexes shown in Figures 7.7 and 7.8. The packing of these complexes can be seen in the packing diagrams shown in Figures 7.5 and 7.6. The sort of hydrogen bonding seen in TGS has also been observed in other crystals with nonlinear properties. For example in the 1:1 complex formed between 4-nitropyridine N-oxide and 4-nitrophenol (Fuquen *et al*, 1992). It has been suggested that hydrogen bonding plays an important role in acentric materials with nonlinear properties. It is conceivable that the changes in the Bragg intensities observed under the influence of laser radiation is due to changes in the hydrogen bonding network.

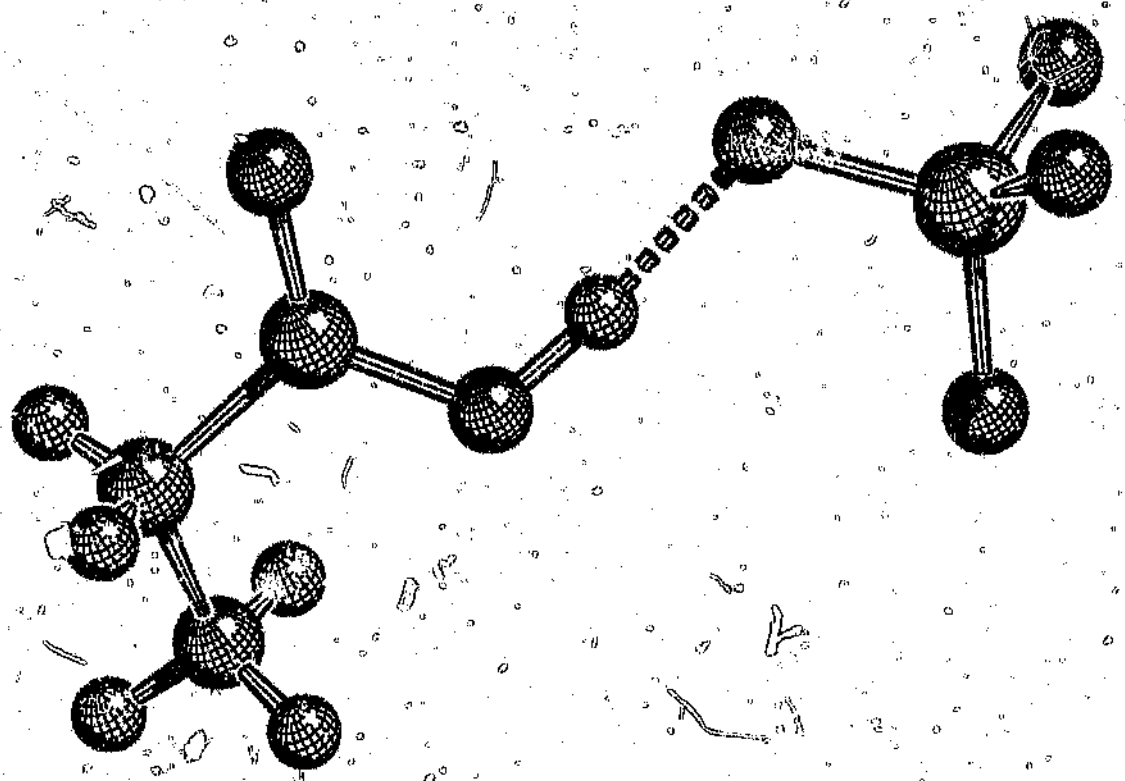


Figure 7.7 : First hydrogen bonded complex in TGS

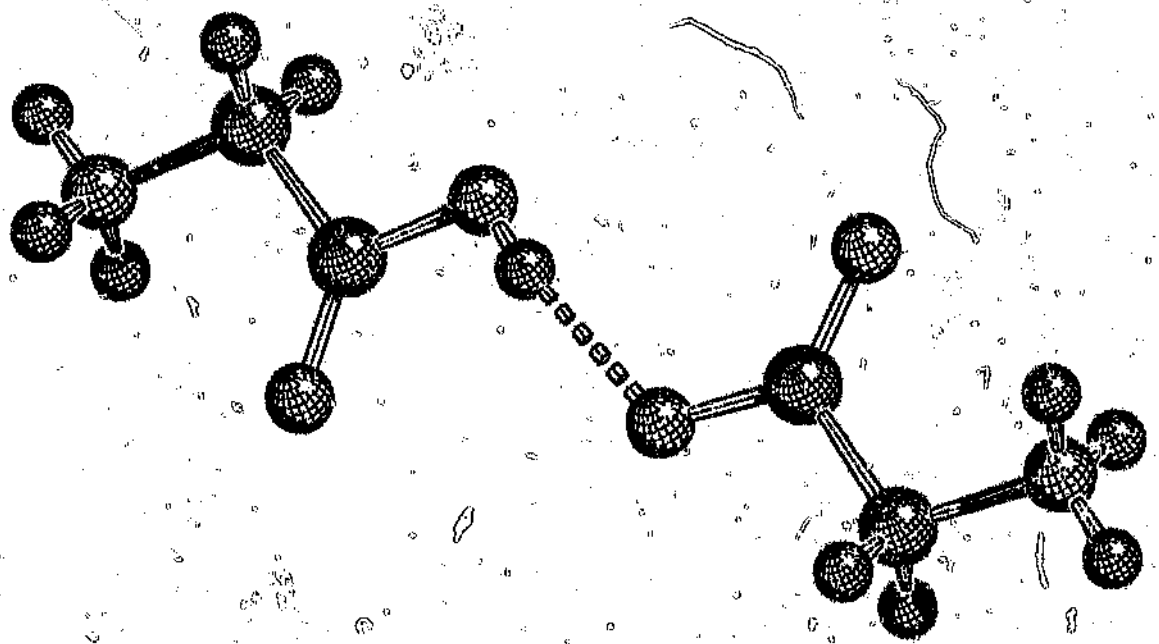
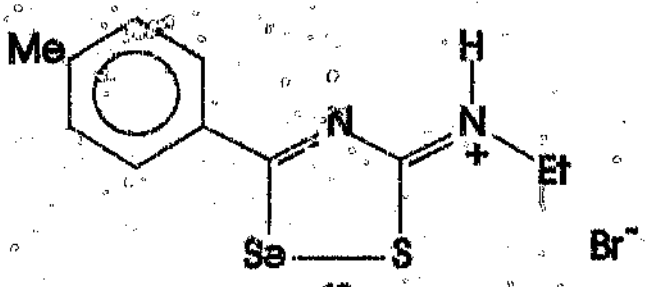


Figure 7.8 : Second hydrogen bonded complex in TGS

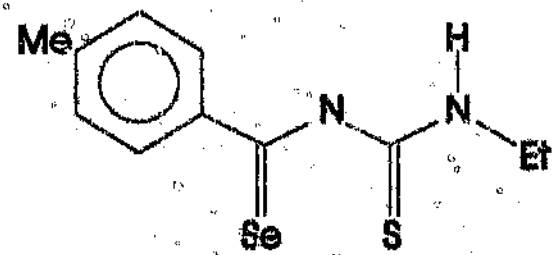
CHAPTER 8

The crystal structure of 5-Ethylamino-3-p-tolyl-1λ⁴,2,4-thia- selenazol-1-ylium Bromide.

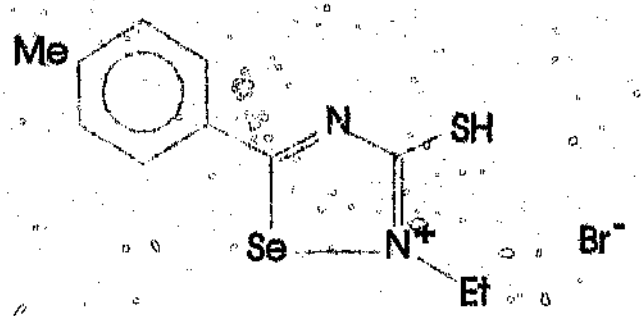
The structure determination of the title compound ***18***, obtained by intermolecular oxidative coupling of compound (xx) with bromine (Lai; 1992), was undertaken to confirm that Se-S coupling in ***18*** had indeed occured, rather that Se-N coupling which would lead to the isomeric salt (xxi). The cation in the salt is a derivative of the 1λ⁴, 2,4-thiaselenazol-1-ylium cation, a new heteroaromatic system whose derivatives are being employed in a new systhesis of hypervalent heterocyclic compounds (Lai; 1992). The length of the Se-S bond [2.1893(8)Å] is nearly the same as the accepted covalent Se-S bond length [2.195(15)Å; Allen, Kennard, Watson, Brammer, Orpen and Taylor, 1987]. The C(2)-Se and C(1)-S bonds are essentially C(sp^2)-Se and C(sp^2)-S single bonds, respectively. The cation in the salt ***18*** is planar and the heterocyclic ring bond lengths indicate that there is some π-electron delocalisation extending over the C(2), N(1), C(1), N(2) sequence, with the C(2)-N(1) and the C(1)-N(2) bonds shorter than the C(1)-N(1) bond.



18



(xx)



(xxi)

The title compound ***18*** was obtained as yellow needle-shaped crystals, from the reaction mixture, after washing with acetonitrile; m.p. 511 - 513K. As the crystals proved to be unstable in the X-ray beam at ambient temperature, data were collected at 123K. This was done using a liquid nitrogen gas-flow cryostat mounted on a CAD4 diffractometer, equipped with standard Enraf Nonius data collection routines. Data reduction, including Lorentz, polarisation and analytical absorption corrections was done using the PC version of the NRCVAX set of programs. Unit cell dimensions and details of the data collection are given in Table 8.1. The structure was solved by direct methods using SHELXS86 and refined by full-matrix least-squares methods based on F^2 using SHELXL93. All non-hydrogen atoms were refined with anisotropic displacement parameters. Hydrogen atoms were placed in geometrically calculated positions and allowed to refine in riding mode in the final cycles of refinement. Figure 8.1 shows a labelled ORTEP diagram of the molecule and the atomic coordinates are listed in Table 8.2.

Table 8.1 : Crystal and refinement data

Compound	***18***
Empirical formula	$C_{11}H_{13}BrN_2SSe$
Formula weight / g.mol^{-1}	364.16
Temperature / K	126(2)
Wavelength / Å	0.71069
Crystal system	Monoclinic
Space group	P $2_1/n$
a / Å	7.237(2)
b / Å	10.4340(10)
c / Å	17.450(2)
α / °	90
β / °	99.42(1)

γ / °	90
Volume / Å^3	1299.9(4)
z	4
ρ / Mg.m^{-3}	1.881
Absorption coefficient / mm^{-1}	6.042
F(000)	716
Crystal size / mm^3	0.34 x 0.15 x 0.14
Range	2.3 ≤ θ ≤ 30
Index ranges : h k l	 -10→10 0→14 0→24
Reflections collected	8911
Independent reflections	3776
R_{int}	0.0268
Data/restraints/parameters	3776/0/148
Max shift, Δz	0
Residual density / e.Å^{-3} $(\Delta\rho)_{max}$ $(\Delta\rho)_{min}$	 1.052 -1.012
Reliability indice: R1 (I > 2σ(I)) wR2 (I > 2σ(I)) R1 (all data) wR2 (all data)	 0.0356 0.0923 0.0606 0.0967
S	0.986

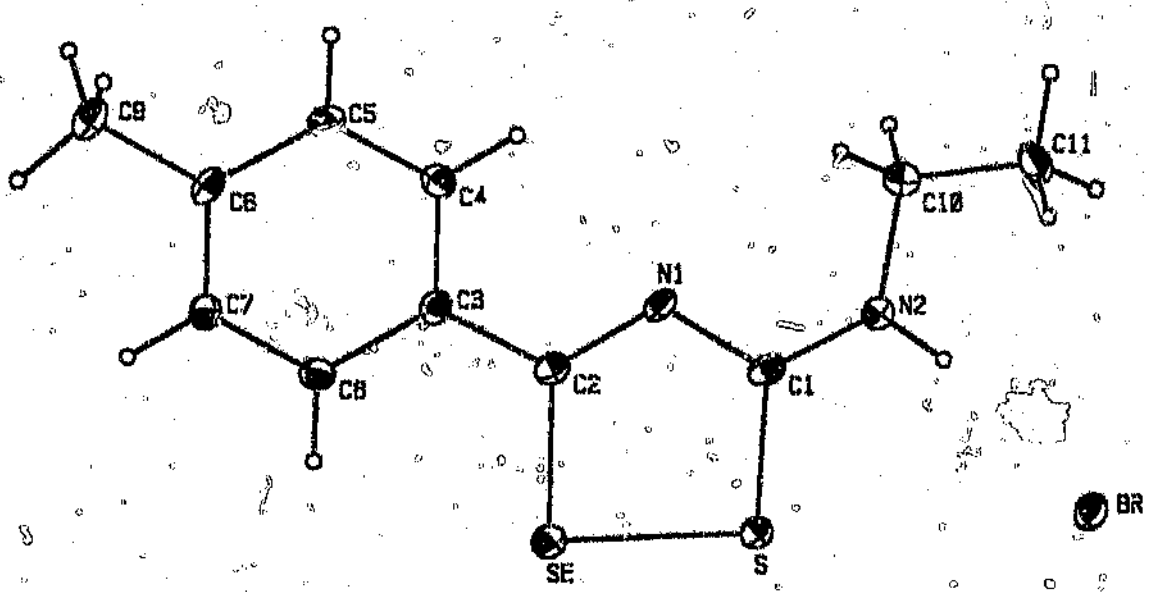


Figure 8.1: Labelled ORTEP diagram of *18*

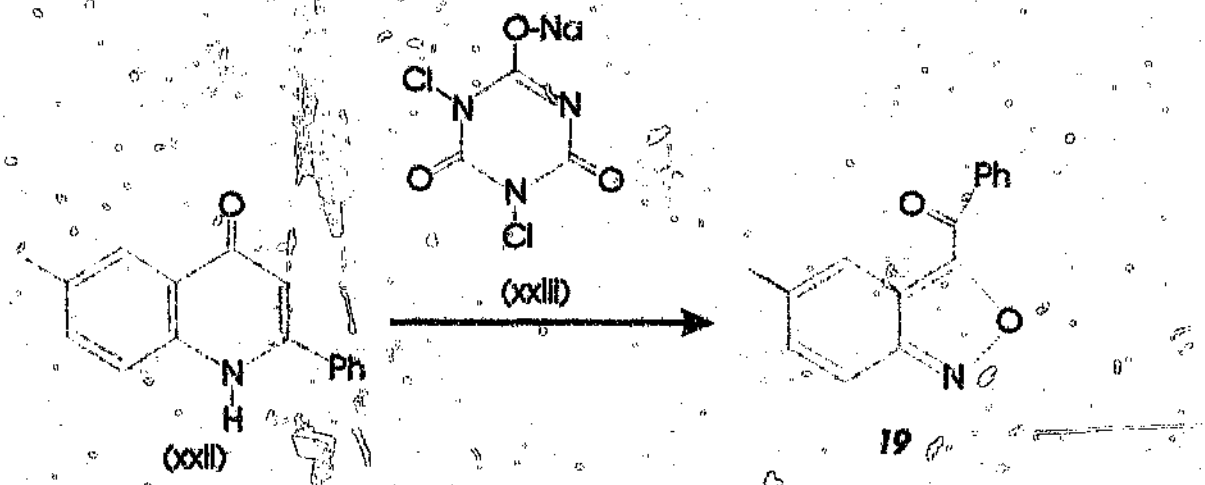
Table 8.2 : Atomic coordinates (x 10^4) and equivalent isotropic displacement parameters ($Å^2$, x10^3) for **18**

	x/a	y/b	z/c	U_{eq}
Br	5532(1)	4582(1)	6666(1)	16(1)
Se	3300(1)	8077(1)	4139(1)	14(1)
S	4137(1)	6724(1)	5091(1)	11(1)
N(1)	3164(4)	9039(3)	5614(2)	11(1)
N(2)	4128(4)	7497(3)	6538(2)	13(1)
C(1)	3786(4)	7845(3)	5811(2)	12(1)
C(2)	2821(4)	9320(3)	4869(2)	11(1)
C(3)	2093(4)	10567(3)	4604(2)	12(1)
C(4)	1695(5)	11477(3)	5142(2)	14(1)
C(5)	1010(4)	12869(3)	4899(2)	13(1)
C(6)	690(4)	13000(3)	4107(2)	13(1)
C(7)	1080(4)	12097(3)	3573(2)	13(1)
C(8)	1756(4)	10883(3)	3809(2)	13(1)
C(9)	-28(5)	14307(3)	3855(2)	17(1)
C(10)	3917(5)	8318(3)	7200(2)	19(1)
C(11)	3487(5)	7515(4)	7865(2)	16(1)

Chapter 9

The crystal structure of 3-benzoyl-5-methyl-2,1-benzisoxazole.

The title compound ***19*** was identified on the basis of a single crystal X-ray structure determination. It had been obtained from the treatment of (xxii) with excess sodium dichloroisocyanurate (xxiii) in methanolic aqueous sodium hydroxide.



The yellow crystal selected for the analysis afforded data reliable enough to allow for the refinement, using isotropic displacement parameters, of the positions of the hydrogen atoms, located using difference Fourier maps. The fused ring system within the title compound is planar, with its atoms deviating from the mean plane by at most 0.013Å. The C(2)-C(1)-C(8)-O(2) torsion angle (-11.8(3)°) indicates that the carbonyl group deviates somewhat from the mean plane of the fused ring system. The C(1)-C(8) bond, of length 1.471(2)Å, shows that there is some delocalisation of electronic charge taking place between the fused ring system and the carbonyl group. In general the bond lengths and angles of the title compound are virtually identical to the corresponding bond lengths and angles in 3-benzoyl-2,1-benzisoxazole (*Sunderalingam and Jeffrey;* 1962).

Cell determination, using 25 high-order reflections, and data collection were done on an Enraf-Nonius CAD4 four-circle diffractometer equipped with a graphite monochromator. Data reduction included corrections for Lorentz and polarisation effects using standard Enraf Nonius routines. Absorption effects were corrected for empirically (North *et al*, 1968). Three standard reflections monitored every hour showed only random fluctuations. Unit cell parameters, as well as details of the data collection, solution and refinement are given in Table 9.1. The structure was solved by direct methods using SHELXS86 and refined using SHELXL93 by least-squares methods, based on F^2. All non-H atoms were refined with anisotropic displacement parameters. Figure 9.1 shows a labelled ORTEP diagram of the molecule and also indicates the numbering scheme used in the analysis. Atomic coordinates and selected bond lengths are listed in Table 9.2 and Table 9.3 respectively.

Table 9.1 : Crystal and refinement data	
Compound	**19**
Empirical formula	$C_{15}H_{11}NO_2$
Formula weight / g.mol^{-1}	237.25
Temperature / K	293(2)
Wavelength / Å	0.71069
Crystal system	Monoclinic
Space group	C 2/c
a / Å	24.415(4)
b / Å	5.7540(10)
c / Å	17.143(2)
α / °	90
β / °	94.463(7)
γ / °	90
Volume / Å^3	2400.9(6)
z	8
ρ / Mg.m^{-3}	1.313
Absorption coefficient / mm^{-1}	0.088
F(000)	992
Crystal size / mm^3	0.3 x 0.2 x 0.2
Range	$2.8 \leq \theta \leq 30$
Index ranges : h k l	 -1→34 -1→8 -24→24
Reflections collected	4379

Independent reflections	3472
R_{int}	0.0561
Data/restraints/parameters	3472/0/207
Max shift, Δz	0.001
Residual density / e Å^{-3}	
$(\Delta\rho)_{max}$	0.391
$(\Delta\rho)_{min}$	-0.261
Reliability indices	
R1 ($I > 2\sigma(I)$)	0.0633
wR2 ($I > 2\sigma(I)$)	0.1924
R1 (all data)	0.0857
wR2 (all data)	0.2042
S	1.079

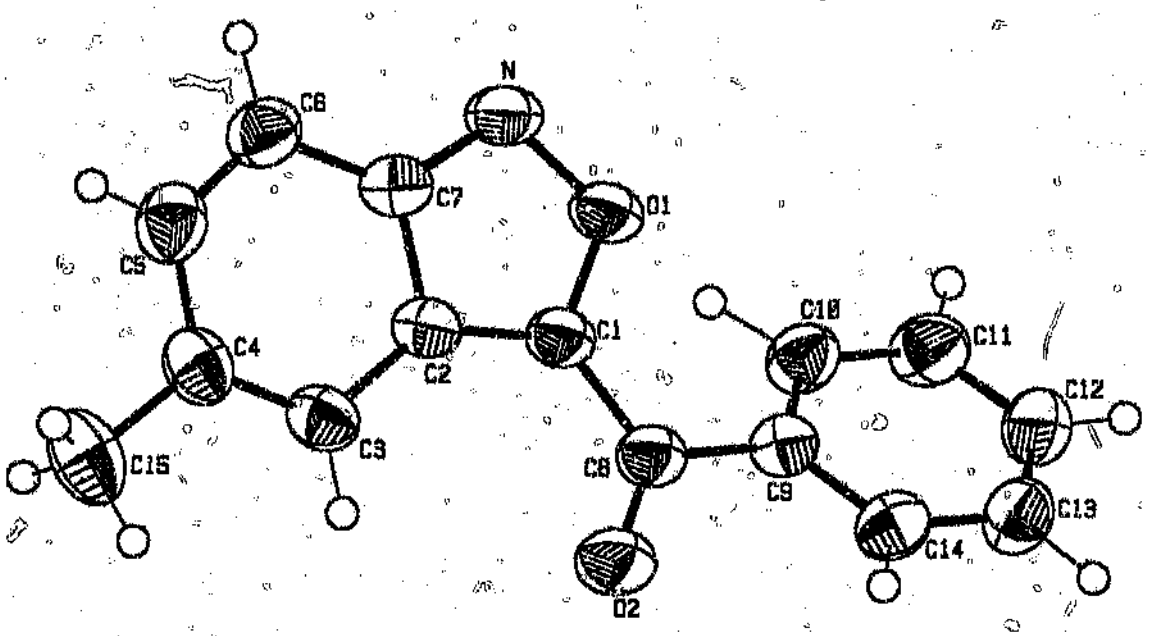


Figure 9.1: Labelled ORTEP diagram of ***19***

Table 9.2: Atomic coordinates (x 10^4) and equivalent isotropic displacement parameters (Å^2, x10^3) for ***19***

	x/a	y/b	z/c	U_{eq}
O(1)	676(1)	2587(2)	1527(1)	54(1)
O(2)	2006(1)	2311(3)	2473(1)	65(1)
N	455(1)	4036(3)	927(1)	55(1)
C(1)	1197(1)	3248(2)	1756(1)	45(1)
C(2)	1337(1)	5126(2)	1317(1)	42(1)
C(3)	1807(1)	6566(3)	1272(1)	48(1)
C(4)	1780(1)	9337(3)	742(1)	53(1)
C(5)	1283(1)	8730(3)	247(1)	58(1)
C(6)	826(1)	7424(3)	270(1)	54(1)

C(7)	851(1)	5551(3)	813(1)	45(1)
C(8)	1514(1)	1951(3)	2378(1)	47(1)
C(9)	1235(1)	238(2)	2861(1)	44(1)
C(10)	668(1)	497(3)	3035(1)	52(1)
C(11)	447(1)	-1166(4)	3478(1)	60(1)
C(12)	712(1)	-3091(3)	3744(1)	60(1)
C(13)	1287(1)	-3330(3)	3592(1)	58(1)
C(14)	1536(1)	-1673(3)	3157(1)	50(1)
C(15)	2264(1)	9915(4)	665(2)	76(1)

Table 9.3: Selected bond lengths (Å) for **19**

O(1)-C(1)	1.358(2)	O(1)-N	1.398(2)
O(2)-C(8)	1.329(2)	N-C(7)	1.374(2)
C(1)-C(2)	1.374(2)	C(1)-C(8)	1.471(2)
C(2)-C(3)	1.423(2)	C(2)-C(7)	1.431(2)
C(3)-C(4)	1.363(2)	C(4)-C(5)	1.442(3)
C(5)-C(6)	1.348(2)	C(6)-C(7)	1.423(2)
C(8)-C(9)	1.487(2)		

Chapter 10
Concluding discussion

In recent years, approximately 10 000 new crystal structures have been added annually to the Cambridge Crystallographic database. This fact is a testimony to the importance of structural data within chemistry. In general, these structures, determined by small molecule crystallographic methods, form the basis on which chemists have now founded their knowledge of molecular structure. In this thesis, the results of 19 successfully refined structures have been presented. These structure determinations, in addition to contributing to the body of known crystal structures, were undertaken for a number of chemical reasons, and the issues addressed included the nature of some chemical bonds, conformational preferences in molecules, hydrogen bonding in crystals as well as the identification and characterisation of reaction products.

Improvements and developments in crystallographic methodology as well as advances in the fields of computing and automated diffractometry have greatly reduced the effort required for the successful completion of a structure determination. It is, however, still far from being as routinely applicable as, for example, proton NMR spectroscopy. The reason for this is that both the precision and accuracy of each crystallographic analysis may be influenced by a number of factors, beyond the control of the crystallographer.

When, for example, measuring the intensities of the X-ray diffraction pattern a multitude of problems may be encountered. These may be categorised as instrumental problems, crystal problems and user problems. These include random errors such as misalignment of the instrument, fluctuations in the power of the X-ray beam, failure of the detecting system, non-uniformity of a low-temperature gas stream, if used, crystals moving on their mounts and intermittent X-ray shutter failures. There are other errors, such as those derived from crystal decay in the X-ray beam, which are systematic and may be corrected from by measuring periodically a few standard reflections to check on the constancy of the experimental

set-up. The absorption of the X-ray beam by the crystal is also systematic and may be minimised by the use of either empirical or analytical absorption correction methods. For the latter the faces of the crystal are accurately measured and indexed, and this information then used to determine appropriate correction factors for each reflection measured. There are also other types of errors that are more difficult to correct for unless more information is available; these include multiple reflection, extinction and thermal diffuse scattering. These type of errors are normally only considered when an extremely accurate crystal structure is required.

Disorder too can cause serious problems during crystallographic investigations. Real crystals deviate from the ideal picture of a periodically perfect repetition of a unit. Because of thermal motion, atoms oscillate around an equilibrium position within the unit cell, and is described by the anisotropic displacement parameters. For some crystals very large movements are possible and this results in dynamic disorder. Because the diffraction experiments show a time-averaged situations, the observed electron density appears to be smeared out. This problem may generally be reduced by performing the diffraction experiment at reduced temperatures. Another type of disorder that may occur in crystals is referred to as static disorder, and in this case the average contents of the unit cell is obtained by averaging over space, i.e. over the different unit cells. An important example of this type of disorder, which is common in minerals, and alloys is the substitutional disorder where the same site is occupied by different types of atoms in different unit cells.

It is clear that although crystal structures can today be determined with greater ease and precision than ever before, cognisance needs to be taken of all the factors that may influence the outcome of the analysis. Care should also be taken when the results of crystallographic analyses are considered or compared.

Bibliography

1. Blundel, J.L and Johnson, L.N., (1976), *Protein Crystallography*, Academic Press, New York.
2. Buerger, M.J. (1970), *Contemporary crystallography*, McGraw Hill
3. Domenicano, A and Hargittai, I. (1992), *Accurate molecular structures, their determination and importance*, Oxford science publications.
4. Giacovazzo, C (1992), *Fundamentals of Crystallography*, Oxford University Press.
5. Ladd, M.F.C and Palmer, R.A. (1993), *Structure determination by X-ray crystallography*, Plenum Press.
6. Luger, P. (1985), *Modern x-ray analysis on single crystals*, Walter de Gruyter, Berlin.
7. Mak, T. C. W and Zhou, G-D, (1992), *Crystallography in modern chemistry, a resource book of structures*, John Wiley and Sons.
8. McKie, D. and McKie, C. (1986), *Essentials of crystallography*, Blackwell scientific publications.
9. Pauling, L. (1960), *The nature of the chemical bond*, Cornell University Press.
10. Pickworth Glusker, J and Trueblood, K.N. (1985), *Crystal structure analysis, a primer*, (2nd ed.), Oxford university press.
11. Stout, R.H and Jensen, L.H. (1989), *X-ray structure determination, a practical guide*. (2nd ed.), Wiley.
12. Woolfson, M.M (1970), *An introduction to X-ray crystallography*, Cambridge university press.

References

1. Albertsson, J.; Oskarsson, Å. and Stahl K., (1979), *J. Appl. Cryst.*, **12**, 537-544.
2. Allen, C.; Boeyens, J.C.A.; Briggs, A.G.; Denner, L.; Markwell, A.J.; Reid, D.H. and Rose, B.G., (1987), *J. Chem. Soc., Chem. Commun.*, 967-968.
3. Allen, F.H.; Kennard, O.; Watson, D.G.; Brammer, L.; Orpen, A.G. and Taylor, T., (1987), *J. Chem. Soc. Perkin Trans II*, S1-S19.
4. Argoud, R. and Muller, J., (1989), *J. Appl. Cryst.*, **22**, 378-380.
5. Baert, F.; Lamoit, J.; Couturier, D.; Roussel, D. and Ricart, G., (1984), *Acta Cryst.*, **C40**, 1071.
6. Billing, D.G.; Boeyens, J.C.A.; Denner, L.; Hellyar, M.D.; Lai, L-L.; Matthee, A.J. and Reid, D.H., (1991), *Acta Cryst.*, **C47**, 2564-2567.
7. Birknes, B.; Hordvik, A. and Saethre, L.J., (1975), *Acta Chem. Scan.*, **A29**, 195-200.
8. Birknes, B.; Hordvik, A. and Saethre, L.J., (1982), *Acta Chem. Scan.*, **A36**, 683-688.
9. Bezzi, S.; Mammi, M. and Garbuglio, C. (1958), *Nature*, **182**, 247-248.
10. Churchill, M.R.; Amoh, K.N.and Wasserman, H.J., (1981), *Inorg. Chem.*, **20**, 1609.
11. Cremer, D. and Pople, J.A. (1975), *J. Am. Chem. Soc.*, **97**, 1354.
12. Coppens, P.; Ross, F.K.; Blessing, R.H.; Cooper, W.F.; Larsen, F.K.; Leipoldt, J.G.; Rees, B. and Leonard, R. (1974), *J. Appl. Cryst.*, **7**, 315.
13. Darwin, C.G., (1914), *Philosophical Magazine*, **27**, 315.
14. Darwin, C.G., (1922), *Philosophical Magazine*, **43**, 800.
15. Fuquen, R.M.; de Almeida Santos, R.H. and Lechat, J.R., (1992), *J. of Cryst. and Spec. Res.*, **22**, 201-204.
16. Gabe, E.J., Le Page, Y and Charland, J-P (1989), *J. Appl. Cryst.*, **22**, 384.
17. Giacometti, G. and Rigatti, G. (1959), *J. Chem. Phys.*, **30**, 1633-1634.
18. Gleiter, R. and Hoffmann, R., (1968), *Tetrahedron*, **24**, 5899-5911.

19. Greubel, K.H.; Gmelin, E.; Moser, N.; Mensing, Ch. and Walz, L., (1990), *Cryogenics*, 9091.
20. Hall, S.R. and Steward, J.M., (1992), Eds. *Xtal3.2 Reference Manual* . Universities of Western Australia and Maryland.
21. Hansen, L.K. and Hordvik, A., (1973), *Acta Chem. Scan.*, **27**, 411-420.
22. Hendrikson, K.; Larsen, F.K. and Rasmussen, S.E., (1986), *J. Appl. Cryst.*, **19**, 390-394.
23. Hordvik, A., (1971), *Acta Chem. Scan.*, **25**, 1822-1834.
24. Hordvik, A. and Julshamn, K., (1971)a, *Acta Chem. Scan.*, **25**, 2507-2515.
25. Hordvik, A. and Julshamn, K., (1971)b, *Acta Chem. Scan.*, **25**, 1835-1848.
26. Hordvik, A. and Porten, J.A., (1973), *Acta Chem. Scan.*, **27**, 485-492.
27. Hordvik, A. and Saethre, L.J., (1972), *Isr. J. Chem.*, **10**, 239-248.
28. Hordvik, A.; Sletten, E. and Sletten, J., (1969), *Acta Chem. Scan.*, **23**, 1852-1870.
29. Iwasaki, F.; Murakami, H.; Yamazaki, N.; Yasui, M.; Tomura, M. and Matsumura, N., (1991), *Acta Cryst.*, **C47**, 998-1003.
30. Karle, J. and Hauptman, H., (1950), *Acta Crystallogr.*, **3**, 181-187.
31. Keller,E. (1988), SCHAKAL88. *A Fortran Program for the Graphical Representation of Molecular and Crystallographic Models.* Albert-Ludwigs Univ. Freiburg, Germany.
32. Kilpatrick, J.E.; Pitzer, K.S. and Spitzer, R., (1947), *J. Amer. Chem. Soc.*,**69**, 2483-2488.
33. Klyne, W. and Prelog, V. (1960), *Experientia*, **16**, 521.
34. Lai, L.-L., (1992), Ph.D. Thesis, University of the Witwatersrand, Johannesburg, South Africa.
35. Mammi, M.; Bardi, R.; Garbuglio, C. and Bezzi, S. (1960), *Acta cryst.*, **13**, 1048-1049.
36. Martin, M.; Rees, B. and Mitschler, A., (1982), *Acta Crystallogr.*, **B38**, 6.
37. North, A.C.T.; Phillips, D.C. and Mathews, F.S., (1968), *Acta Crystallogr.*, **A24**, 351.
38. Patterson, A.L., (1934)., *Phys. Rev.*, **46**, 372-376
39. Patterson, A.L., (1935)., *Z. Kristallogr.*, **90**, 517-542.

40. Ravi, G.; Arebukumar, S. and Ramasamy, P., (1993), *J. of Crystal Growth*, **133**, 212-216.

41. Schomaker, V.; Wasser, J.E.; Marsh, R.E. and Gergman, G., (1959), *Acta Cryst.*, **12**, 600.

42. Sheldrick, G.M., (1985), SHELXS86, In *Crystallographic Computing 3*, edited by G.M. Sheldrick, C. Kruger and R. Goddard, pp 175-189, Oxford Univ. Press.

43. Sheldrick G.M., (1993), SHELXL93, *J. Appl. Cryst*, (In preparation).

44. Solans, X.; Franco, F. and Mikavitiles, G. (1985), *J. of Ferroelectrics*, **62**, 59.

45. Staskun, B., (1980), *J. Org. Chem.*, **45**, 2482.

46. Strel'tsov, V.A. and Zarodnik, V.E., (1989), *Kristallografia*, **34**, 1369.

47. Struchkov, Yu. T.; Anisimov, K.N.; Osipova, O.P.; Kolobova, N.E. and Nesmeyanov, A.N., (1967), *Dokl. Akad. Nauk SSSR*, **172**, 107.

48. Sundaralingam, M. and Jeffrey, D.A., (1962), *Acta Cryst.*, **15**, 1035.

49. Rheingold, A.L.; Meckstroth, W.K. and Ridge, D.P., (1986), *Inorg. Chem.*, **25**, 3706.

50. Zhukov, S.G.; Fetisov, G.V. and Aslanov, L.A., (1991), *J. Appl. Cryst.*, **24**, 74-76.

Appendix

Lists of structure factors, anisotropic thermal parameters, H-atom coordinates and complete geometrical parameters have been included in compressed form on the accompanying DOS disk. The files include the neccessary escape codes forprinting on an HP laser printer with A4 paper, and may be decompressed with PKUNZIP

Author: Billing David Gordon.
Name of thesis: Applications of small molecule crystallography.

PUBLISHER:
University of the Witwatersrand, Johannesburg
©2015

LEGALNOTICES:

Copyright Notice: All materials on the University of the Witwatersrand, Johannesburg Library website are protected by South African copyright law and may not be distributed, transmitted, displayed or otherwise published in any format, without the prior written permission of the copyright owner.

Disclaimer and Terms of Use: Provided that you maintain all copyright and other notices contained therein, you may download material (one machine readable copy and one print copy per page)for your personal and/or educational non-commercial use only.

The University of the Witwatersrand, Johannesburg, is not responsible for any errors or omissions and excludes any and all liability for any errors in or omissions from the information on the Library website.